University of Minho
School of Sciences

Carlos Bruno Pereira Oliveira

Development of new supramolecular hypergelators based on non-natural amino acid residues

December 2021

Carlos Bruno Pereira Oliveira **Development of new supramolecular hypergelators based on non-natural amino acid residues**

Uminho | 2021

University of Minho
School of Sciences

Carlos Bruno Pereira Oliveira

Development of new supramolecular hypergelators based on non-natural amino acid residues

Master`s Dissertation
Medicinal Chemistry

Performed under the supervision of
Doctor Peter John Jervis and
Doctor Paula Margarida Ferreira

December 2021

DIREITOS DE AUTOR E CONDIÇÕES DE UTILIZAÇÃO DO TRABALHO POR TERCEIROS

Acknowledgement

This work was only possible with the contribution and brilliant guidance of many people. I am grateful to all whom, in one way or another, helped me through this amazing journey.

First, I would like to thank my incredible supervisors, Dr. Peter Jervis, Dra. Paula Margarida Ferreira, and Dr. José Alberto Martins for all their support during the development of this work and for giving me freedom to think for myself. I apologize for all my endless questions and thank you for your enormous patience. Thanks to them both my confidence and love for chemistry has increased exponentially. Also, their confidence, positive energy and guidance helped me not only to overcome difficulties but also to learn from them.

I would like to express my gratitude to Dr. Loic Hillou from the Instituto de Polímeros e Compósitos (IPC) for all the help and for making available the equipment where the rheology assays were carried out. I also thank Dr. David Pereira from Faculdade de Farmácia of Universidade do Porto for conducting the cytotoxicity tests.

I thank to the Centro de Química and the Departamento de Química of the Universidade do Minho for offering the necessary resources for the development of this project. A special thanks to Elisa Pinto for the NMR spectra. I also thank the NMR Portuguese network (PTNMR (Portuguese NMR network) PINFRA/22161/2016 financed by FCT and Portugal 2020).

I would like to thank to Fundação para a Ciência e a Tecnologia for funding through project PTDC/QUI-QOR/29015/2017.

Thank you to my lab colleagues, Valéria, André, Carolina, Sérgio and Teresa for the good lab environment and the help provided, it wouldn't be the same without them.

Finally, I would like to thank my family, especially my parents, my brother and my grandparents for their support, encouragement, understanding, patience, and strength I needed to continue following my dreams.

FCT Fundação para a Ciência e a Tecnologia

REPÚBLICA PORTUGUESA

STATEMENT OF INTEGRITY

I hereby declare having conducted this academic work with integrity. I confirm that I have not used plagiarism or any form of undue use of information or falsification of results along the process leading to its elaboration. I further declare that I have fully acknowledged the Code of Ethical Conduct of the University of Minho.

Development of new supramolecular hypergelators based on non-natural amino acid residues

Abstract

Employing amino acids and peptides as molecular building blocks provides unique opportunities for generating supramolecular hydrogels, owing to their inherent biological origin, bioactivity, biocompatibility, and biodegradability. However, they can suffer from proteolytic degradation. Ultrashort peptides (< 8 amino acids) attached to an aromatic capping group are particularly attractive alternatives as minimalistic low molecular weight hydrogelators. Peptides with low critical gelation concentration (CGC) are especially desirable, due to the low weight percentage required to obtain a hydrogel, making them more cost-effective. In this work, seven non-natural peptides were prepared. These peptides were based on different subclasses: dehydro*di*peptides, dehydro*tri*petides and non-canonical (in structure and stereochemical configuration) dipeptides. Their self-assembly properties were studied, and the results showed that all compounds, with the exception of 3-indolepropionyl-D-4-benzoylphenylalanyl-D-homophenylalanine, can form self-standing hydrogels with ultralow critical gelation concentrations using a pH trigger. Scanning transmission electron microscopy images showed a network of entangled fibres for all six hydrogels, while vesicular/aggregated structures were observed for the dipeptide which failed to produce a hydrogel. Circular dichroism spectroscopy was performed to evaluate the aggregation of peptides into characteristic secondary structures. Generally, the results suggest β-sheet or random coil-like structures. According to the rheology results, the hydrogelators are viscoelastic materials with an elastic modulus G` that falls in the range of native tissue (0.37 kPa brain – 4.5 cartilage). The cytotoxicity of the new compounds was also tested using human keratinocytes (HaCaT cell line). In general, the results suggest that all seven compounds are not cytotoxic, although some peptides have shown a small impact in cell viability.

In sustained release assays, the effect of the charge of the model drug compounds on the rate of cargo release from the hydrogel network was evaluated. The hydrogels showed a sustained release of methyl orange (anionic) and ciprofloxacin (neutral), while methylene blue (cationic) was retained by the hydrogel network. The non-natural peptides developed within this work constitute promising biomaterials to be further explored and used as new therapeutic platforms for localized drug delivery systems.

Keywords: Dehydrodipeptides, dehydrotripeptides, non-canonical dipeptides, self-assembly, supramolecular hydrogels, critical gelation concentration, drug delivery systems.

Desenvolvimento de novos hipergeladores baseados em resíduos de aminoácidos não naturais

Resumo

Neste trabalho, foram sintetizados sete *di* e *tri*péptidos contendo aminoácidos não-naturais o que os torna resistentes à proteólise. Assim, foram preparados três dipéptidos e dois tripéptidos contendo o desidroaminoácido desidrofenilalanina e dois dipéptidos com resíduos de D-homofenilalanina e D-4-benzoilfenilalanina. As propriedades de auto-associação destes péptidos foi estudada e os resultados mostraram que todos os péptidos, com a exceção do dipéptido de D-4-benzoilfenilalanil-D-homofenilalanina *N*-protegido com o ácido 3-indolpropenoico, formam hidrogéis com concentrações críticas de gelificação baixas. Estes hidrogéis foram obtidos utilizando o método de alteração do pH utilizando a glucono-δ-lactona. As imagens de microscopia eletrónica de transmissão de varrimento revelaram uma rede de fibras entrelaçadas nos seis hidrogéis, enquanto que o composto que não formou um hidrogel mostrou estruturas vesiculares. Os espetros de dicroísmo circular foram efetuados para avaliar as estruturas secundárias resultantes da agregação dos péptidos. Os resultados evidenciaram estruturas em folha β e *random coil*. Estudos reológicos mostraram que os hidrogéis são materiais viscoelásticos com valores para o módulo de elasticidade G` situados entre os encontrados para os vários tecidos biológicos (0.37 kPa cérebro – 4.5 kPa cartilagem). A citotoxicidade dos péptidos foi testada em queratinócitos humanos (HaCaT). Os resultados obtidos sugerem que os péptidos em estudo não são citotoxicos, apesar de terem um pequeno impacto na viabilidade celular. Nos ensaios de libertação controlada, foi estudado o efeito da carga de compostos modelo na taxa de libertação a partir dos hidrogéis. Verificou-se a libertação do alaranjado de metilo (aniónico) e da ciprofloxacina (neutra) a partir dos hidrogéis e a retenção do azul de metileno (catiónico). Os novos hidrogéis baseados em péptidos não-naturais desenvolvidos neste trabalho constituem uma classe de biomateriais bastante promissora cujo estudo irá prosseguir com o objetivo de criar novas plataformas terapêuticas para a entrega localizada e controlada de fármacos.

Palavras-chave: Desidrodipéptidos, desidrotripéptidos, dipéptidos não-canónicos, auto-associação, hidrogéis supramoleculares, concentração crítica de gelificação, libertação de fármacos.

Índex

Index of figures

Index of tables

Index of schemes

Abbreviations and Acronyms

3D	Three-dimensional
Boc	*tert*-Butyloxycarbonyl
Boc_2O	*tert*-Butyl dicarbonate
CD	Circular dichorism
$CDCl_3$-d_1	Deuterated chloroform
CGC	Critical gelation concentration
COX-1	Cyclooxygenase-1
COX-2	Cyclooxygenase-2
DMAP	4-dimethylaminopyridine
DMSO-d_6	Deuterated dimethylsulfoxide
DNA	Deoxyribonucleic acid
DOX	Doxorubicin
ESI	Electrospray Ionization
Et_3N	Triethylamine
Phe-Phe	Phenylalanylphenylalanine
Fmoc	Fluorenylmethoxycarbonyl
Ind	Indole
G*	Complex modulus
G'	Elastic modulus
G''	Viscosity modulus
GdL	D-glucono-δ-lactone
HBTU	*N,N,N',N'*-Tetramethyl-*O*-(1*H*-benzotriazol-1-yl)uronium hexafluorophosphate
HRMS	High Resolution Mass Spectrometry
J	NMR coupling constant in Hz
LDH	Lactate dehydrogenase
L-DOPA	Levadopa
LMWHs	Low molecular weight hydrogelators
MB	Methylene blue
MeCN	Acetonitrile
MO	Methyl orange

Naph	Naphthalene
NMR	Nuclear magnetic resonance
Npx	Naproxen
Cbz	Benzyloxycarbonyl / carboxybenzyl
NSAID	Nonsteroidal anti-inflammatory drug
PAG	Photoacid generators
PEG	Polyethylene glycol
PLA	Polylactic acid
Ppm	Parts per million
RGD	Arginylglycylaspartic acid
rt	Room temperature
STEM	Scanning transmission electron microscopy
T_{gel}	Temperature of hydrogelation
TEM	Transmission electron microscopy
TFA	Trifluoroacetic acid
THF	Tetrahydrofuran
TLC	Thin layer chromatography
TMG	*N*,*N*,*N*′,*N*′-tetramethylguanidine

Chapter 1

Introduction

1 Introduction

1.1 The marvellous world of Hydrogels

The first mention of the term "hydrogel" appeared in the literature at the beginning of the 19th century, to describe colloidal gels derived from inorganic salts (1). Later in 1960, Wichterle and Lim provided one of the earliest records of cross-linked hydroxyethyl methacrylate (HEMA) hydrogels, with the ambitious goal of using them in permanent contact applications with human tissues (2).

As suggested by Buwalda *et al.*, the history of hydrogels can be divided into three main sections (3):

1) A first generation of hydrogels, formed through a wide range of cross-linking procedures involving chemical modifications of a monomer or polymer with an initiator, with the general aim of developing materials with high swelling, good mechanical properties, and relatively simple rationales.
2) Later, a different concept of hydrogel materials emerged - a second generation of materials capable of responding to specific stimuli, such as variations in temperature, pH, or concentration of specific molecules in solution.
3) Finally, a third generation of hydrogels focusing on the development of stereo-complexed (e.g., PEG-PLA interaction) hydrogels cross-linked by other physical interactions (e.g., cyclodextrins) (4).

Hydrogels, a network of three dimensional (3D) self-assembled polymer fibrillar chains, are unique semi-solid-like materials containing mainly water (usually >99%) (5). Their capacity to trap high amounts of water is attributed to the presence of hydrophilic functional groups linked to the polymeric chains, such as: -OH, -CONH, -$CONH_2$ and SO_3H, (5,6). Due to their biocompatibility, favourable structural features and high-water content, hydrogels have attracted considerable attention over the years (**Figure 1**) as promising biomaterials for biomedical and biotechnological applications (7). Such applications include tissue engineering, drug delivery systems, cell culture scaffolds, bioimaging, biosensors and wound healing (5–7).

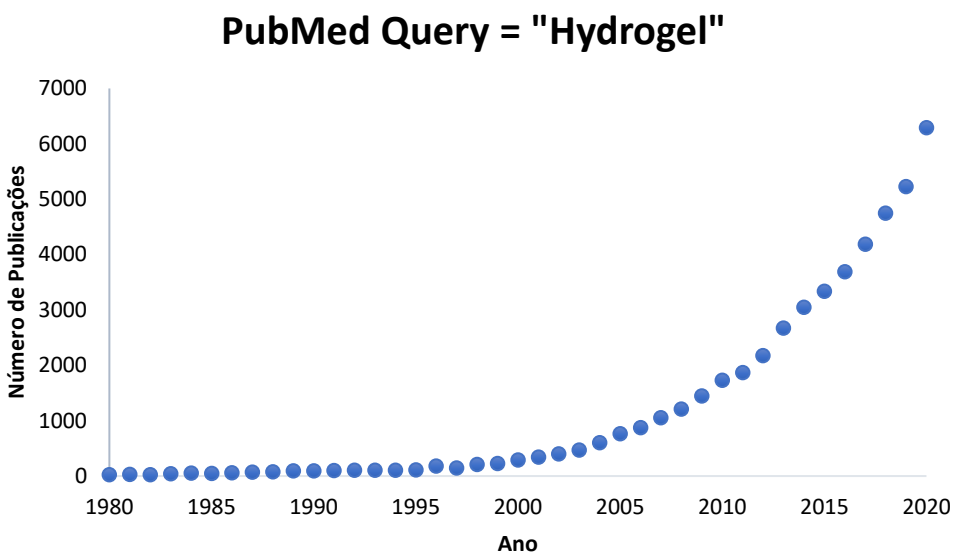

Figure 1: Histogram showing the increase in publications related to the keyword "hydrogel" from 1980 to 2020. A proper exponential fitting is also detectable.

The use of hydrogels in controlled drug delivery has always been one of the most explored applications. Besides the high biocompatibility of these biomaterials, the highly porous structure of the hydrogels allows loading of drugs in the gel matrix and subsequent drug release. This porous structure can be tuned by controlling the density of the cross-links in the gel matrix and the affinity of the hydrogels for the aqueous environment in which they are swollen (8).

1.2 Classifying Hydrogels

Hydrogels can be classified into different categories, depending on the materials involved, the crosslinking, their response to stimuli and their ionic charge (9), as shown in **Figure 2**.

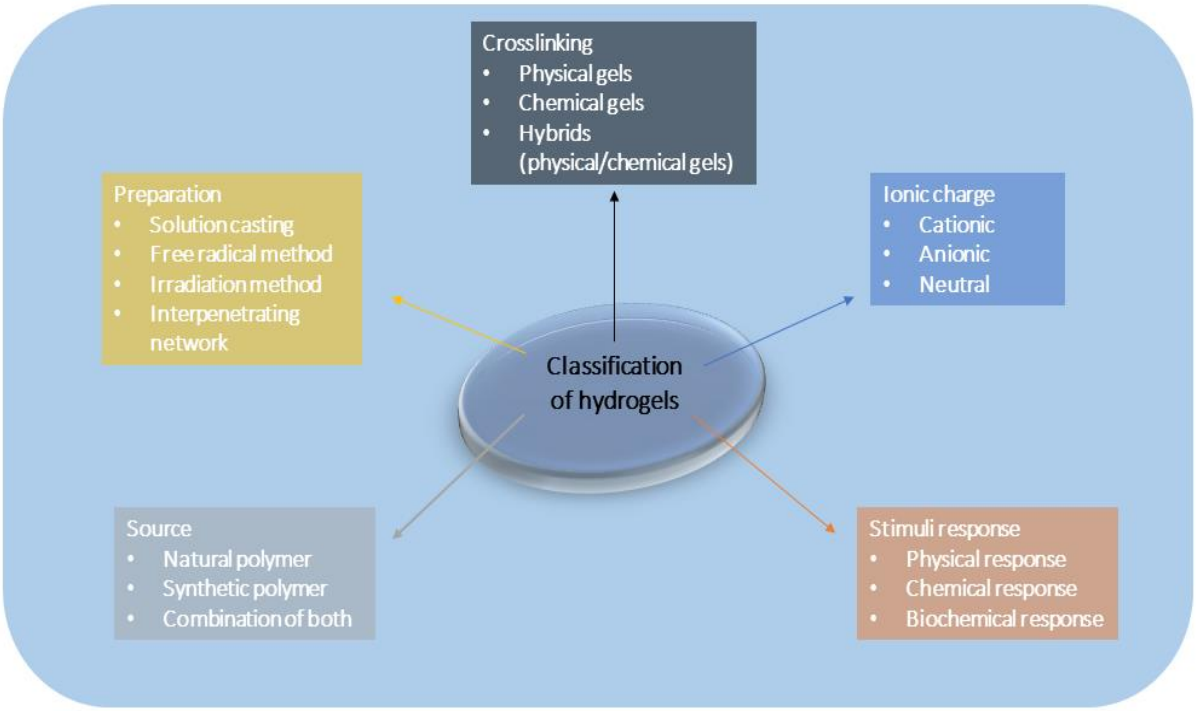

Figure 2: Classification of hydrogels.

The polymers involved in the structure of hydrogels can be natural, synthetic or a combination of both. Further classification into homopolymer hydrogels, copolymer hydrogels, block copolymer hydrogels and terpolymers is possible (9–14). Moreover, hydrogels are prepared by polymer cross-linking, which can be physical or chemical, depending on the nature of the material (15). The network of chemical hydrogels is held together by covalent interactions. This type of interactions produce mechanically resistant and irreversible hydrogels. Chemical hydrogels undergo significant volume changes during the transition from solution to gel state (15). The cross-links can be formed in many ways, such as crosslinking by complementary groups, high energy radiation, free radical polymerization and using enzymes (16,17). On the other hand, physical gels are networks held together by non-covalent interactions such as hydrogen bonds, electrostatic interactions or π-π interactions. These intermolecular interactions can be disrupted by changes in the environment, such as temperature, pH, ionic strength, presence of specific solutes and stress (**Figure 3**). Consequently, the formation of physical hydrogels can be reversible, and the transition to gel is faster when compared with chemical hydrogels (18).

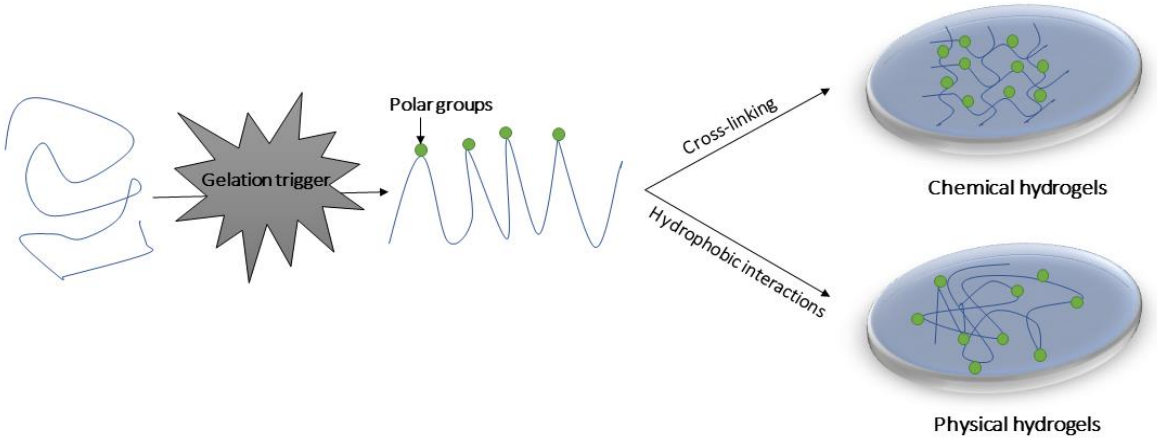

Figure 3: Representation of the types of crosslinking, chemical and physical hydrogels. Adapted from (17).

Finally, hydrogels can also be classified based on the ionic charge, as cationic, anionic, and neutral hydrogels. The charge on the overall network depends on the charge on the polymer (19–22).

1.3 Supramolecular Hydrogels: where less is more

"Simplicity is the ultimate sophistication" - this Leonardo Da Vinci phrase is particularly fitting for supramolecular hydrogels. These gels are a fascinating and useful class of biomaterials, which arise from the self-assembly of small molecules into different hierarchical structures, such as tubes, spheres, films, tapes, and fibers from nano to microscale sizes (5,23). At a sufficiently high concentration, these fibers entangle or otherwise form cross-links, which leads to a network that is able to immobilize the solvent through surface tension and capillary forces (23). These hydrogels differ from permanently covalently cross-linked polymer hydrogels, because the cross-linking can be reversed by the input of energy, - for example, by heating (23). Such hydrogels are often brittle and at times opaque, which greatly limits their application in various biomedical and biotechnological fields (24).

In recent years, special interest has emerged in low molecular weight (LMW) hydrogelators with a molecular mass of <1000 Da, which self-assemble in an aqueous environment to form supramolecular gel matrices (7,23). LMW hydrogelators are expected to exhibit low bioaccumulation, as they are formed using low concentrations of small building blocks which upon degradation can be effectively removed *via* the renal system. Consequently, LMW hydrogelators are very attractive for *in vivo* applications.

LMW hydrogelators self-assemble due to the presence of multiple non-covalent interactions, which allow the monomeric building blocks to self-associate into ordered fibrous structures, which later entangle and interact with each other, to form the 3D hydrogel network (7,25), as shown in **Figure 4**.

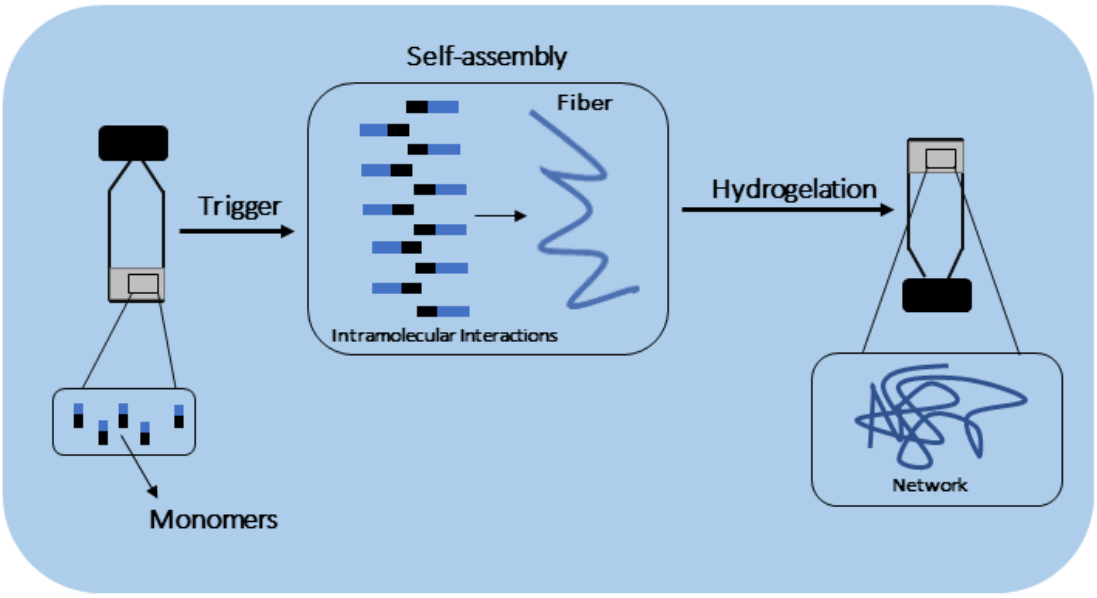

Figure 4 Representation of the hierarchical process that leads to gelation of LMW hydrogelators. Adapted from (25).

Several methods have been described and used to trigger gelation, such as pH change, heating-cooling cycle, enzymatic catalysis, the addition of chelating metal ions and sonification (26).

This self-assembly process to form hydrogels is reminiscent of the self-assembly processes that can be found in many biological systems, either to achieve biological function - such as the formation of biological membranes upon self-assembly of phospholipids, DNA double helix formation through specific hydrogen bounding interactions, protein microtubules and microfilaments as functional units for intracellular interplay – or as part of a pathogenic process, such as the formation of amyloid fibrils relevant to several neurological disorders or diseases (27).

1.4 Low molecular weight supramolecular peptide hydrogelators

The utilization of amino acids and peptides as molecular building blocks of hydrogels provides unique opportunities for generating supramolecular hydrogels, owing to their inherent biological origin, bioactivity, biocompatibility, and biodegradability (28).

Ultrashort peptides (< 8 amino acids) attached to an aromatic capping group are particularly attractive alternatives as minimalistic LMW hydrogelators (5). Hydrophobic stacking interactions, such as π-π stacking due to aromatic-containing residues and bulky protecting groups, have been found to play a crucial role in their self-assembly (5). The most common way to modify a peptide is to cap the *N*-terminus or the *C*-terminus or both (29–31). In some particular cases, ultrashort peptides without an aromatic capping group can also give hydrogels (32). There are many aromatic capping groups described

in the literature, which are used to protect the *N*-terminus of peptides, such as fluorenylmethoxycarbonyl (Fmoc), carboxybenzyl (Cbz), naphthaloyl (Naph) or pyrenyl (Pyr) groups (**Figure 5**) (33).

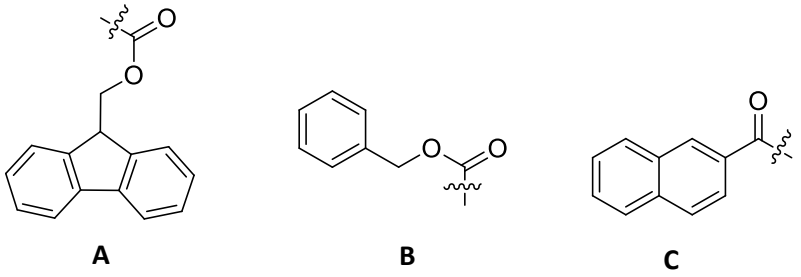

Figure 5: Structure of various *N*-protecting groups: fluorenylmethoxycarbonyl (Fmoc) (A), carboxybenzyl (Cbz) (B), naphthaloyl (Naph) (C).

To generate supramolecular hydrogels, these ultrashort peptides must have a balance of hydrophilic and hydrophobic properties - if a hydrogelator is too hydrophilic, it may stay in aqueous solution; if it is too hydrophobic, then precipitation may occur before the onset of the gelation process (32). Normally, log P values below 2.8 generate unstable hydrogels and log P values above 5.5 indicate that peptides are too hydrophobic and do not produce a homogenous hydrogel. Therefore, to produce a strong and stable hydrogel, the log P value should be between 2.8 and 5.5 (34).

While various peptide hydrogelators have been utilized for biomedical and biotechnological applications, peptides of low critical gelation concentration (CGC) are especially desirable, due to the low quantities of hydrogelator required for obtaining a hydrogel (35). These peptides have the advantage of not only be more cost-effective, but also a higher biocompatibility. In 2005, Muller *et al.*, reported a hexadecapeptide hydrogelator with a CGC value of 0.007 wt% (36). Over the years, efforts have been made with the goal of finding smaller molecules and minimalist building blocks as hydrogelators with optimized CGC values. In 2014 Yang *et al.*, reported an ultrashort peptide hydrogelator which exhibited a CGC value of 0.01 wt% (37). Finally, last year Gazit and co-workers reported a minimalist ultrashort dipeptide-based hydrogelator, Fmoc-Lys(Fmoc)-Asp(OH)-OH, which showed the lowest CGC ever reported, 0.002 wt%, a "hypergelator" (**Figure 6**)(38).

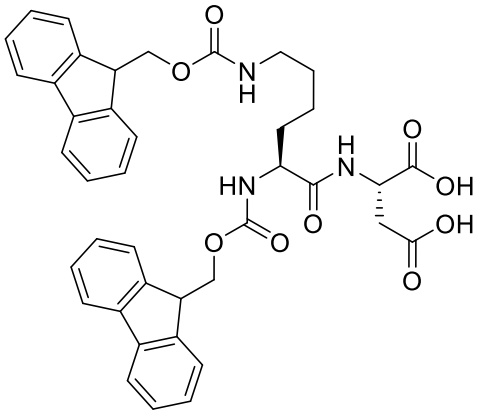

Figure 6: Structure of the hypergelator Fmoc-Lys(Fmoc)-Asp-OH.

Fmoc-protected amino acids or peptides have emerged as excellent building blocks for the development of functional self-assembled structures (39). In fact, the first report on dipeptide hydrogels *N*-protected with a Fmoc group dates back to 1995, when Vegners *et al.*, synthesized a dipeptide, Fmoc-Leu-Asp-OH that gave a hydrogel with a CGC of 0.2 wt% at physiological pH (40). Since then, a lot of work in this area has been carried out on hydrogels based on Fmoc-capped peptides. While most building blocks include only one *N*-terminal protecting Fmoc group, the dipeptide designed by Gazit *et al.* includes an additional Fmoc group, protecting the lysine side chain (**Figure 7**) (38).

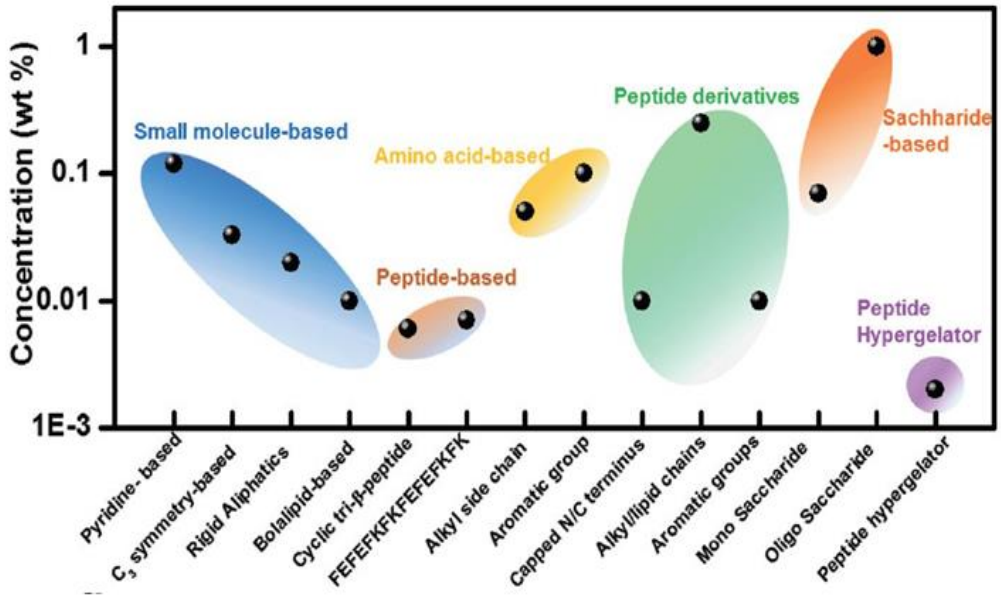

Figure 7: Comparison of the critical gelation concentration of different classes of hydrogelators, including Gazit and co-workers hypergelator (purple) (38).

The modulation of the self-assembly process could potentially be obtained *via* hydrogen bonding of the amino acid or peptide chain, aromatic, and hydrophobic interactions from the fluorenyl ring, and steric optimization from the methoxycarbonyl moiety. The two hydrophilic carboxylic acids of the Asp residue balance the hydrophobicity generated by the extra Fmoc group, maintaining the balance between the hydrophobic and hydrophilic functionalities necessary for the self-assembly process. Although Gazit's hypergelator is very unique and interesting, there are potential limitations arising from the presence of the Fmoc groups. The Fmoc group is susceptible to cleavage at pH values above 10, which can be problematic as Fmoc-containing peptides hydrogelators are often dissolved in basic aqueous solutions prior to gelation. Upon cleavage of the Fmoc group from a peptide chain, a highly reactive dibenzofulvalene is generated. Although the toxicity of dibenzofulvalene has not been determined directly, Thordarson *et al.*, studies indicated that Fmoc-Phe-Phe-OH degradation products show cytotoxicity (41). To avoid this, various capping groups have been studied. Adams and co-workers studied the use of a naphthalene-based capping groups. These capping groups are advantageous because they are not base-labile and boast several sites for additional functionalization (42). In addition, ultrashort peptide hydrogelators *N*-protected with naphthalene can generate very stiff hydrogels (43). Also, other capping groups are being used and studied, such as carboxybenzyl (Cbz) and cinnamoyl groups, which due to their decreased aromaticity, require hydrophobic peptide sequences such as diphenylalanine to give hydrogels (42).

The peptide chain of Gazit and co-workers hypergelator consists of canonical amino acids which are susceptible to proteolytic degradation *in vivo*. This problem can be overcome by incorporating unusual (non-proteinogenic) amino acid residues, such as *D*-amino acids, β-amino acids, *N*-alkylated amino acids, α-amino acids and dehydroamino acids (32).

1.5 Structure of dehydroamino acid residues and dehydropeptides

The key feature of dehydroamino acid residues when compared with the corresponding canonical amino acid residues is the presence of a double bond, usually between the carbon α and β atoms. When the double bond is in this position, they are known as α,β-dehydro-α-amino acids (for simplicity, we shall refer to dehydroamino acids). The presence of the double bond has various effects. Structurally, the planar geometry around the double bond means that the stereogenic center of the corresponding canonical amino acid is no longer present. There is less molecular flexibility, with fixed bond angles around the C-α and C-β carbon atoms. The overlapping p-orbitals ensure that bond rotation around Cα and Cβ is suppressed, and therefore, if R^1 and R^2 are different, then there are two possible geometric isomers, *E*

and *Z* (**Figure 8**).

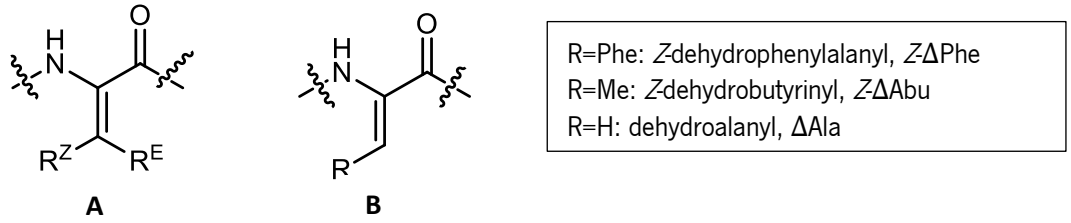

Figure 8: (A)-General structure of dehydroamino acid residue. (B)- *Z*-dehydroamino acid residues relevant to supramolecular hydrogels.

As shown in **Figure 8A**, the *E* isomer features the substituent *cis* to the carbonyl, whereas in the *Z* isomer the substituent is *cis* to the nitrogen atom. In dehydroamino acids, the *Z* isomer is the thermodynamically stable (32). The most important dehydroamino acid residues involved in supramolecular structures are dehydrophenylalanine, dehydroaminobutyric acid, and dehydroalanine (**Figure 8B**) (32).

In our research group, new dehydropeptides capable of generating hydrogels are being developed (26,33,44–48) (**Figure 9**). The presence of the dehydroamino acid residue increases the proteolytic resistance of these hydrogels.

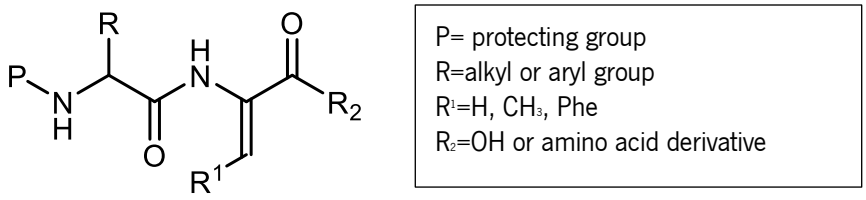

Figure 9: General structure of the dehydropeptides developed in our research group.

1.6 Stimuli for hydrogelation

As previously mentioned, supramolecular hydrogels differ from polymeric hydrogels because they result from molecular self-assembly driven by weak, non-covalent interactions. This difference not only renders more ordered molecular arrangement, but also manifests itself in the process of hydrogelation, as a stimulus or a trigger is necessary to change the thermodynamic equilibrium for starting the self-assembly process. The choice of the gelation method is crucial, and the optimal gelation conditions vary with the structure of the hydrogelator. Changing the hydrogelation method can lead to very different materials, or even result in an effective gelator becoming an ineffective gelator (23). Several triggers have been described and used to start gelation, such as pH change, heating-cooling cycle, enzymatic catalysis,

the addition of chelating metal ions and sonification (26).

1.6.1 pH change

A change in pH is one of the most effective and simplest method to trigger supramolecular hydrogelation, because a small amount of acid or base rapidly leads to a large pH shift *via* a diffusion-limited process. This method is particularly useful for generating supramolecular hydrogels when the gelator contains charged groups.

C-Deprotected peptide-based hydrogelators are the most common that form supramolecular hydrogels on the basis of a pH change (49). A typical procedure consists of adding an aqueous solution of hydrochloric acid (HCl) to a basic solution of the peptide hydrogelator (35). Although this method has proved to be effective, it has a limitation - the decrease in pH which induces hydrogelation occurs faster than the mixing of mineral acids, which can result in heterogenous hydrogels (35) (**Figure 10B**).

Adams and co-workers pioneered the use of glucone-δ-lactone (GdL) to produce homogenous and reproducible hydrogels from LMW hydrogelators (50). GdL is water-soluble and hydrolyses in water to form gluconic acid (**Scheme 1**). With GdL the rate of dissolution is higher than the rate of hydrolysis, resulting in a uniform decrease in pH across the entire sample. Furthermore, this method allows us to target a specific final pH, which gives further insight into the mechanism by which gelation occurs (50).

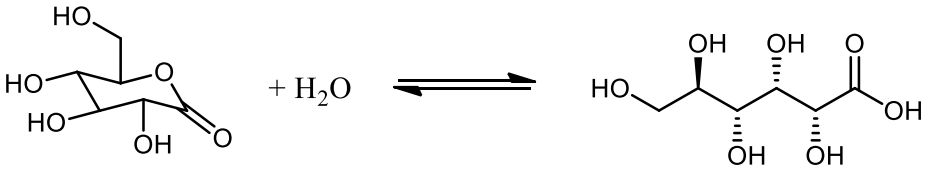

Scheme 1: The hydrolysis of glucone-δ-lactone to gluconic acid in water.

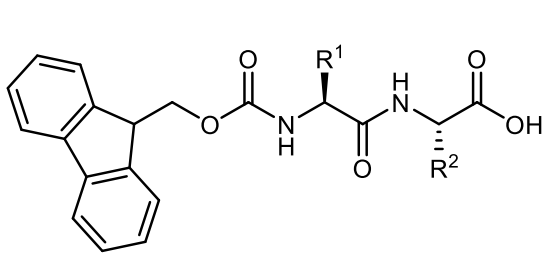

R^1 and R^2 - Amino acid side-chain.

A

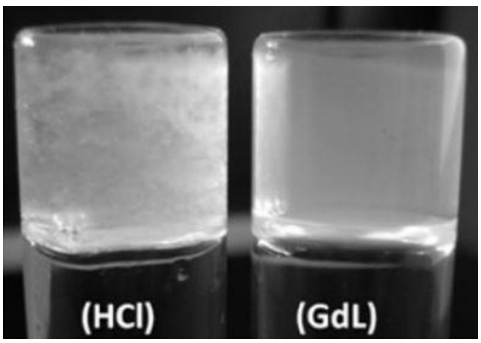

B

Figure 10: A) Structure of a Fmoc-dipeptide hydrogelator. (B) Photographs of hydrogels prepared from Fmoc-Leu-Gly-OH. On the left, the pH was changed with HCl, turbid inhomogeneities can be seen in this hydrogel. On the right, the pH was changed using GdL. Here, a transparent, uniform gel is formed. In both cases the final pH is 3.9 (35).

More recent routes for adjusting the pH to induce hydrogelations have included the use of photoacid generators (PAG) (51). When exposed to UV light, PAG releases protons, and these can be used as triggers in a number of ultrashort peptide systems. Adams *et al.* showed that using a PAG to adjust the pH has the advantage induce gelation in a particular location. This means that such materials could be used in the future to make patterned channels of gels to use in microfluidics and biosensors (51).

1.6.2 Heating/cooling cycles or Ultrasound

A clean and fast way to induce hydrogelation, is through a heating and cooling cycle. Generally, LMW hydrogelators are soluble in water in low concentration at high temperatures. This method consists of heating the solution of the hydrogelator and, upon cooling, a hydrogel is formed. As the temperature decreases, so does the solubility, and due to one-dimensional non-covalent forces, fibrous structures are formed, giving the hydrogel (49). Though this method is commonly used for making supramolecular hydrogels, there is the possibility that precipitation occurs upon cooling before gelation can take place.

Nandi *et al.*, applied various techniques to demonstrate the effects of temperature and elucidated the activation barriers for the assembly of riboflavin-melamine hydrogels, the formation of which is induced by cooling a homogenous solution of the mixture from 80 °C or 120 °C to 30°C (49). This method has been reported many times as a trigger for hydrogelation of ultrashort peptide hydrogelators. Vegners *et al.*, reported the hydrogelation of Fmoc-Leu-Asp-OH, Fmoc-Ala-Asp-OH and Fmoc-Ile-Asp-OH induced by a heating/cooling cycle (40).

Besides heating, ultrasound is commonly used in chemical laboratories or in industry as a stimulus to speed dissolution, dispersion, or to clean up the surface by breaking weak intramolecular forces. In fact, it is quite common to use ultrasound to assist the formation of supramolecular hydrogels, but the systematic study of ultrasound to control the properties of soft materials is a rather recent event (49). Essentially, the force of ultrasound readily rearranges the aggregation of molecules by cleaving self-locked structures through intramolecular interactions, usually involving the precipitation of water molecules.

1.6.3 Enzymatic catalysis

Another method to induce hydrogelation is to use an enzyme to trigger the self-assembly of a hydrogelator, resulting in the formation of supramolecular hydrogels (52). Enzymatic reactions are a well-known dynamic feature in nature. Taking advantage of this, Ulijin et al. reported the use of a thermolysin to catalyze reverse hydrolysis to create oligopeptides for hydrogelation (53). Later, Bing Xu's group designed ultrashort peptide hydrogelators which consisted of two β-amino acids and one α-amino acid residue to evaluate if enzymatic hydrogelation takes place both *in vitro* and *in vivo* (52). Since then, a lot of work has been carried in this area, with new hydrogelator designs that forms supramolecular hydrogels triggered by enzymatic catalysis.

There are two different approaches when operating with enzymes – creating or breaking a bond. Both ways can turn a precursor into a hydrogelator, which later can self-assemble and generate the supramolecular hydrogel. For example, attaching a tyrosine with a phosphate group to the *C*-terminal end of the hydrogelator can be used as a substrate for phosphatases and to give hydrogels (54) (**Scheme 2**). The phosphatase dephosphorylates the tyrosine residue thus reducing the water solubility of the overall compound. Consequently, the hydrophilicity of the conjugate is reduced, resulting in self-assembly (54). Furthermore, the concentration of enzyme used in the process influences the mechanical properties of the hydrogels, which is advantageous because the kinetics of gel formation can be controlled by the concentration of enzyme used. Generally, higher concentrations of enzyme result in gels with higher elastic moduli. On the other hand, low concentrations of enzyme generate thinner fibers which result in weaker hydrogels (54).

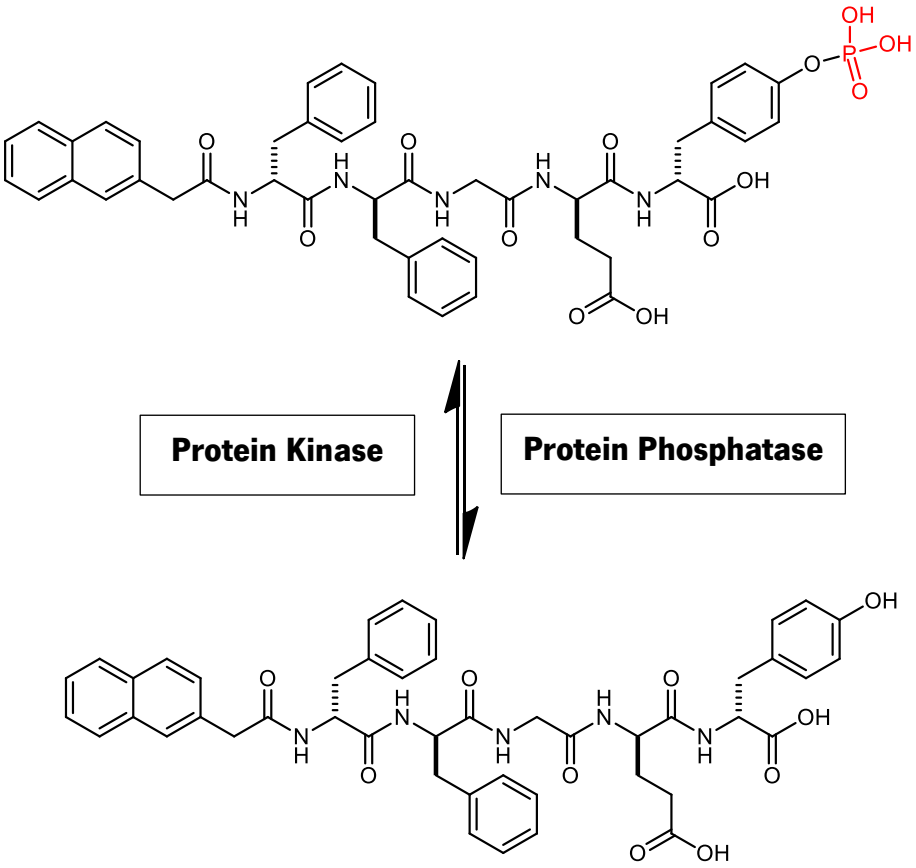

Scheme 2: Enzymatic *in situ* generation of a hydrogelator by dephosphorylation of a tyrosine phosphate (54).

1.6.4 Addition of chelating metal ions

The use of different anions and cations as triggers to induce hydrogelation has been reported as an efficient strategy. Metal triggered hydrogelation has been demonstrated for various peptide-based materials, with a particularly elegant example using Zn^{2+} ions to induce a structural change in a β-hairpin peptide, resulting in hydrogelation (55).

Schneider *et al.*, demonstrated that a twenty-residue peptide is capable of undergoing hydrogelation in response to heavy metal ion binding (56). The unstructured peptide binds monomethylarsonous acid, Pb^{2+}, Zn^{2+}, Cd^{2+} or Hg^{2+} and subsequently folds into an amphiphilic β-hairpin that rapidly self-assembles into a β-sheet rich fibrillar network (56) (**Figure 11**).

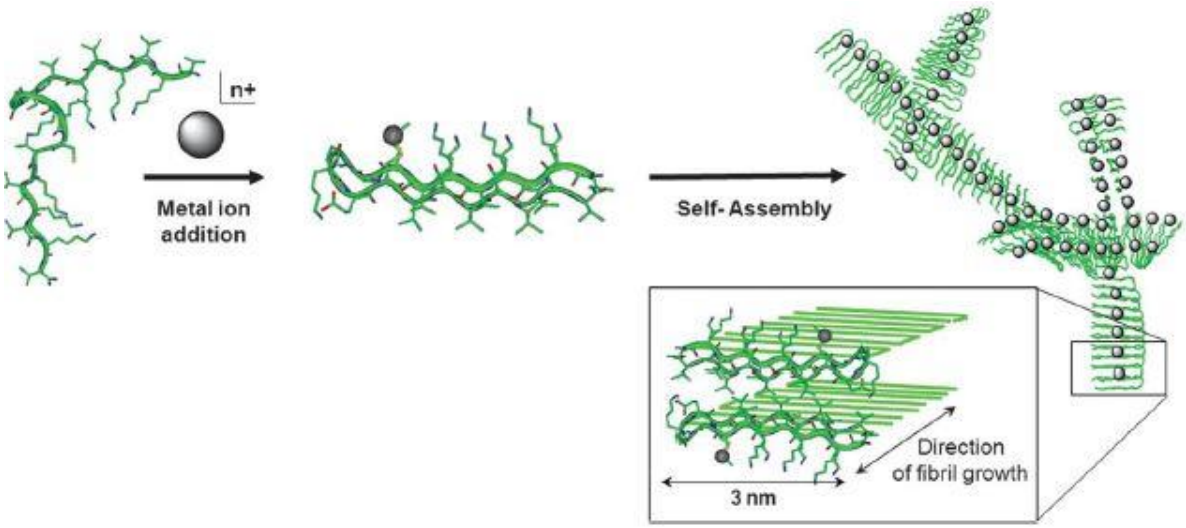

Figure 11: Proposed mechanism of metal ion triggered folding and self-assembly of the twenty-residue peptide (56).

Adams *et al.*, showed that the addition of cations to a series of ultrashort peptide hydrogelators with high pH values resulted in hydrogelation (57). Also, when the solution contained long and worm like micelles, the addition of cations generated crosslinks between the micelles, which led to hydrogelation (57).

1.7 Characterization of supramolecular hydrogels

The continuous search for new and optimized hydrogelators and the requirement of more information on supramolecular hydrogels at both the macroscopic and molecular levels, require more accurate analysis and characterization of the hydrogels. The macroscopic properties of hydrogels can be studied using techniques such as rheology; while spectroscopy, microscopy or diffraction allow the study of hydrogels at the molecular level.

Given the highly complex nature of supramolecular hydrogels, complementary techniques should be used to characterize their properties. Herein, some of the most commonly used techniques to characterize hydrogels will be presented and discussed.

1.7.1 Rheology and differential scanning calorimetry (DSC)

Rheology studies the flow of supramolecular hydrogels and can provide tertiary information about the type, number, and strength of networks responsible for the observed hydrogelation (49).

The basic principle of rheology is the application of a stress to a material and study its deformation and flow (58). When a stress is continuously applied to a material, there are two possible opposite outcomes: either the material deforms slightly but resists, or the material flows continuously, being either a solid or a liquid, respectively. However, there are materials that exhibit both behaviors depending on the time scale of the deformation process. Because of this, it is easier to classify materials in terms of their rheological behavior, as elastic or viscous (58). If the amount of deformation of the material is proportional to the applied stress, it is said to be elastic. On the other hand, if the deformation rate is proportional to the applied stress, the material is considered to be viscous (58).

Oscillatory rheometry, as a comprehensive technique to characterize viscoelastic materials, is becoming a routine measurement of supramolecular hydrogels (49). Oscillatory rheometry measures the response of supramolecular hydrogels to an applied oscillatory stress, which is quantified by the elastic properties, such as G* (complex modulus), G´ (storage or elastic modulus), and G´´ (loss modulus or viscosity) (49,58). To determine the formation of supramolecular hydrogels, two rheological experiments are usually performed: a frequency variation, where the linear response of the module (G' and G'') is measured within a fixed voltage range, and a variation of the shear stress, where the non-linear behaviour of the module is analysed at a fixed frequency (58).

For supramolecular hydrogels, as they are a more solid-like system, the contribution of the elastic behaviour is higher than the viscous behaviour (G´>G´´), which means that the gelation point can be determined when G´ becomes greater than G´´.

The temperature of hydrogelation (T_{gel}) is also one of the most studied characteristics of a hydrogel. T_{gel} is determined by the point that non-covalent crosslinks or global molecular arrangements are broken by thermal energy (49). Using differential scanning calorimetry (DSC), T_{gel} can be determined, especially when there is a sharp phase transition associated with hydrogelation. Both the rheological and thermodynamic properties are important to better understand the mechanical and physical properties of supramolecular hydrogels.

1.7.2 Circular dichroism (CD) spectroscopy

Circular dichroism (CD) is one of the most used techniques to study the stereo structures and intra/intermolecular interactions of various classes of chiral supramolecular systems. CD refers to the differential absorption of left and right circularly polarized light. This technique has several advantages, as it is very sensitive, destruction free, and usually requires very low quantities of sample, typically in the sub microgram-scale (58–60).

When an achiral sample is exposed to both right- and left-handed circularly polarised light, it can absorb both polarisations of light equally, resulting in a "zero" spectrum. Contrarily, a chiral molecule absorbs the two polarisations differently, hence giving rise to a spectrum, either positive or negative (58).

LMW supramolecular hydrogelators are molecules that usually contain chiral centres. The chiral information at the molecular scale can be translated into gel-phase assemblies, making CD spectroscopy an efficient way to provide insight into the assembly of the hydrogelator molecules into a well-defined secondary structure (58). Illustrative examples of CD spectra characteristic of the presence of β-sheets, α-helices, and random coil secondary structures for the poly-L-lysine and for the placental collagen protein are shown in **Figure 12** (60).

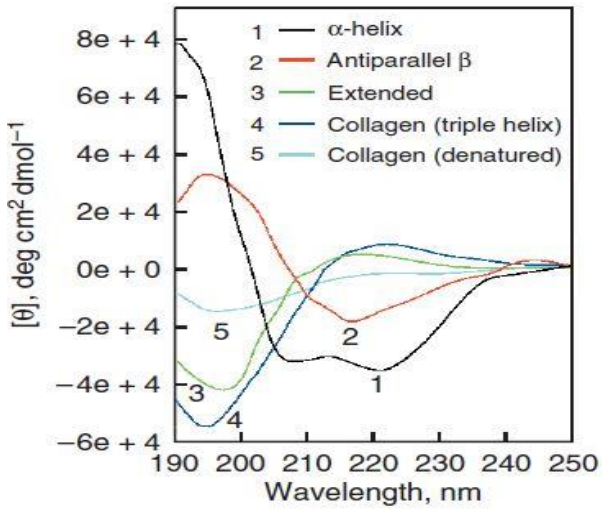

Figure 12: CD spectrum of poly-L-lysine: (1) α-helical conformation; (2) anti-parallel β-sheet conformation at pH 11.1, (3) extended conformation at pH 5.7 and placental collagen; (4) native triple-helical and (5) denatured forms (60).

CD is an excellent method of determining the secondary structure of proteins (60). When the chromophores of the amides of the polypeptide backbone of proteins are aligned in arrays, their optical transitions are shifted into multiple transitions as a result of "exciton" interactions (60). The result is that different structural elements have characteristic CD spectra. For example, α-helical proteins have negative bands at 222nm and 208 nm and a positive band at 193 nm. Proteins with well-defined antiparallel β-helices have negative bands at 218 nm and positive bands at 195 nm, while disordered proteins have very low ellipticity above 210 nm and negative bands at 195 nm (60).

With LMW supramolecular hydrogelators protected with aromatic capping groups, such as naphthalene or carboxybenzyl, the CD spectra is a bit trickier as there are various factors which can influence the spectra, such as: the rigidity of the protein, the hydrogen bonding, and the interactions between the aromatic amino acids (61).

1.7.3 Fluorescence spectroscopy

Fluorescence spectroscopy is widely used in biochemical, medical, and chemical research fields for analysing organic compounds (58). The basic principle of fluorescence is the use of a beam of light, usually ultraviolet (UV) light, to excite the electrons and causes them to emit light, typically, visible light.

In fluorescence spectroscopy, the species is first excited by absorbing a photon, going from its ground state to one of the various vibrational states in the excited electronic state. Collisions with other molecules make the excited molecule lose vibrational energy until it reaches the lowest vibrational state of the excited singlet electronic state. After this, the molecules drop down to one of the vibrational levels in the ground electronic state again, followed by the emission of a photon. As molecules drop onto any of the vibrational levels in the ground state, the emitted photons will have different frequencies (58).

In the literature, various ultrashort peptides have been studied by fluorescence. The existence of hydrophobic pockets and π-π interactions within the supramolecular hydrogel are verifiable by fluorescence. The technique can also be used to study the orientation of aromatic moieties in the solution and the gel states (26,49,61).

1.7.4 Scanning transmission electron microscopy (STEM)

Electron microscopy techniques, such as STEM, use a beam of accelerated electrons as a source of illumination. Since the wavelength of an electron is rather short, electron microscopy has the capacity to reveal the structures of small objects with high resolutions, going up to a nanometer (49). STEM

provides valuable information about the morphology of the molecular aggregates/nanofibrils leading to hydrogelation. This technique has the advantage of being fast and efficient since griding, polishing or ion milling are not required.

1.7.5 Molecular modelling

Considering the molecular data collected from techniques such as microscopy and rheology, nowadays it is possible to use molecular modelling for proposing a plausible arrangement of the molecular organization in supramolecular hydrogels (49). Investigators have developed some relevant model systems from computer simulations on the hydrogelation process in organic solvents. However, there are currently not many reliable modelling approaches for describing the self-assembly of small molecules in water because of the inherent kinetic nature of hydrogels and the lack of an accurate description of hydrophobic interactions, which as previously mentioned, are the driving forces for small molecules self-assemble in water to generate supramolecular hydrogels (49).

1.8 Applications of LMW supramolecular hydrogels

As previously mentioned, due to their intrinsic biocompatibility, favourable structural features and high-water content, peptide-based hydrogels have attracted considerable attention over the years, as promising biomaterials for biomedical and biotechnological applications (7). In this section, the most important applications for peptide-based hydrogels will be discussed, with an emphasis on drug delivery systems, as they one of the most promising fields for hydrogel applications, and a dominant theme in this thesis.

1.8.1 Drug delivery systems

The unique physical properties of peptide-based hydrogels have attracted a particular interest in drug delivery applications. Conventional drug administration usually requires high dosages or repeated administration to stimulate a therapeutic effect, which can cause low overall efficacy and patient compliance, resulting in severe side effects and/or toxicity (8,62,63). The most common approach for delivering pharmaceuticals is by oral administration, which is frequently limited by poor targeting and short circulation times (<12 hours) (64). To address these issues, studies on using hydrogels as drug delivery systems are gaining attention because they can offer spatial and temporal control of drug availability to cells and tissues and leverage beneficial outcomes of therapeutics by enhancing their

efficacy and by reducing their toxicity and required dosage. The highly porous structure of these hydrogels permits loading of drugs into the gel matrix and subsequent drug release at a rate dependent on the diffusion coefficient of the small molecule or macromolecule through the gel network. This porous structure can be tuned by controlling the density of the cross-links in the gel matrix and the affinity of the hydrogels for the aqueous environment in which they are swollen.

The use of hydrogels for drug delivery brings many advantages. From a pharmacokinetic perspective, a depot formulation can be created, from which drugs slowly elute, maintaining a high local concentration of drug in the surrounding tissues over an extended period of time (8). In addition, hydrogels are very biocompatible, owing to their high-water content and their physiochemical similarity to the native extracellular matrix (ECM), both compositionally and mechanically. Hydrogels can be designed to be biodegraded *via* enzymatic and hydrolytic pathways or by pH, temperature, or electric fields. Also, hydrogels are readily deformed, which means that they can adapt to the shape of the surface to which they are applied. These bio-adhesive properties of hydrogels can be advantageous when the gels are applied to irregularly shaped surfaces. For example, the intestinal epithelium and mucosa are biological barriers that are usually wet, dynamic, and slippery, which can constitute a problem for good adhesion. It is reported in literature that hydrogels containing 3,4-dihydroxy-L-phenylalanine (L-DOPA) have shown to adhere on epididymal fat pad and external liver surfaces for up to 1 year, promoting bio-adhesion (65–67).

Despite these advantages of hydrogels for drug delivery applications, there are still some limitations to consider. The low tensile strength of many hydrogels limits their use in load-bearing applications and can result in the premature dissolution, or flow away, of the hydrogel from a targeted local site. Also, the quantity and homogeneity of drug loading into hydrogels may be limited, particularly in the case of hydrophobic drugs. The high-water content and large pore sizes of some hydrogels can result in fast drug release, over a few hours to a few days. These limitations restrict the use of hydrogel-based drug delivery therapies in clinics.

One particularly interesting example of using ultrashort peptides as drug delivery systems was reported by Xu *et al.*, in which dipeptides conjugated with various non-steroidal-inflammatory drugs (NSAID), such as naproxen, flurbiprofen, ibuprofen and aspirin, were used to obtain multifunctional supramolecular hydrogelators (68). They showed that conjugating diphenylalanine with naproxen generate hydrogelators imparted with anti-inflammatory properties with a more favorable COX-2/COX-1 inhibition selectivity than naproxen alone (68). Our research group also reported that conjugating dehydrodipeptides with naproxen provides improved anti-inflammatory properties as well (46,69).

Hydrogel delivery systems can be categorized into three groups based on their size: macroscopic hydrogels, microgels and nanogels. Since hydrogels can be applied or formed into almost any shape and/or form, the size of the hydrogel is important. It is the macroscopic design of the hydrogel that determinates the delivery route.

1.8.1.1 Macroscopic hydrogels

Macroscopic hydrogels are usually either implanted surgically into the body or placed in contact with the body for transepithelial drug delivery (70), as their size is typically on the order of millimeters to centimeters. These macroscopic hydrogels can be divided into three categories according to their delivery routes: *In situ*-gelling gels, macroporous gels and shear-thinning gels.

1.8.1.1.1 *In situ*-gelling hydrogels

These hydrogels can be injected in liquid form and undergo a sol-gel transition inside the body. The resulting hydrogels take the shape of the space in which the gel was injected in. The sol-gel transition can be achieved through different methods. Slow-gelling systems are one way to achieve this gelation process. In this method, the gelation process is initiated outside of the body, but as it occurs slowly, the solution can be injected before solidification occurs. This method has been applied with various gelation mechanisms, such as charge interaction (71), stereocomplexation (72), and Michael addition (73). Another strategy being explored, is the development of thermosensitive hydrogels. Injectable thermosensitive hydrogels are promising biomaterials that have a low critical solution temperature (LCST) above which they undergo transition from sol phase to gel phase. Their characteristics allow therapeutic agents to be easily encapsulated into the solution and to be injected in solution state, followed by forming a hydrogel *in situ* at physiological temperature (74).

Recently, Wei and Tang *et al.*, studied the antitumor effects of Emodin (EM) loaded peptide-hydrogels *in situ* (75). These hydrogels are in an injectable solution before administration, and semi-solid or solid hydrogels form *in situ* at the site of drug administration through phase transition, stimulated by external conditions, such as light, temperature or pH. In this particular case, the RADA16-I peptide was used as gelator. RADA16-I is an ionic complementary self-assembling peptide and the gelation process was triggered by pH. In this work, the results showed that the RADA16-I-EM *in situ* hydrogels significantly reduced the tumor growth rate and reduced the toxic side effects of EM on normal organs *in vivo* compared with the free EM in subcutaneously implanted murine Hepa1-6 liver tumor models. This is primarily attributed to the RADA16-I-EM hydrogels, as they effectively deliver EM into the tumor tissue

(75). This work highlights *in situ* gelling hydrogels for drug administration and localized sustained drug delivery and demonstrates their potential in further biomedical applications.

1.8.1.1.2 Shear-thinning hydrogels

Some hydrogels can be pre-gelled outside of the body and then injected by application of shear stress. These hydrogels flow like a low-viscosity fluid under shear stress during injection, but quickly self-heal after the removal of the shear stress, regaining their initial stiffness. This behavior results from the reversible properties of the physical crosslinks. Physical crosslinks are reversible due to the dynamic competition between pro-assembly forces, such as hydrophobic interactions, electrostatic interactions and hydrogen bonding, and anti-assembly forces, like solvation and electrostatic repulsion (76). The MAX1 family has been developed through the years to make injectable hydrogels for drug delivery (76,77). The MAX peptides are a family of self-assembling β-hairpin peptides usually used as injectable therapeutic delivery systems (76). Miller *et al.* have recently reported a series of novel β-hairpin peptides that bind to Zn^{2+} ions and produce fibrillar structures. They designed nine novel peptides, all based on the MAX1 peptide. Mutations of the Lys and Val residues at different positions along the sequence of MAX1 to His and Cys residues were implemented to create potential binding sites to Zn^{2+} ions. The locations and the number of Cys and His in the Zn^{+2} binding site affected the molecular mechanism of the self-assembly of the peptide and consequently its structural characteristics (77). In cases where there were four His residues and of three His residues in the Zn^{+2} binding site, the nanofibers where more rigid and less twisted. Contrarily, in cases of two, three or four Cys residues in the Zn^{+2} binding site, the nanofibers were more twisted, flexible, and brittle (77).

Although the MAX1 peptide family is very well known for its shear-thinning properties, there are still other supramolecular peptide-based hydrogels that have being investigated for their shear-thinning/self-healing properties. Recently, Bai *et al.* designed a series of aromatic dipeptides that form shear-thinning hydrogels with self-healing and tunable mechanical properties (78). They reported the design and synthesis of Fmoc-conjugated Phe-Phe, Tyr-Leu, Leu-Leu and Tyr-Ala. The results showed that the synergic effect of hydrophobic interactions and hydrogen-bonding interactions is a crucial factor that affect mechanical strength and self-healing properties of hydrogels. By increasing the hydrophobic interactions among molecules, the mechanical stiffness is enhanced, and by increasing the hydrogen-bonding interactions, the self-healing process is enhanced (78).

1.8.1.1.3 Macroporous hydrogels

Another approach to make injectable hydrogels, is to create large hydrogels with interconnected pores that can mechanically collapse and recover reversibly. When the gel is delivered via injection with a needle, water is squeezed out from the pores, and the gel collapses, allowing it to pass through the needle. Once the gel is outside the needle and the mechanical constraint imposed by the needle walls is removed, the hydrogel recovers its initial shape almost immediately in the body. These hydrogels behave like a foam and can be reversibly compressed at up to 90% strain without any permanent damage to the gel network (79). Through the years, many different methods have been described to fabricate these kinds of hydrogels, such as gas foaming (80), microemulsion (81), freeze drying (82), and cryogelation (83). One example is the work reported by Kirsebom *et al.*, in which they describe the formation of macroporous self-assembled hydrogels through cryogelation of Fmoc-Phe-Phe-OH (83).

1.8.1.2 Microgels and nanogels

Using small hydrogel particles can be an alternative strategy for minimally invasive drug delivery. When compared to their macroscopic analogues, microgels and nanogels have some advantages. Because of their small size, they are needle-injectable, and they provide a large surface area for bioconjugation, which leads to easy natural clearance and penetration enhancement through tissues barriers (56).

Recently, microgels and nanogels, formed by self-assembly of short peptides, have emerged as promising biomaterials and exhibited enormous potential in biomedical fields, such as controlled drug release. An example is given by Xing *et al.*, as they reported on stimulus-responsive short peptide nanogels for controlled intracellular drug release (84). They presented an environmental responsive nanogel system that self-assembles with DOX and P-glycoprotein inhibitor, which exhibits acid-sensitive properties for controlling drug release and simultaneously inhibiting the efflux function of P-glycoprotein. This system effectively reverses multi-drug resistance for improved tumor treatment. The results showed that this system provided a useful strategy to overcome cancer drug resistance (84).

1.8.2 Tissue engineering

Tissue engineering is a research field that aims to replace/repair tissue or even organs that have been damaged because of disease, injury, or trauma. There are three main components: cells, scaffolds and signaling biomolecules (or growth factors) which are generally referred to as the tissue engineering

triad (85). Scaffolds play a vital role in providing the beneficial microenvironment for regenerative cell survival, proliferation, and differentiation, as well as carrying signaling biomolecules for mediating cellular response. Therefore, a 3D porous biomimetic scaffold that can mimic the natural ECM is critical. As previously mentioned, due to the intrinsic properties of peptide-based hydrogels, they are being investigated as scaffolds in regenerative medicine (86).

In 2010, Chauhan *et al.*, reported on a 3D cell growth and proliferation of mammalian cells on an easy to functionalize and biocompatible dipeptide hydrogel (87). Also, Nilsson *et al.*, reported on multicomponent dipeptide hydrogels as ECM scaffolds for cell culture applications (86). The group designed two dipeptide hydrogelators, Fmoc-3F-Phe-Arg-NH_2 and Fmoc-3F-Phe-Asp-OH (**Figure 13**), which have the requisite mechanical and biochemical properties to support the viability and growth of NIH 3T3 fibroblast cells (86). The studies show that noncovalent supramolecular display of Arg and Asp provides materials that can effectively mimic the cell adhesive functions of the fibronectin RGD peptide, without covalent connection between the Arg and Asp amino acids (86). Multicomponent co-assembled hydrogel materials that elicit RGD-like responses in cell culture applications expands the possibilities in the design of novel materials for tissue engineering.

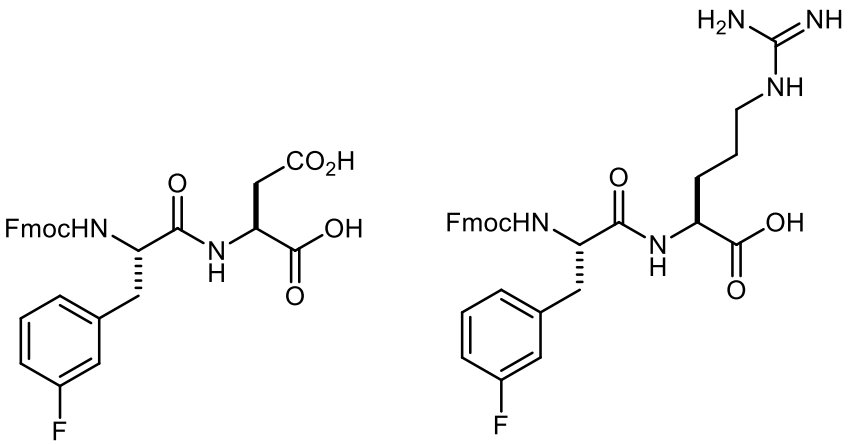

Figure 13: Structures of Fmoc-3F-Phe-Asp-OH (A) and Fmoc-3F-Phe-Arg-NH_2 (B).

1.8.3 Biosensors

Bioimaging enables multi-dimensional and multi-scale visualization of biological structures and events in a non-invasive and real-time manner, providing insights on biological processes, signaling networks, and pharmaceuticals effects, thus holding significance in both biology research and diagnostic applications (88). Owing to their superior loading capacity and biocompatibility, imaging agent-conjugated (or encapsulated) peptide-based hydrogels are capable of imaging *in vivo* biological events with enhanced signals. Notably, by rational design of the hydrogelators, the gelation process can occur on the region of interest, rendering precise and sensitive bioimaging of the disease *in vivo* (88).

Yang *et al.*, used a self-assembled hydrogel of the Fmoc-Phe-Phe-OH dipeptide to build a smart bio-interface, which was used for enzyme-based electrochemical biosensing and cell monitoring purposes (89). Similarly, Park *et al.*, used Fmoc-Phe-Phe-OH dipeptide hydrogel encapsulating enzyme bioreceptors and fluorescent reporters to make enzyme-based optical biosensors (90). Finally, Alves *et al.*, also used the Fmoc-Phe-Phe-OH dipeptide hydrogel containing an antigen, for the detention of Leishmaniasis disease in patient samples (91).

1.9 Supramolecular hydrogels based on non-natural amino acids with ultralow CGC

As previously stated, peptides with low CGC are especially desirable due to the low weight percentage required to obtain a hydrogel, which makes them more cost-effective and more biocompatible in cases where the monomeric hydrogelator is cytotoxic (**Figures 14-16**).

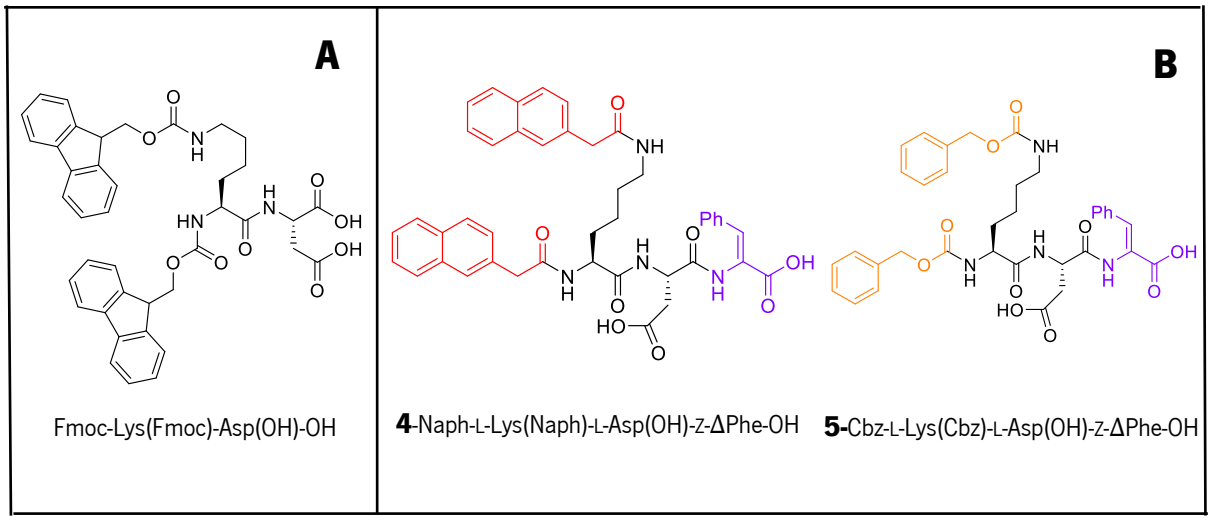

Figure 14: (A) Structure of the hypergelator developed and studied by Gazit and co-workers. (B) Structure of the dehydrotripeptides hypergelators synthetized and studied for their hydrogelation ability.

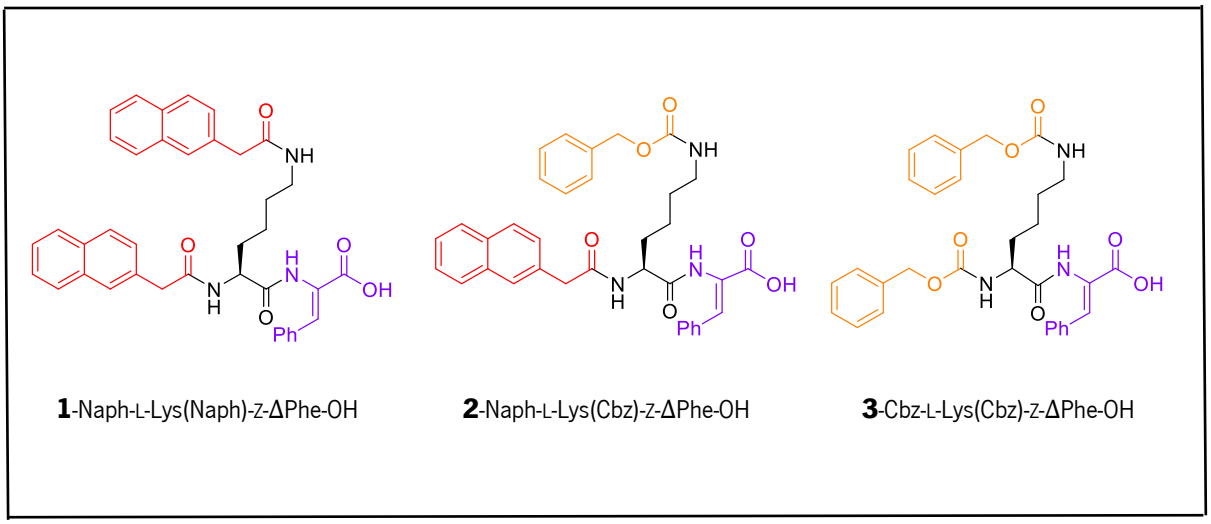

Figure 15: Structure of the dehydrodipeptides hypergelators synthetized and studied for their hydrogelation ability.

With the aim of developing novel hypergelators, we targeted two sets of new peptides based on non-natural amino acids:

1. Inspired by the dipeptide developed by Gazit research group, which is the gelator with the lowest CGC (0.002 wt%) ever reported (38), a first set of five novel hydrogelators was designed (**Figure 14, 15**). The rationale behind the design of these peptide hydrogelators was to maintain the ultra-low values of CGC presented by Gazit`s molecule, and at the same time optimize some of its deficiencies. As mentioned previously, the Fmoc group is susceptible to cleavage at pH values above 10, which can be problematic. For example, when gelation is triggered by a pH change, peptides gelators are initially dissolved in basic aqueous solutions prior triggering hydrogelation, which will degrade the gelator. In addition, upon cleavage of the Fmoc group from the peptide chain, a highly reactive dibenzofulvalene is generated. Although the toxicity of dibenzofulvalene derived from Fmoc-based peptides has not been determined directly, a study performed by Thordarson *et al.* indicated that the degradation products of Fmoc-Phe-Phe-OH show significant cytotoxicity (41). In addition, the peptide chain of Gazit's hydrogelator consists of canonical amino acids, which are susceptible to proteolytic degradation by enzymes *in vivo*. Taking all of this information into account, we aimed to switch the Fmoc aromatic capping group for the more biocompatible carboxybenzyl (Cbz) and/or naphthylacetyl (Naph) capping groups, as they are stable at both high and low pHs and are reported to produce stiff hydrogels (43). For the peptide chain of the new hydrogelators, we considered two main groups: three dipeptides (compounds **1**, **2** and **3**),

which maintain the lysine amino acid, but the aspartic acid is switched by a dehydrophenylalanine and two tripeptides (compounds **4** and **5**), which maintain the lysine and aspartic acid core, but also feature a dehydrophenylalanine residue added to the peptide chain. The presence of a dehydroamino acid residue is known to increase the enzymatic stability of the hydrogelator for *in vivo* applications, as it increases the proteolytic resistance of the hydrogel (32). Dehydrophenylalanine residues are also known to enable the gelation process through the restriction of conformational freedom. Dehydropeptide gelators have been successfully employed by the research group on many occasions (26,33,44–48).

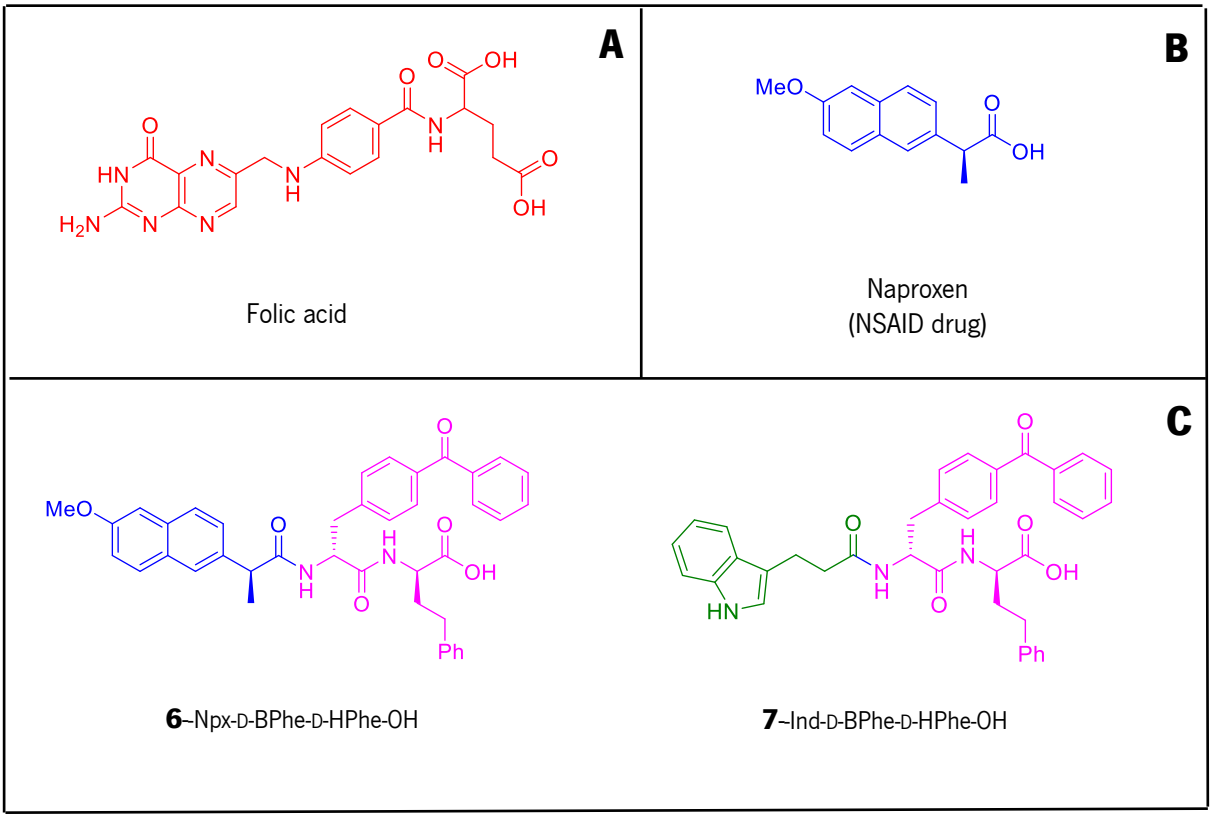

Figure 16: (A) Structure of Folic acid. (B) Structure of Naproxen. (C) Structure of the hypergelators synthetized and studied for their hydrogelation ability.

2. A second set of unique peptides (**6** and **7**) was targeted, with the aim of studying their hydrogelation properties (**Figure 16**). In a recent study by Huang *et al.*, five compounds were identified as ligands of the folate receptor from a screen of a DNA-encoded chemical library of over 30 million compounds (92). Two of the identified folate receptor ligands contained *N*-capped dipeptide structures similar to those of known supramolecular hydrogelators (compounds **6** and **7**), and one of these two compounds contained a similar

structure to known anti-inflammatory compounds (compound **6**). These peptides contain the basic structure of peptide hydrogelators – a dipeptide consisting of aromatic amino acid residues, containing an aromatic capping group at the *N*-terminus. A folate receptor ligand as a hydrogelator is an interesting concept, as it potentially provides an opportunity to selectively target drug delivery to cancer cells, as these over-express folate receptors (92). D-4-benzoylphenylalanine and D-homophenyl alanine are unusual amino acids - unnatural in both basic structure and enantiomeric configuration – and should provide enzymatic resistance. Their aromatic sidechains should make these compounds ideal peptide hydrogelators. Furthermore, the capping group of compound **6** is naproxen (**Figure 16B**), a non-steroidal anti-inflammatory drug (NSAID). Naproxen has been successfully incorporated into the structures of hydrogelators previously, often resulting in retained or improved anti-inflammatory activity (26). The capping group of compound **7** is an indole 3-propionic acid, which is a known antibiotic. Overall, the structures of **6** and **7** seem attractive structures for studying hydrogelation.

Chapter 2

Results and discussion

2 Results and discussion

2.1 Dehydrodipeptides with lysine *N*-capped with aromatic moieties

Three dehydrodipeptides (**1**-**3**) (**Figure 17**) containing a lysine residue *N*-capped with aromatic moieties and a dehydrophenylalanine residue were prepared and tested as hypergelators.

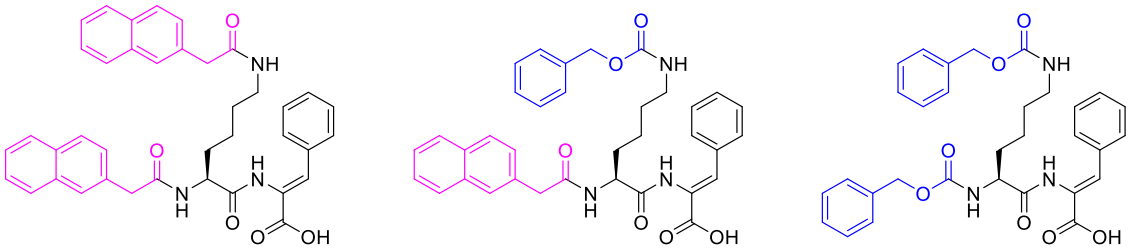

Figure 17: Structures of the lysine dehydrodipeptides *N*-protected with aromatic groups **1-3**.

2.1.1 Synthesis of dehydrodipeptides 1-3

The dehydrodipeptides **1-3** were synthesized using a conventional stepwise protocol (**Scheme 3**) (93).

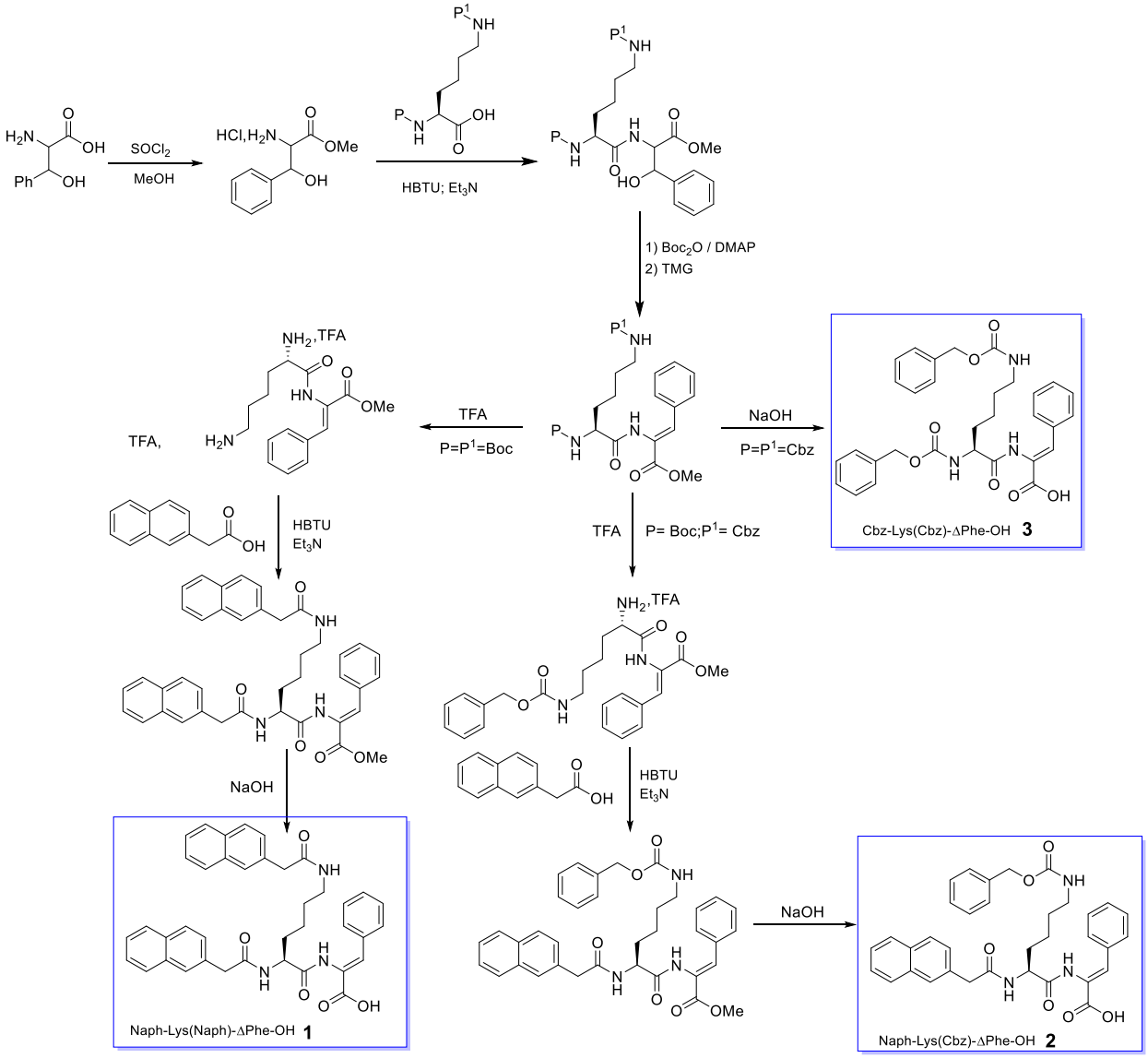

Scheme 3: Synthesis of the lysine-containing dehydrodipeptides **1**-**3**.

Starting from β-hydroxyphenylalanine [H-D,L-Phe(β-OH)-OH], an initial esterification using thionyl chloride in methanol afforded the corresponding methyl ester of the β-hydroxyphenylalanine [H-D,L-Phe(β-OH)-OMe]. This was followed by an amide coupling reaction with the lysine derivative in the presence of 2-(1*H*-benzotriazole-1-yl)-1,1,3,3-tetramethylaminium hexafluorophosphate (HBTU), which afforded the corresponding dipeptide as a diastereomeric mixture. HBTU is a standard coupling agent commonly used for the activation of free carboxylic acids in peptide synthesis. The reaction mechanism involves the deprotonation of the amino acid carboxylic acid, followed by an attack on the imine carbon atom of HBTU giving an *O*-acyl urea and the anion of 1-hydroxybenzotriazole. The latter reacts with the *O*-acyl urea to give the active ester and tetramethylurea. Finally, the active ester reacts with the amine to produce the amide and 1-hydroxybenzotriazole (**Scheme 4**) (94).

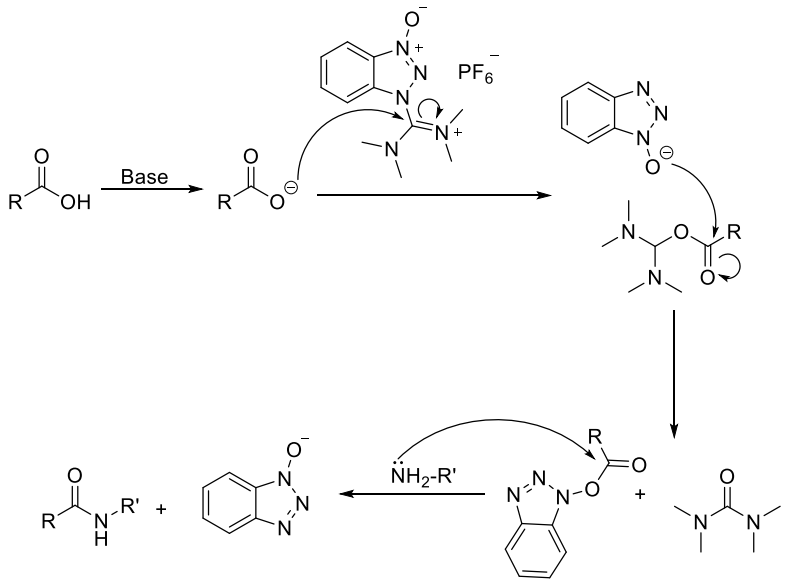

Scheme 4: HBTU coupling mechanism (94).

The β-hydroxydipeptide was dehydrated by treatment with di-*tert*-butyl dicarbonate (Boc_2O) in the presence of 4-dimethylaminopyridine (DMAP), followed by *N,N,N′,N′*-tetramethylguanidine (TMG), to afford the protected dehydrodipeptide. This reaction involves the formation of a carbonate intermediate which is then eliminated by treatment with base (TMG). The reaction is stereospecific towards the *Z*-isomer (**Scheme 5**) (93). The stereochemistry of the dehydrodipeptides prepared in this work was confirmed by NOE difference experiments by irradiating the α-NH proton and observing an NOE effect on the β-phenyl protons of the dehydropheylalanine residue.

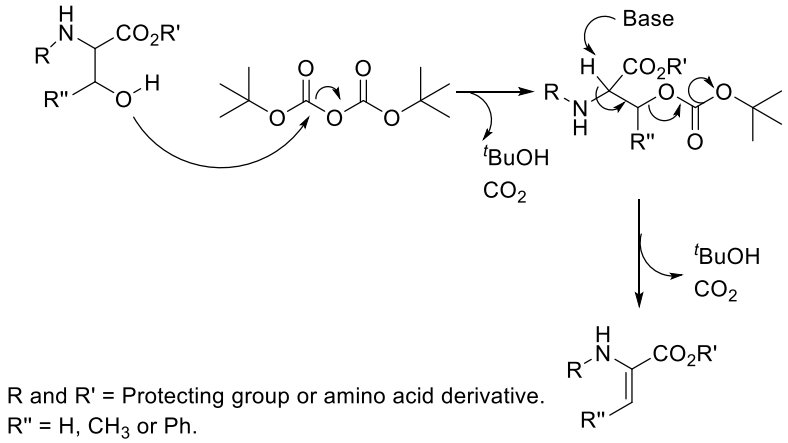

Scheme 5: Mechanism of dehydration of β-hydroxyamino acid derivatives with Boc_2O/DMAP and TMG (93).

In the case of peptides **1** and **2**, a deprotection step with trifluoroacetic acid to remove the *tert*-butoxycarbonyl group is followed by coupling with 2-(naphthalen-2-yl) acetic acid, in the presence of HBTU, to give the methyl esters of compounds **1** and **2**. The methyl ester of compound **3** was obtained after the dehydration reaction of the corresponding lysine-β-hydroxyphenylalanine dipeptide *N*-protected with the carboxybenzyl group. A final hydrolysis reaction using NaOH (1 M) delivered the desired compounds **1**-**3**.

The ^{1}H NMR spectra of compounds **1**-**3** in DMSO is shown is **Figure 18**.

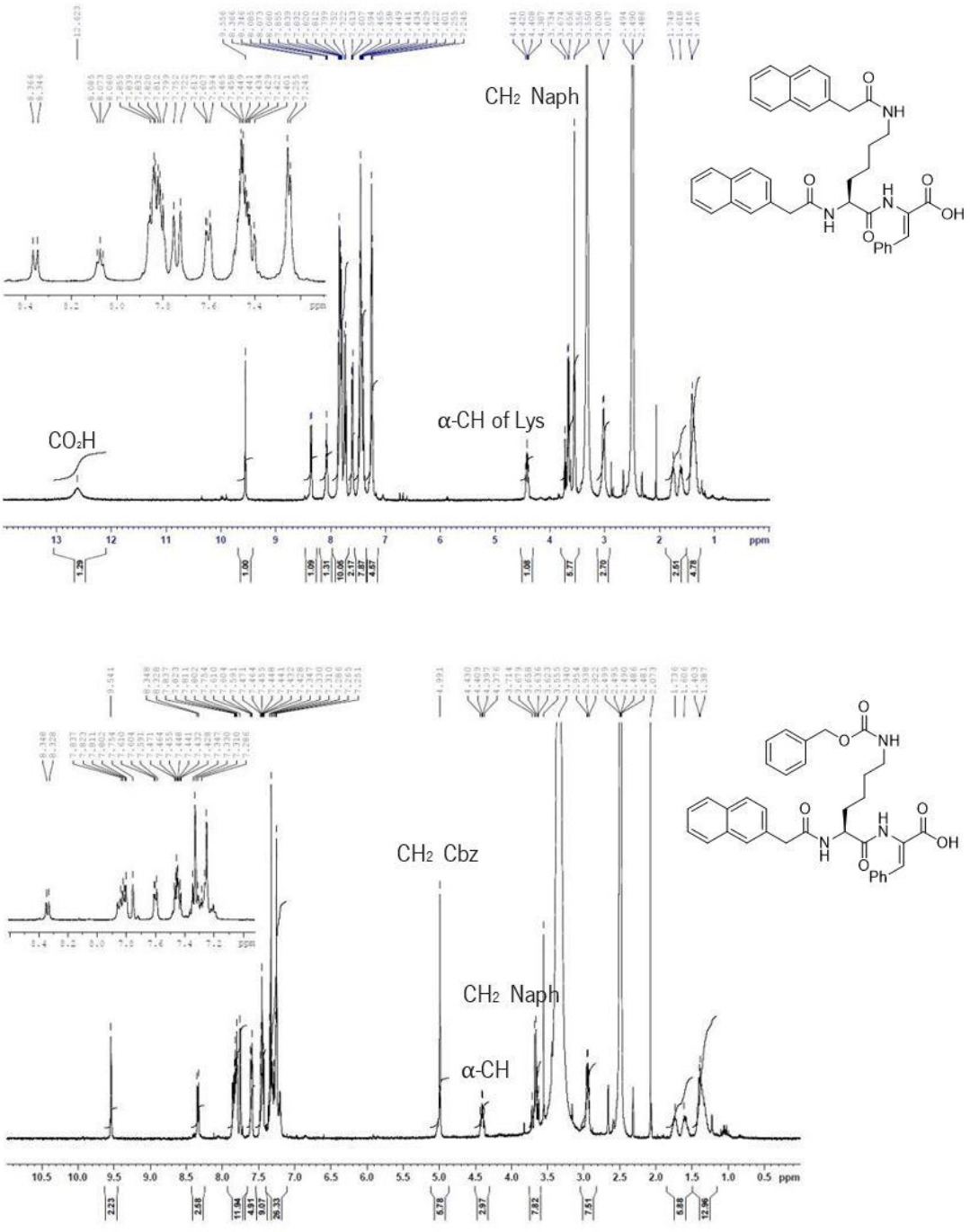

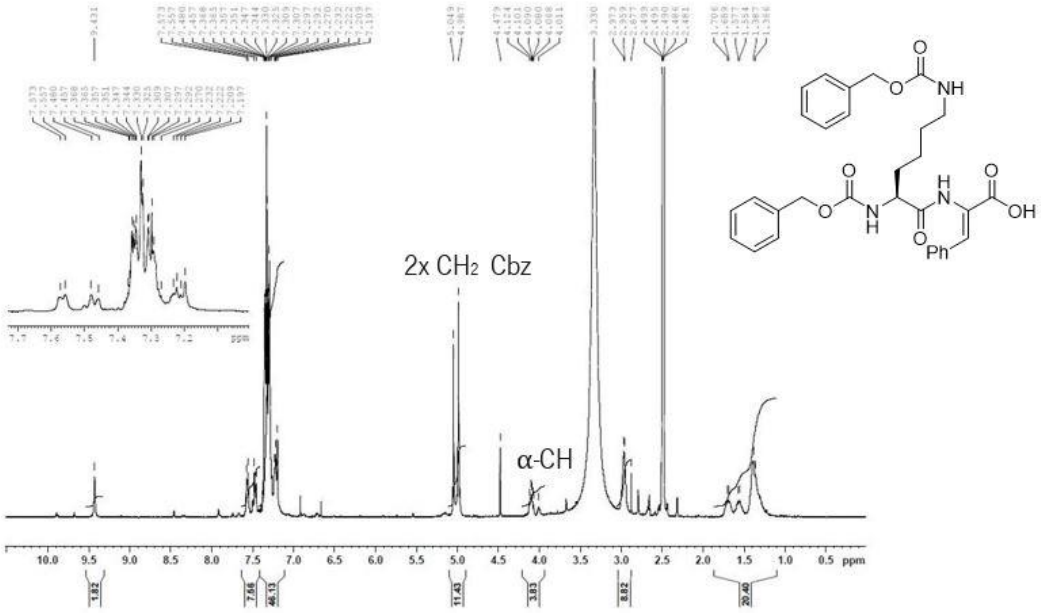

Figure 18: ^{1}H NMR spectrum (400 MHz) of compound **1**-**3** in DMSO-d_6.

In the spectra of the three compounds, it is possible to observe the NH proton of the dehydrophenylalanine residue between 9.43 ppm and 9.56 ppm. The absence of the singlet due to the three protons of the methyl ester moiety (3.55 ppm - 3.67 ppm; Chapter 4: Experimental procedures) is also characteristic of these spectra.

2.1.2 Preparation of hydrogels

As previously mentioned, LMW hydrogelators self-assemble due to the presence of multiple non-covalent interactions, which allow the monomeric building blocks to self-associate into ordered fibrous structures, which later entangle and interact with each other, to form the 3D hydrogel network (7,25). The hydrogelation process of ultrashort peptides, is dependent on a delicate balance between hydrophobicity and hydrophilicity. Several methods have been described and used to trigger gelation, such as pH change, heating-cooling cycles, enzymatic catalysis, the addition of chelating metal ions and sonification (26).

Generally, the ultrashort peptides synthesized **1-3** exhibited limited solubility in buffer solutions in the physiological pH range (6.0-8.0). However, they could be dissolved in water upon pH adjustment to pH 10, by the addition of sodium hydroxide 1 M. Hydrogelation was triggered by a slow pH drop, achieved by the aqueous hydrolysis of added D-glucono-δ-lactone (GdL) to D-gluconic acid. As mentioned in Section **1.6**, subsection **1.6.1**, hydrogelation using GdL has been shown to be advantageous compared to the

addition of mineral acids such as HCl, since the formation of D-gluconic acid is slower than the rate of diffusion, leading to more uniform hydrogels (35). In these conditions, peptides **1-3** produced free-standing hydrogels (**Figure 19**). The critical gelation concentration (CGC) of compounds **1-3** was assessed by varying the peptide concentrations and conducting vial inversion tests (**Table 1**).

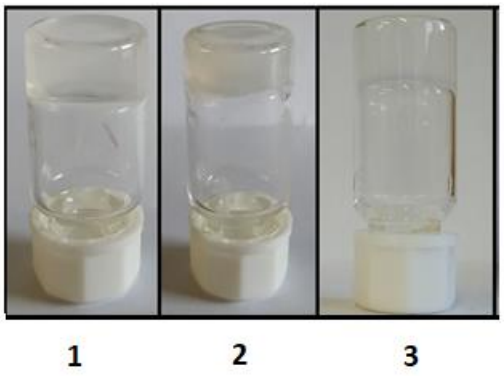

Figure 19: Optical images of hydrogels formed by hydrogelators **1**, **2** and **3**.

Table 1: Optimized gelation conditions of peptides **1-3**.

Peptide	Critical Gelation Concentration (CGC)		[GdL] (wt%)	pH	cLogP*
	wt%	mM			
1	0.05	0.0008	0.4	4.8	6.36
2	0.07	0.001	0.4	5.1	5.48
3	0.2	0.004	0.4	5.0	6.42

*cLogP value obtained from https//molinspiration.com

Although the CGC values obtained were the lowest ever to be reported within the research group (**Figure 20**) and are significantly lower than the usual CGCs reported for low molecular weight peptide based supramolecular hydrogels, they are still higher than those reported in the literature for some gelators.

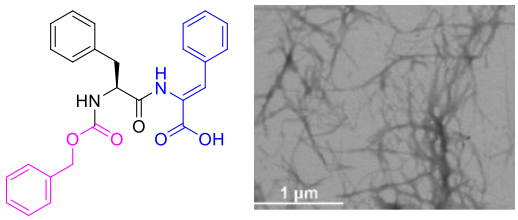

Z-Phe-ΔPhe-OH; CGC = 0.1 wt% [48]
clogP = 5.94

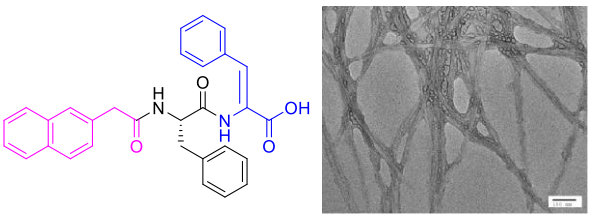

Naph-Phe-ΔPhe-OH; CGC = 0.14 wt% [95]
clogP = 5.01

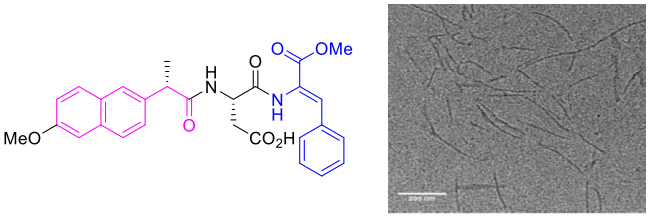

Npx-Asp-ΔPhe-OMe; CGC = 0.4 wt% [45]
clogP = 4.17

Figure 20: Structure and STEM and TEM images of hydrogels obtained from compounds Z-Phe-ΔPhe-OH (48), Naph-Phe-ΔPhe-OH (95) and Npx-Asp-ΔPhe-OMe (45).

Gazit and co-workers described a minimalistic ultrashort peptide-based hydrogelator with a CGC of 0.002 wt% (38). This hypergelator is based on a dipeptide comprised of lysine and aspartic acid, *N*-capped with a fluorenylmethoxycarbonyl group [Fmoc-Lys(Fmoc)-Asp(OH)-OH] (**Figure 21**).

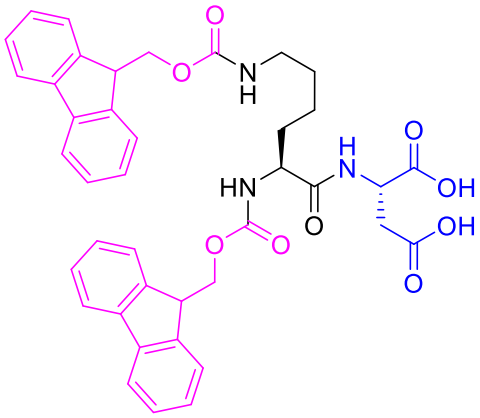

Fmoc-Lys(Fmoc)-Asp-OH
CGC 0.002 wt%; 0.03 mM
(cLogP 5.51)

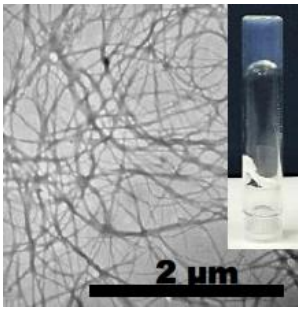

Figure 21: Structure and TEM micrograph of the hypergelator Fmoc-Lys(Fmoc)-Asp-OH (38).

To give hydrogels, the corresponding peptide based hydrogelators must have the correct balance between hydrophilicity and hydrophobicity. If the compound is too hydrophilic it stays in solution; if it is too hydrophobic, precipitation may occur before the onset of the gelation process (32). The log P of efficient peptide hydrogelators should ideally be between 2.8 and 5.5 (34). Peptides with values of log P below 2.8 generate unstable hydrogels whilst peptides with log P values above 5.5 are too hydrophobic and do not produce a homogenous hydrogel. The calculated log P values of dehydrodipeptides **1**-**3** are equal or higher than 5.5. When compared with Fmoc-Lys(Fmoc)-Asp-OH, compounds **1** and **3** are more hydrophobic and this could be one of the reasons to explain the higher CGC. In the case of peptide **2** the calculated log P is similar to that reported for Fmoc-Lys(Fmoc)-Asp-OH however the CGC of the latter is 40 times lower than that of compound **2**.

The peptide Fmoc-Lys(Fmoc)-Asp-OH has two carboxylic acid moieties at the *C*-terminus that compensate for the hydrophobicity arising from the two Fmoc groups. Dehydrodipeptides **1**-**3** have a hydrophobic aromatic dehydrophenylalanine residue instead of aspartic acid. Another reason to explain the higher CGC of dehydrodipeptides **1**-**3** could be the gelation methodology used. The hydrogels of compounds **1**-**3** were prepared using a pH trigger whereas the hydrogel of the dipeptide Fmoc-Lys(Fmoc)-Asp-OH was prepared using the solvent switch methodology. As previously described the CGC depends on the method used to trigger gelation (23). The pH change method would not be suitable for Fmoc-Lys(Fmoc)-Asp-OH gelator of Gazit, because Fmoc groups are labile at high pHs, whereas the solvent switch method was not a successful gelation method for compounds 1-3. Therefore, it is impossible to make exact comparisons.

Dehydrodipeptide **1** showed the lowest CGC, 0.04 wt%, probably due to the two-naphthalene lysine protecting groups. Although with a lower CGC the hypergelator described by Gazit *et al.* (**Figure 20**) has some limitations namely the susceptibility of the Fmoc group to cleavage and the possibility of *in vivo* proteolysis.

2.1.3 STEM

The nanostructure of hydrogels **1**-**3** was studied using scanning transmission electron microscopy (STEM). The STEM images displayed interlaced fibers that assemble into the 3D-networks of hydrogels (**Figure 22**).

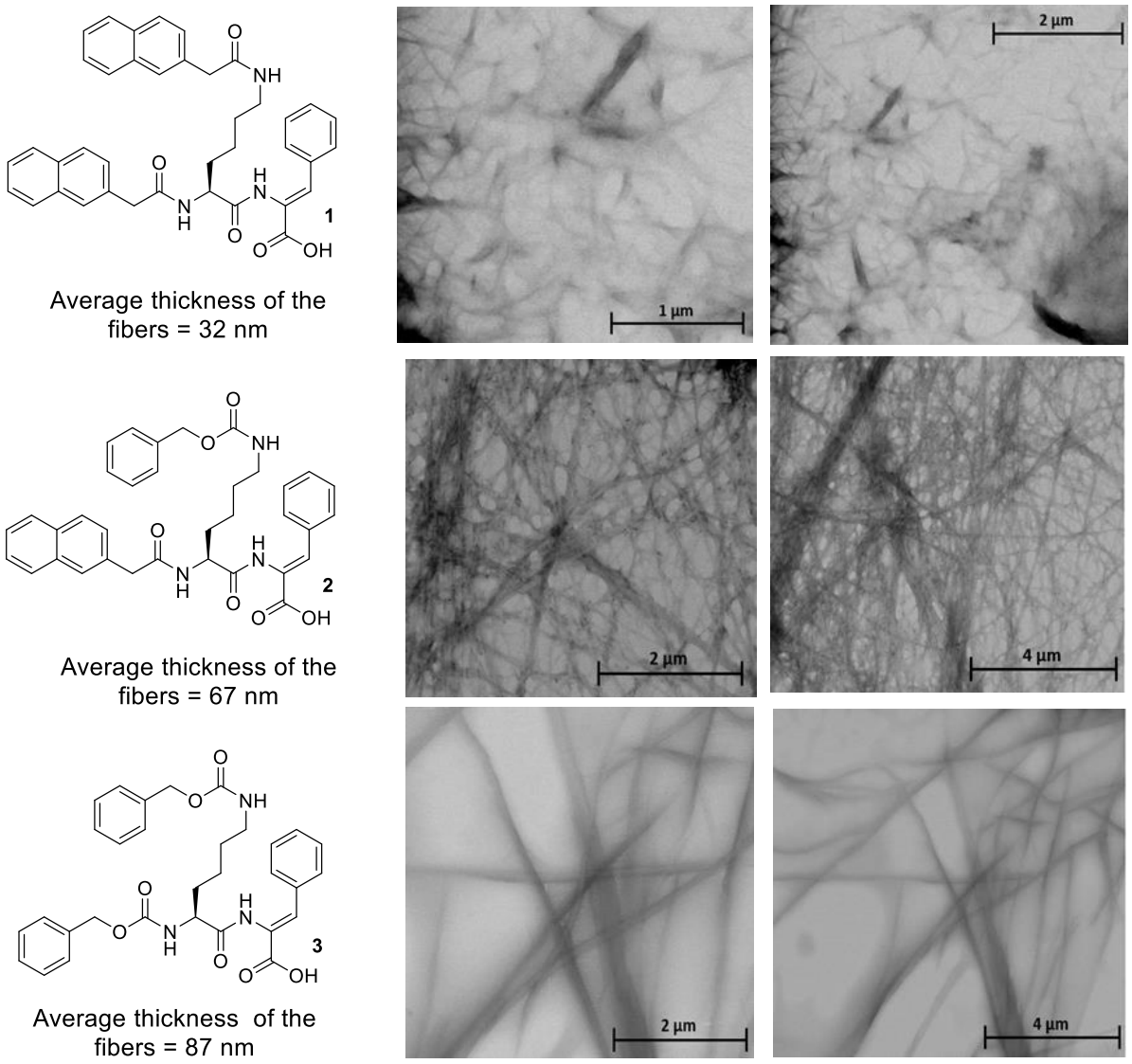

Figure 22: Scanning transmission electron microscopy (STEM) images of hydrogels **1-3** at 0.2 wt%.

From the observation of **Figure 22**, it is possible to conclude that there is a tendency for forming hydrogels with thicker fibers when the dehydropeptide have carboxybenzyl capping groups, compared to those containing naphthalene protecting groups. This is an interesting observation, suggesting that (depending on the end application) the thickness of the fibers could be tuned by judicious choice of the protecting groups used.

2.1.4 Circular Dichroism

Circular dichroism (CD) is among the most commonly used techniques to study the stereostructures and intra/intermolecular interactions of chiral supramolecular systems. CD refers to the differential absorption of left and right circularly polarized light. This technique constitutes a valuable tool for assessing the secondary structure of peptides and proteins (58–60). The determination of the secondary structure of peptides in solution using CD rely on spectral data acquired between wavelengths of 190 nm to 230 nm. Over this spectral range, peptides with a α-helix secondary structure show a CD spectrum with negative bands at 222 nm and 208 nm and a positive band at 193 nm. The CD spectra of peptides with an antiparallel β-sheet display a negative band at 218 nm and a positive band at 195 nm. Finally, a random coil peptide exhibits low ellipticity above 210 nm and negative bands near 195 nm (96) (**Figure 23**).

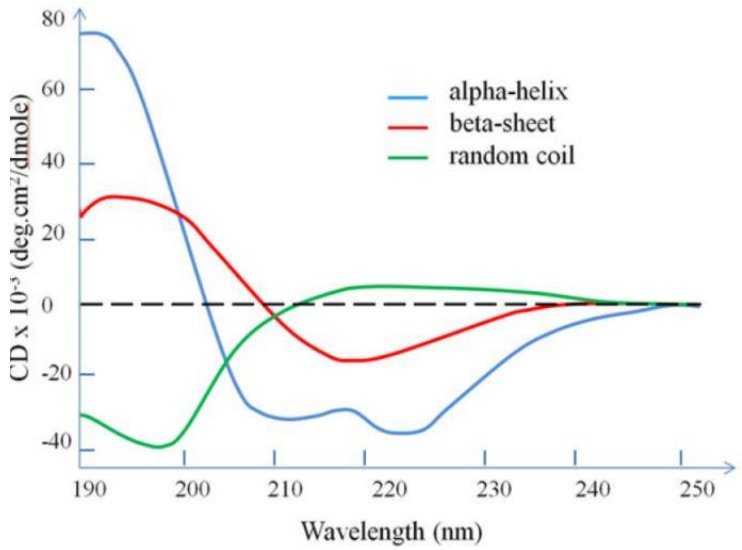

Figure 23: Standard CD spectra characteristic of the three basic secondary structures of a peptide chain: α-helix, β-sheet, and random coil (96).

The CD spectra of compounds **1**-**3** are shown in **Figure 24**. These spectra were obtained with hydrogelator concentrations far below the CGC values, owing to instrumental limitations. Consequently, the secondary structures assessed by CD spectra are merely indicative, since less-organized self-assembled fibrils are expected to exist in solution.

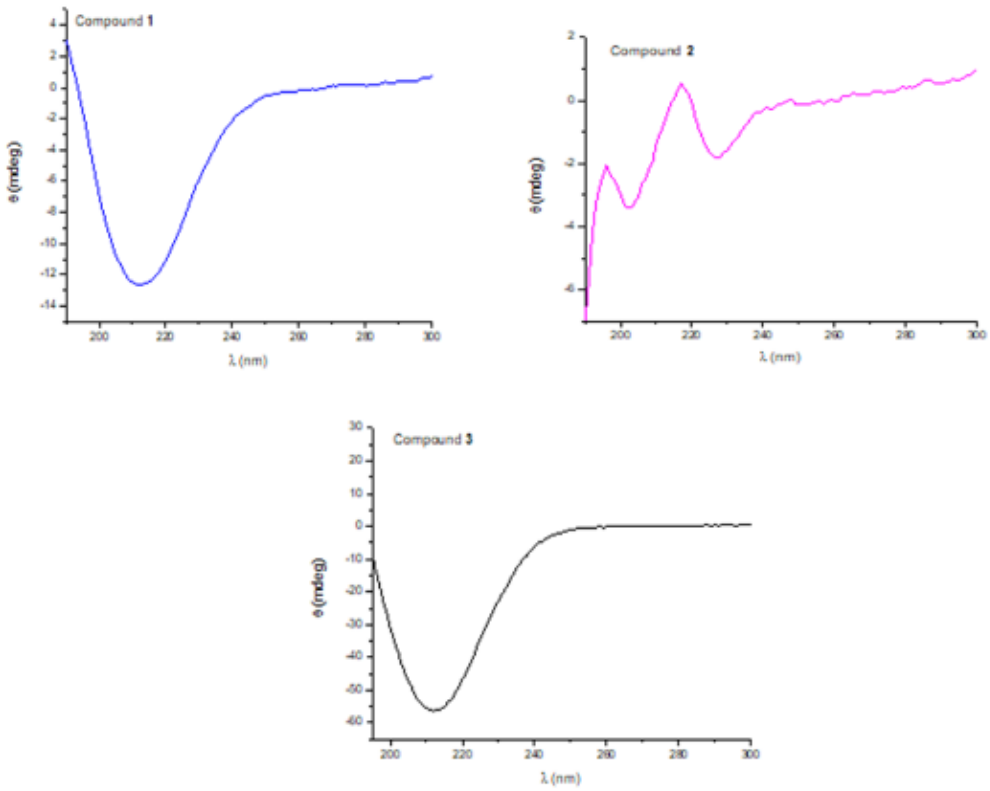

Figure 24: CD spectra of aqueous solutions of compounds **1-3** (0.01 wt%).

The CD spectrum of dehydrodipeptides **1** and **3** are very similar, displaying negative bands at 215 nm and 213 nm, respectively (**Figure 24**). These results suggest a β-sheet aggregation pattern. The CD spectrum of dehydrodipeptide **2** suggests a predominance of random coil due to the two small negative bands at 202 nm and 228 nm. The CD spectrum of the hydrogel Fmoc-Lys(Asp)-Asp-OH (**Figure 25**) indicates the absence of specific secondary structures, although a peak at 307 nm suggests strong π-stacking interactions.

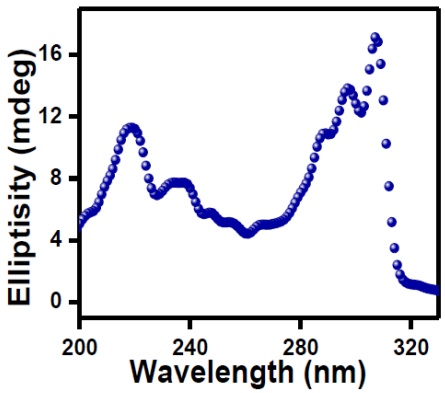

Figure 25: CD spectra of the Fmoc-Lys(Fmoc)-Asp hydrogel (0.5wt%) (38).

The only structural difference between hydrogelator **2** and hydrogelators **1** and **3** is the presence of different capping groups (naphthalene acetyl and carboxybenzyl) protecting the lysine amines. This data clearly suggests that the particular capping groups on lysine affects the self-assembly process.

2.1.5 Rheological studies

As previously mentioned, rheological studies provide structural information about the type, number, and stiffness of the overall network responsible for hydrogelation. Consequently, rheology is an important tool used to characterize supramolecular hydrogels.

The gelation kinetics of dehydrotripeptides **1-3** are presented in **Figure 26**.

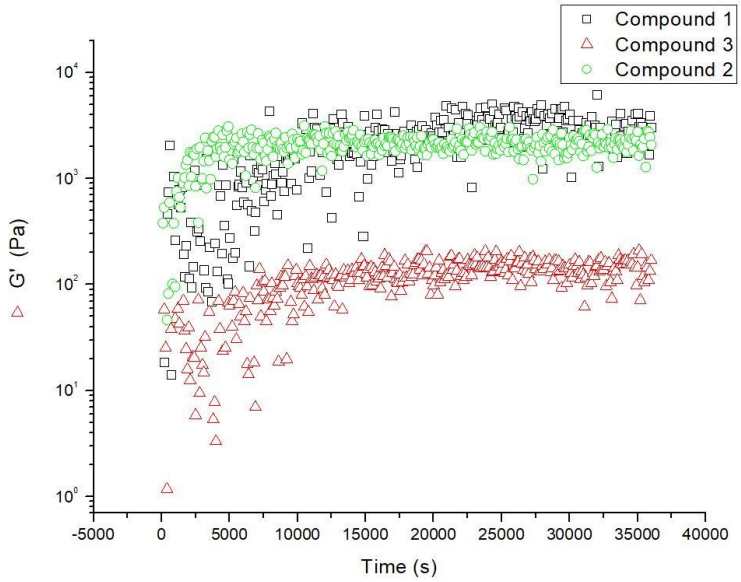

Figure 26: Elastic modulus during the kinetic process of gelation for compounds **1-3** at 0.2wt%.

From the results obtained dehydrodipeptide **2** had the fastest kinetics, giving a gel in approximately 20 minutes. On the other hand, the hydrogels from dehydrodipeptides **1** and **3** displayed a gelation time of 2.8 hours and 2.6 hours, respectively.

Upon reaching the structural equilibrium established by the reading of G` and G`` with time, a frequency sweep from 100Hz down to 0.1 Hz was performed with a strain of 0.01% to give the mechanical spectra displayed in **Figure 27**.

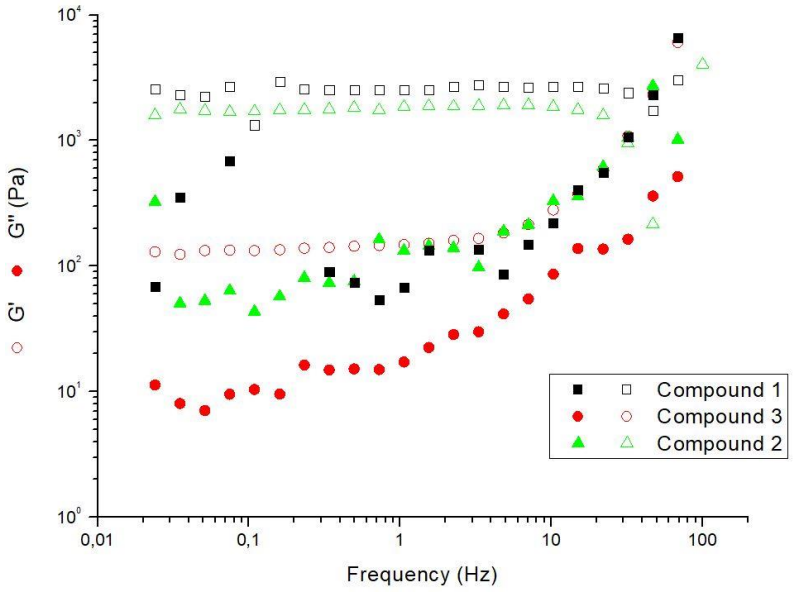

Figure 27: Frequency dependence of the shear elastic G' and G'' moduli for the compounds **1-3** at 0.2wt%.

All three hydrogels from dehydrodipeptides **1-3** showed a G` essentially constant over the frequency domain tested, whereas G`` displays local minimums. For all three dehydrodipeptides **1-3**, there is an increase of both G` and G`` with frequency at larger frequencies. However, this could simply be due to experimental issues (sample inertia) polluting the data at this specific frequency regime. In general, the mechanical spectra are similar, suggesting that the elastic network responsible for the hydrogels mechanical response share structural similarities. As expected, the G` is higher than G`` for all three hydrogels (**Table 2**).

Table 2: G' and G'' for hydrogels **1-3** at 0.2wt%.

Hydrogel	G' (Pa)	G'' (Pa)
1	3.63×10^3	221
2	1.83×10^3	145
3	1.84×10^2	28

By comparing the G` values of hydrogels obtained from dehydrodipeptides **1**-**3**, it is noticeable that hydrogels **1** and **2** are the stiffest and hydrogel **3** is the least elastic. Also, hydrogels **1** and **2** show G` values similar to those obtained for other hydrogelators obtained from dehydrodipeptides in our research group (**Table 2**) (48). The value of G' of hydrogel **3** is rather low which could be a potential disadvantage for using this specific hydrogel for sustained drug release.

Following the frequency sweep, the hydrogels of **1-3** were submitted to a strain sweep, where the frequency was maintained at 1 Hz (**Figure 28**).

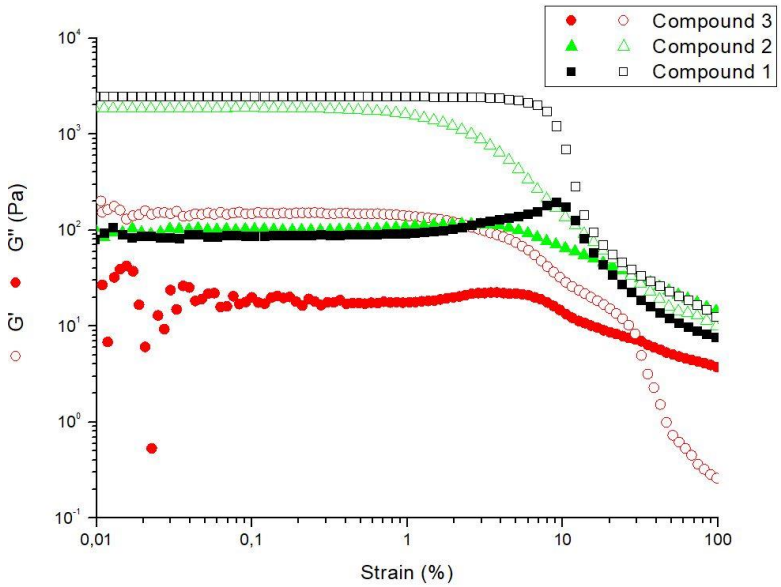

Figure 28: Strain dependence of the shear elastic G' and loss G'' moduli for compounds **1-3** at 0.2 wt%.

Hydrogels of dehydrodipeptides **1, 2** and **3** break up at a strain of 102%, 73,3%, and 35%, respectively. Interestingly, hydrogel from **1** was both the more elastic and stronger among the three dehydrodipeptides hydrogels. On the other hand, the hydrogel formed from **3** was the least elastic and the weakest, while the hydrogel formed from **2** showed a balance between the other two hydrogels, both in elasticity and strength. This data points to the influence of the aromatic capping groups. Dehydrodipeptides *N*-protected naphthalene acetyl groups produced better hydrogels than peptides *N*-protected with carboxybenzyl groups.

2.1.6 Drug release assays

As previously discussed, due to their intrinsic characteristics, these supramolecular hydrogels possess enormous potential to be used as drug delivery systems overcoming pharmacokinetics limitations of certain drugs, such as poor aqueous solubility or short half-lives *in vivo*. The hydrogel from dehydrodipeptide **1** was selected to be studied for its capacity to entrap, and then release, model compounds. To this effect, two dyes and an antibiotic were incorporated in the hydrogel matrix. Thus, methylene blue (MB), methyl orange (MO) and ciprofloxacin were chosen as cationic, anionic, and overall neutral cargo (**Figure 29**). The release of each cargo molecule from the two hydrogels was assessed.

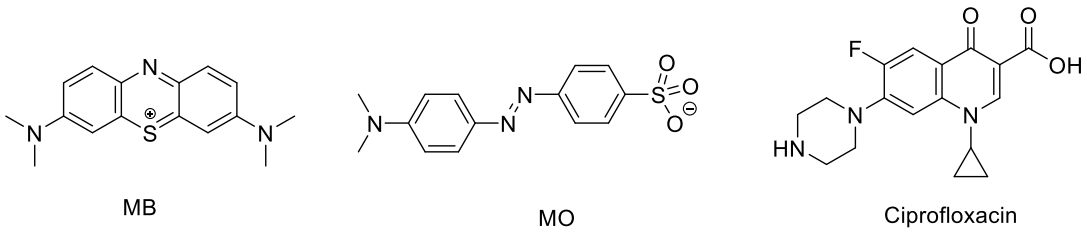

Figure 29: Small molecule cargo for release: methylene blue (MB), methyl orange (MO) and ciprofloxacin.

Hydrogels of **1** containing the model compounds were prepared using the same conditions described but with the water component (1 mL) being replaced by methylene blue solution (0.1 nM), methyl orange solution (0.2 nM) or ciprofloxacin solution (0.2 nM). In a slightly modified version of the method described by Abraham *et al.*, (97), water (1.5 mL) was carefully layered on top of the hydrogel surface and then the percentage of the compound release was recorded *versus* time. This analysis was carried out by UV-Vis spectroscopy for the dyes and by HPLC for ciprofloxacin.

The assays of hydrogel **1** with cationic MB, revealed that the top layer remained colorless and transparent over 7 days, suggesting that only a small amount of MB was released from the hydrogel matrix (**Figure 30**). The results obtained showed that the cationic MB was retained by the hydrogel network. The results obtained for the release of MO showed that this compound was released by the network of the hydrogel **1** (**Figure 31**, **Table 3**) in 37 %. Ciprofloxacin was used as an overall neutral cargo to provide a direct comparison between the cationic and anionic cargo. In this case it was found that hydrogel **1** released 23 % of ciprofloxacin. **Figure 31** reveals that a plateau was reached after 48 h.

Figure 30: Representative images of hydrogels obtained from compound **1** loaded with MO (left), MB (centre) and ciprofloxacin (right) layered with water (1.5 mL) after a saturating release study (168 h).

Table 3: Release % of model drugs from hydrogel 1 after 168 h.

Hydrogelator	MB released (%)	MO released (%)	Ciprofloxacin released (%)
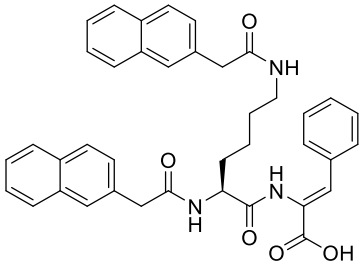 **1**	0.9	37.4	23.2

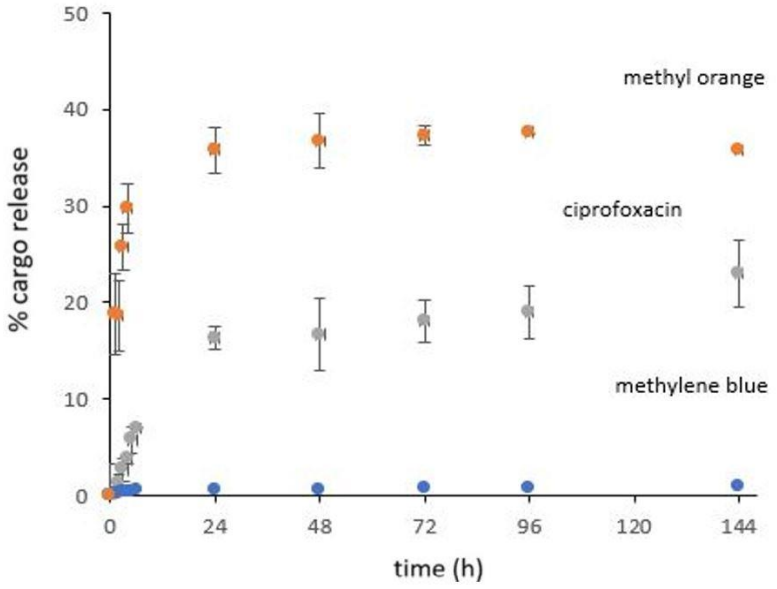

Figure 31: Percentage of cargo release vs time over 168 h. Release of methylene blue, methyl orange and ciprofloxacin from hydrogelator **1.**

To describe the release of the cargo from the hydrogel network, the Korsmeyer-Peppa's model was used. This mathematical model includes both diffusion and erosion of polymer (**Figure 32**).

The following equation describes the Korsmeyer-Peppa's model:

$$\frac{M_t}{M} = kt^n$$

M_t: amount of cargo released at time t;

M: Total amount of cargo used for the release study;

k: release rate constant incorporating structural and geometric characteristics of drug dosage form;

n: release exponent.

In this model, the n value is associated with the diffusion mechanism of the drug as described in **Table 4** (98,99).

Table 4: Interpretation of diffusional release mechanisms.

Release exponent (n)	Drug transport mechanism
0.5	Fickian diffusion
0.45 < n = 0.89	Non – Fickian transport
0.89	Case II transport
Higher than 0.89	Super case II transport

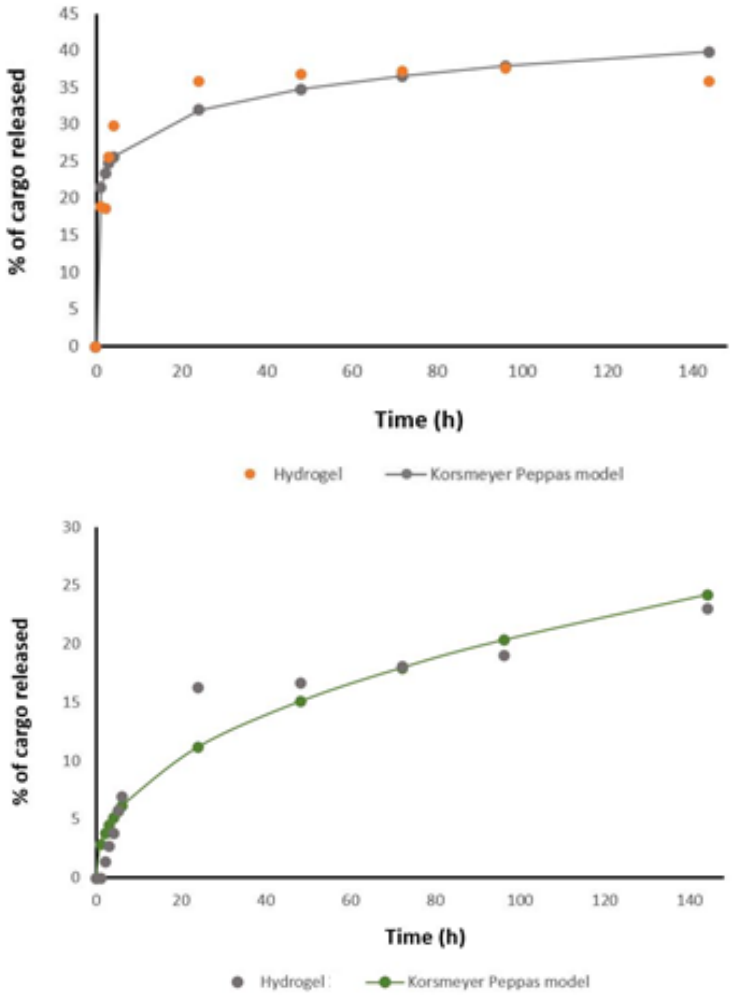

Figure 32: Data to Korsmeyer-Peppas Model to describe the release kinetics of MO and ciprofloxacin from hydrogel **1**.

The determined parameters of this model (k and n) and the value of R^2 are presented in **Table 5**. The data show that release of ciprofloxacin from hydrogel **1** is faster (higher k value) than methyl orange and in both cases is associated with a diffusion-controlled release mechanism (n value).

Table 5: Release coefficients of the Korsmeyer-Peppas model obtained for methyl orange and ciprofloxacin release profiles in hydrogels from **1**.

Cargo	k	*n*	R^2
Methyl Orange	21.5687	0.1235	0.9090
Ciprofloxacin	29.9747	0.4309	0.9679

2.2 Hydrogelation of tripeptides based on dehydrodipeptides with lysine *N*-capped with aromatic moieties

Considering the hypergelator described by Gazit and co-workers (**Figure 21**) (38) and our results obtained with the hydrogelators **1**-**3** based on a *N*-diprotected lysine and a dehydrophenylalanine residue, we decided to introduce an aspartic acid in dehydrodipeptides **1** and **3** to obtain new hydrogelators with lower critical gelation concentrations. The aspartic acid will increase the hydrophilicity of the new tripeptides **4** and **5** (**Figure 33**).

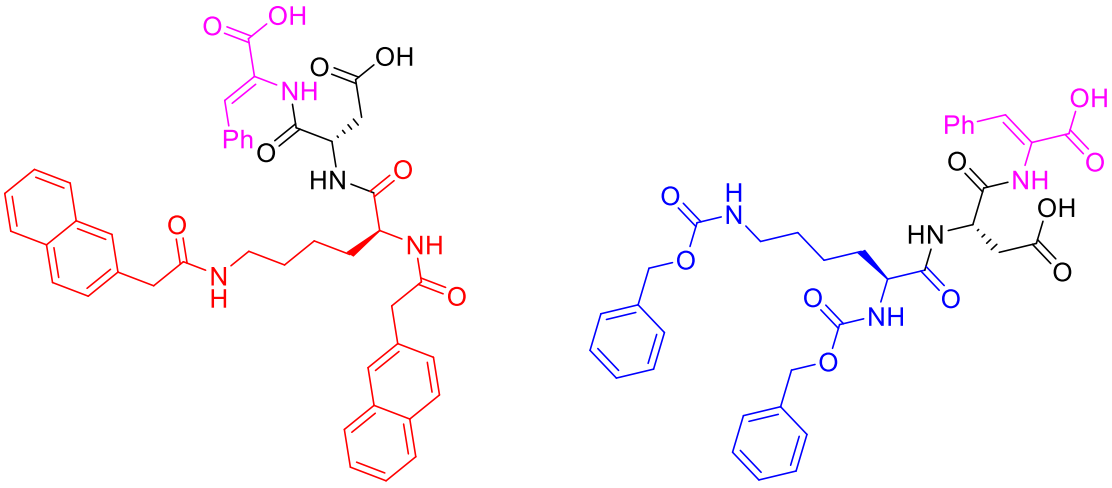

Naph-Lys(Naph)-Asp(OH)-ΔPhe-OH, **4**

Cbz-Lys(Cbz)-Asp(OH)-ΔPhe-OH, **5**

Figure 33: Structure of the lysine dehydrotripeptides *N*-protected with aromatic groups **4** and **5**.

2.2.1 Synthesis of tripeptides 4 and 5

Dehydrotripeptides **4** and **5** were prepared according to **Scheme 6** using a conventional stepwise protocol.

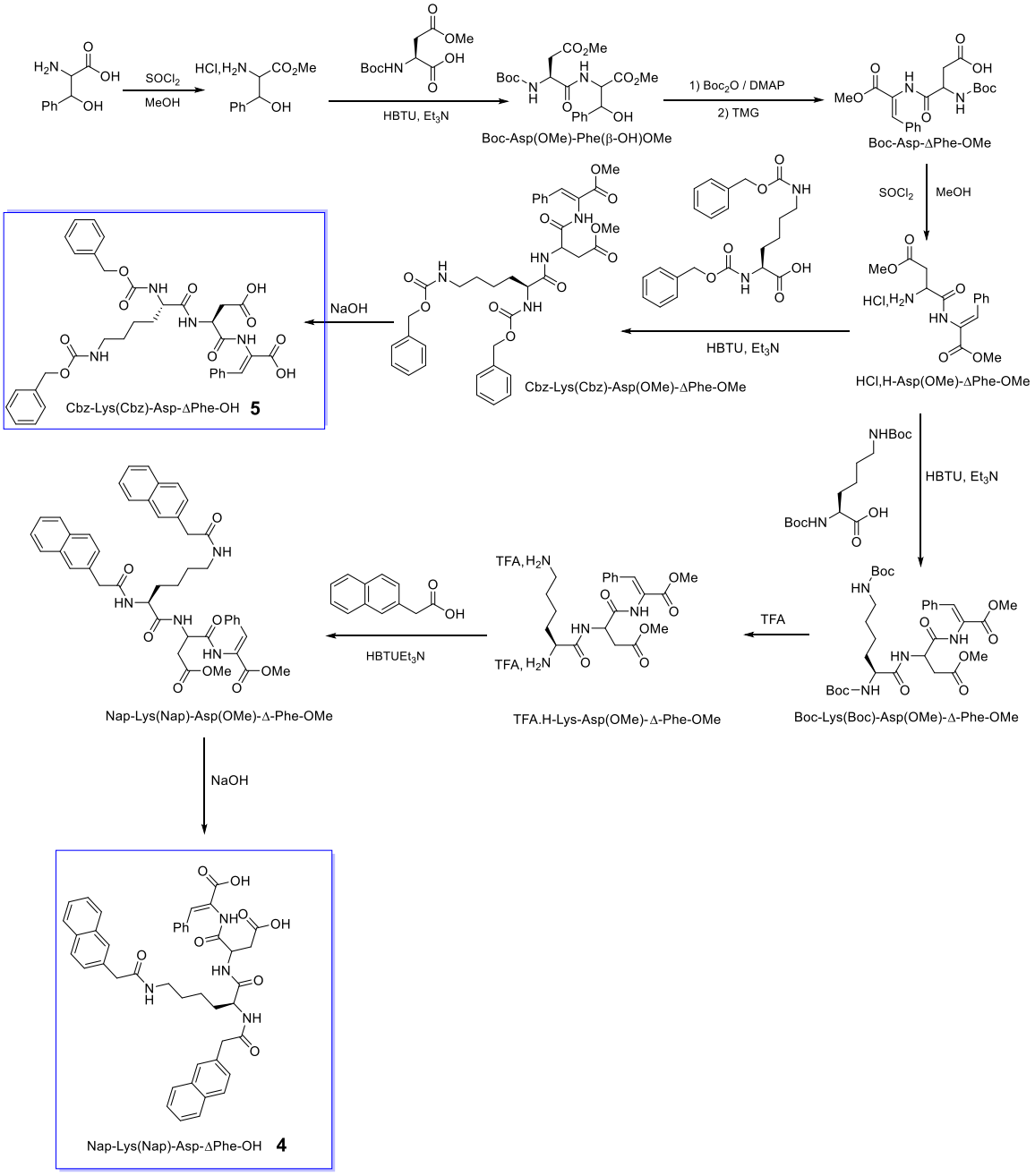

Scheme 6: Synthesis of dehydrotripeptides **4** and **5**.

The synthesis of dehydrotripeptides **4** and **5** involved the synthesis of the dehydrodipeptide Boc-Asp(OMe)-ΔPhe-OMe. Thus, the methyl ester of β-hydroxyphenylalanine (H-D,L-Phe(β-OH)-OMe) prepared earlier (Section **2.1**, subsection **2.1.1**) was coupled with an aspartic acid derivative (Boc-Asp(OMe)-OH) in the presence of HBTU to afford the corresponding dipeptide (Boc-Asp(OMe)-Phe(β-OH)-OMe) as a diastereomeric mixture. The β-hydroxydipeptide was dehydrated by treatment with Boc_2O in the presence of DMAP, followed by TMG. Although we are aiming to obtain the dehydrodipeptide Boc-Asp(OMe)-ΔPhe-OMe, the ^1H NMR showed only one three-proton singlet at 3.75 ppm indicating that one of the methyl esters suffered hydrolysis possibly due to the use of TMG. Remarkably, the hydrolysis reaction was selective and just one of the methyl esters was cleaved. A possible mechanism to explain the hydrolysis from the β-methyl ester of aspartic acid involves the deprotonation of the dehydrophenylalanine NH (more acidic due to conjugation with the α,β-double bond) followed by an intramolecular attack on the β-carbonyl carbon atom of aspartic acid to give a succinimide derivative that can easily open to give Boc-Asp-ΔPhe-OMe (**Scheme 7**). This mechanism might also explain the fact that both tripeptides were obtained as isomeric mixtures.

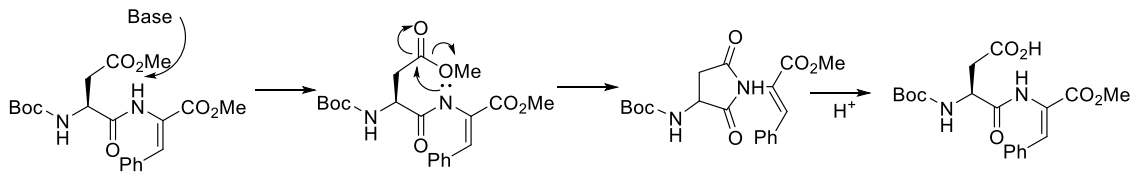

Scheme 7: Proposed mechanism for the hydrolysis of the methyl ester of Boc-Asp(OMe)-ΔPhe-OMe.

In order to protect the β-carboxylic acid of aspartic acid and simultaneously remove the Boc group, the compound obtained in the previous reaction was treated with thionyl chloride in methanol to afford the dehydrodipeptide H-Asp(OMe)-ΔPhe-OMe • HCl. The structure of this compound was confirmed by ^1H NMR spectroscopy. The spectrum showed the presence of two methyl esters resonances at 3.68 ppm and 3.70 ppm as well as the disappearance of the nine-proton singlet at 1.42 ppm assigned to the *tert*-butoxycarbonyl (Boc) group and the appearance of a three-proton broad singlet at 8.40 ppm, which corresponds to an NH_3^+ group. (**Figure 34**).

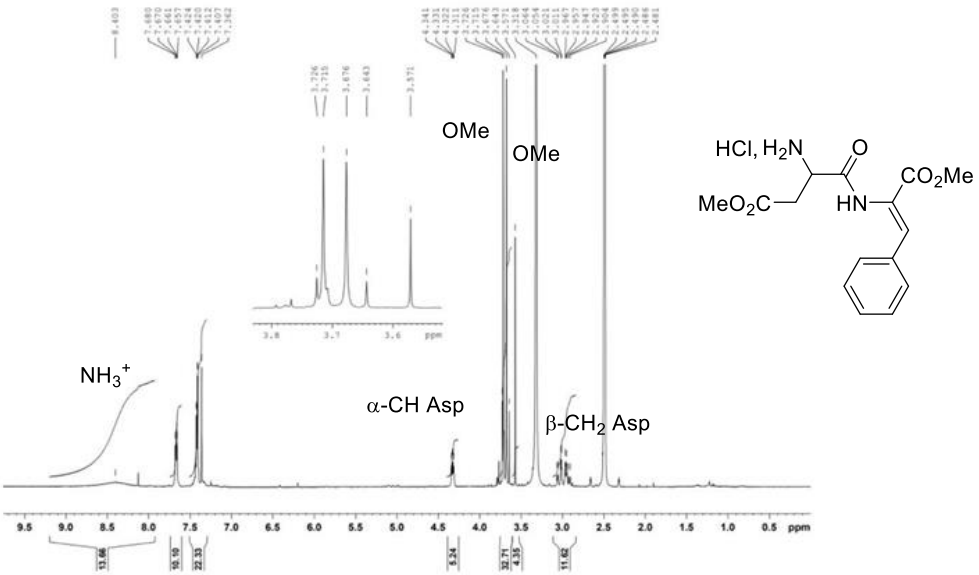

Figure 34: ^{1}H NMR spectrum (400 MHz) of compound H-Asp(OMe)-ΔPhe-OMe • HCl in DMSO-d_6.

Compound H-Asp(OMe)-ΔPhe-OMe • HCl was then coupled with *N*-diprotected lysine derivatives Boc-Lys(Boc)-OH and Cbz-Lys(Cbz)-OH in the presence of HBTU and trimethylamine to give the corresponding dehydrotripeptides in good yields. The dehydrotripeptide Cbz-Lys(Cbz)-Asp(OMe)-ΔPhe-OH was treated with a NaOH solution in dioxane to give the hydrogelator **5**. Removal of the Boc groups from compound Boc-Lys(Boc)-Asp(OMe)-ΔPhe-OMe was carried out with TFA. The *N*-deprotected dehydrotripeptide was then coupled with 2-(naphthalen-2-yl)acetic acid in the presence of HBTU to give Naph-Lys(Naph)-Asp(OH)-ΔPhe-OMe. The latter gave dehydrotripeptide **4** after basic hydrolysis of the methyl esters. Analysis of the ^{1}H and ^{13}C NMR spectra of compounds **4** and **5** show that these compounds were obtained as diastereomeric mixtures. **Figure 35** shows the ^{1}H NMR spectra of compound **5**.

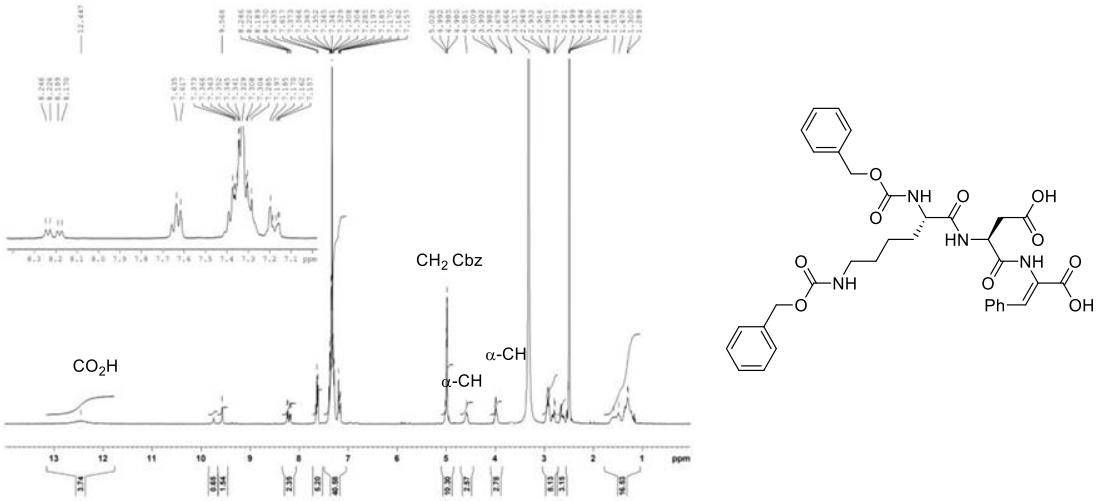

Figure 35: ^{1}H NMR spectrum (400 MHz) of compound Cbz-Lys(Cbz)-Asp-ΔPhe-OH in DMSO-d_6.

2.2.2 Preparation of hydrogels

The preparation of hydrogels from dehydrotripeptides **4** and **5** was carried out by solubilizing the peptide in water by adjustment to pH 10 with a solution of NaOH followed by the addition of D-glucono-δ-lactone (GdL). The slow aqueous hydrolysis of GdL to gluconic acid trigger gelation (**Figure 36**).

Figure 36: Optical images of hydrogels formed by hydrogelators **4** and **5**.

Table 6 shows the Critical Gelation Concentration (CGC) of dehydrotripeptides **4** and **5**.

Table 6: Optimized conditions for gelation of peptides **4** and **5**.

Peptide	Critical gelation concentration (CGC)		GDL Concentration (wt%)	pH	cLogP*
	wt%	mM			
4	0.04	0.0006	0.4	4.8	4.96
5	0.1	0.002	0.4	5.2	5.03

cLogP* value obtained from https//molinspiration.com

Compared with the dehydro*di*peptides **1** and **3**, the dehydro*tri*peptides show lower CGCs. These results show that the introduction of an aspartic residue contribute to a reduced CGC of the dehydrodipeptides. However, the dehydrotripeptides show a higher CGC when compared with the hypergelator described by Gazit (38) Fmoc-Lys(Fmoc)-Asp-OH (CGC 0.002 wt%).

2.2.3 STEM

The nanostructures of the supramolecular assemblies of dehydrotripeptides **4** and **5** were studied using STEM. The STEM images (**Figure 37**) displayed interweave fibers that assemble into 3D-network in hydrogels.

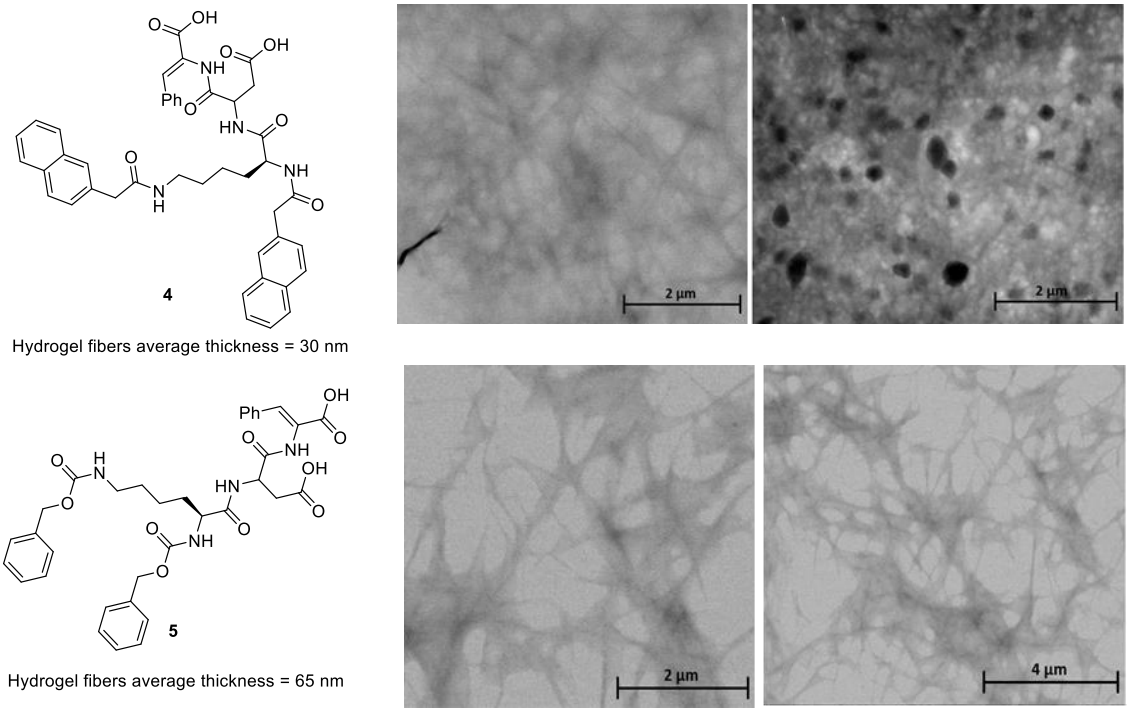

Figure 37: STEM images of hydrogels based on dehydrotripeptides **4** and **5** (0.2 wt%).

The networks of the hydrogels obtained from the dehydrotripeptides **4** and **5** were very different from those obtained from dehydrodipeptides **1** and **3**. The thicknesses of the fibers, which form the hydrogels, are on average 30 nm and 65 nm for **4** and **5** respectively. This suggests that the presence of an aspartic acid residue influences the thickness of the fibers. This could be explained by different interactions between the molecules. In certain STEM images of the hydrogel of dehydrotripeptide **4** it is possible to observe two different structures, a fibril network and aggregates/spheres. Gazit`s group reported that the hypergelator Fmoc-Lys(Fmoc)-Asp(OH)-OH revealed an unusual two-step assembly when forming the hydrogel (38). In order to investigate the unusual two-step gelation time-dependent TEM images of the hydrogelation of Fmoc-Lys(Fmoc)-Asp(OH)-OH (**Figure 38**). It is possible to observe a morphological transformation from spheres to fibers over time suggesting a molecular rearrangement of the hypergelator (38).

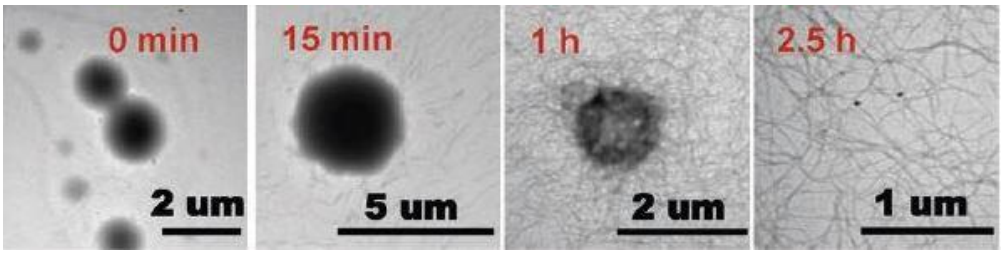

Figure 38: TEM images of Fmoc-Lys(Fmoc)-Asp(OH)-OH hydrogel at different time points (38).

This behavior has also been observed for other Fmoc-protected gelators (100), but to the best of our knowledge, there are no reports of this type of two-step gelation with naphthylacetyl protected dehydropeptides. We hypothesize that dehydrotripeptide **4** undergoes a similar gelation mechanism based on a two-step assembly, but in a much slower sphere-to-fiber rate. This hypothesis will be further discussed in subsection **2.2.5 – Rheological studies** (**Figure 39**).

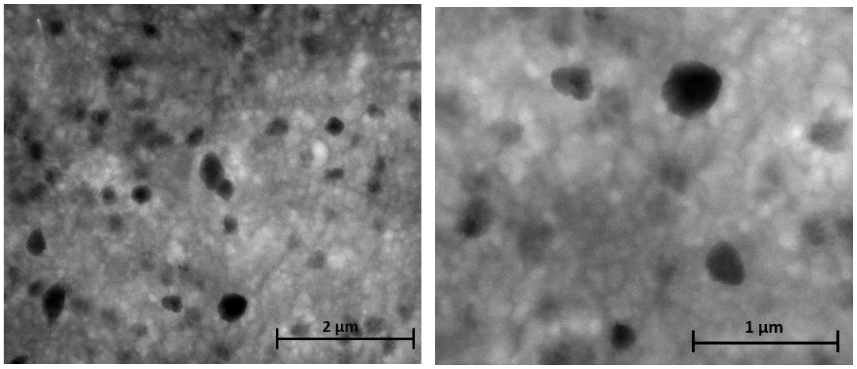

Figure 39: STEM images of dehydrotripeptide **4**.

2.2.4 Circular Dichroism

The CD spectrum of dehydrotripeptides **4** and **5** are very similar, with both compounds having a negative band at 215 nm (**Figure 40**), suggesting a predominance of a β-sheet pattern. The CD spectra of these are similar to those observed for dipeptides **1** and **3**.

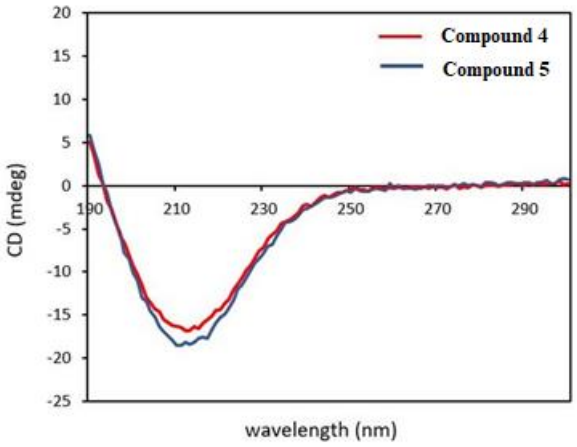

Figure 40: CD spectra of diluted aqueous solutions of compounds **4** and **5** (0.01 wt%).

2.2.5 Rheological studies

The gelation kinetics of dehydrotripeptides **4** and **5** are represented in **Figure 41**.

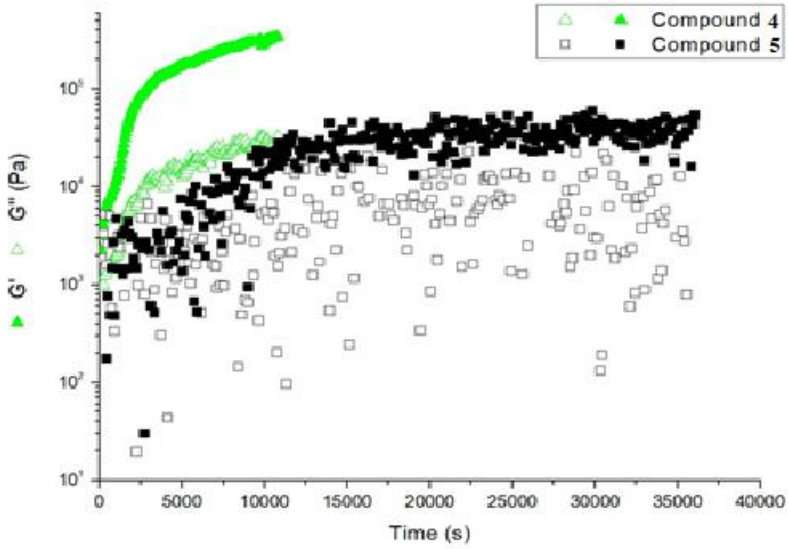

Figure 41: Elastic (G')and viscous (G'') moduli during the kinetic process of gelation for compound **4** and **5** 0.2wt%.

Dehydrotripeptide **4** displays a G` (storage/elastic modulus) significantly higher than G` ` (loss/viscosity modulus) after 2.8 hours, which indicates that the hydrogels form relatively fast, within the same time frame of other hydrogels based on ultra-short dehydropeptide. When compared with the hypergelator Fmoc-Lys(Fmoc)Asp-OH the latter shows a similar kinetics of 2.5 hours (38). Compound **5** has slower gelation kinetics, taking more than 4 hours to reach the maximum G' value. This means that the gelation process is almost twice as long as that observed with dehydrotripeptide **4**. The kinetics of hydrogelation is a very important parameter to be taken into account for biomedical applications since hydrogels with relatively fast kinetics can be injected as solutions and undergo a sol-gel transition inside the body. These kinds of injectable hydrogels are designated as *in-situ* hydrogels (74). The dehydrotripeptide **4** is a good candidate for this kind of application, since the gelation time is relatively fast.

After reaching the structural equilibrium, established by reaching the maximum G` and G` ` values with time (**Figure 41**), a frequency sweep from 100Hz down to 0.1 Hz was performed with a strain of 0.001% to give the mechanical spectra displayed in **Figure 42**.

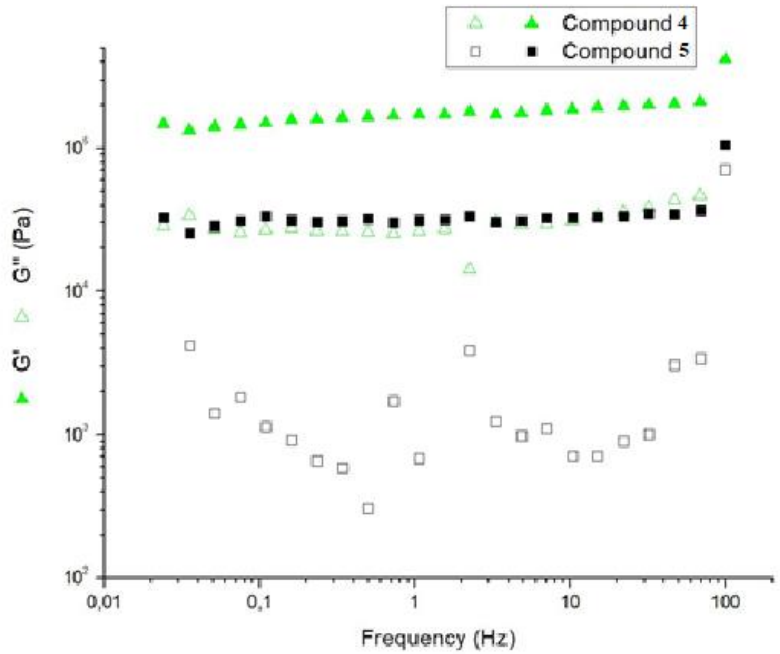

Figure 42: Frequency dependence of the shear elastic G' and G'' moduli for the compounds **4** and **5** at 0.2wt%.

For both hydrogels from dehydrotripeptides **4** and **5**, G` is essentially constant over the frequency domain tested, whereas G` ` of dehydrotripeptide **5** displays a local minimum. Generally, all mechanical spectra are qualitatively similar, suggesting that the elastic network responsible for the hydrogels

mechanical response share structural similarities. As expected, the G` is higher than G`` for both hydrogels (**Table 7**).

Table 7: G' and G'' for hydrogel **4** and **5** at 0.2wt%.

Hydrogel	G' (Pa)	G'' (Pa)
4	3.43×10^{6}	2.49×10^{4}
5	5.44×10^{4}	7.94×10^{3}

According to the G' values presented in **Table 7**, the hydrogel from dehydrotripeptide **4** is stiffer (more elastic) than **5** (higher G`). The hydrogel obtained from Fmoc-Lys(Fmoc)-Asp-OH has a G` value below 1×10^{4} Pa at 0.5 wt% below both G` values of hydrogels **4** and **5** at 0.2 wt% (38). Thordarson and coworkers reported an exceptionally strong hydrogel based on a *N*-capped fenilalanylfenilalanine with a G` of 3×10^{5} (101). The G` value of dehydrotripeptide **4** is significantly higher.

After the frequency sweep, the hydrogels of **4** and **5** were submitted to a strain sweep, where the frequency was maintained at 1 Hz (**Figure 43**).

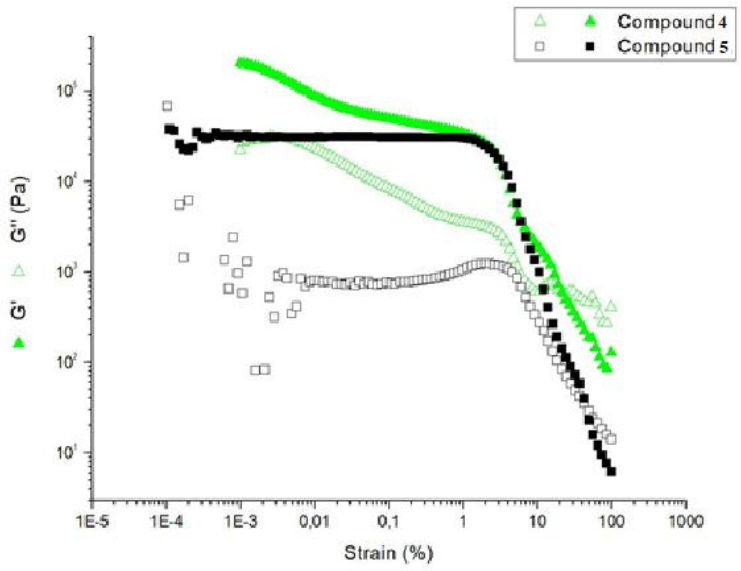

Figure 43: Strain dependence of the shear elastic G' and loss G'' moduli for compound **4** and **5** at 0.2 wt%.

The hydrogel of dehydrotripeptide **4** breaks up more easily than the hydrogel from **5**, breaking up at a strain of 21.5 % and 55.5 %, respectively. These results alone suggest that the thickness of the nanofibers have a direct correlation with the strength of the gel, since hydrogels of **5** possess thicker fibers than hydrogels from **4** (**Figure 37**).

Finally, a second kinetics was measured for ten minutes after the breakup (**Figure 44**). In both cases, it was possible to measure a second kinetics, which means that both hydrogels of **4** and **5** are self-healing hydrogels. Consequently, both these gels are expected to be injectable. These hydrogels flow like a low-viscosity fluid under shear stress during injection, but quickly self-heal after the removal of the shear stress, regaining their initial stiffness or reforming with a lower stiffness. This behavior results from the reversible properties of the physical crosslinks.

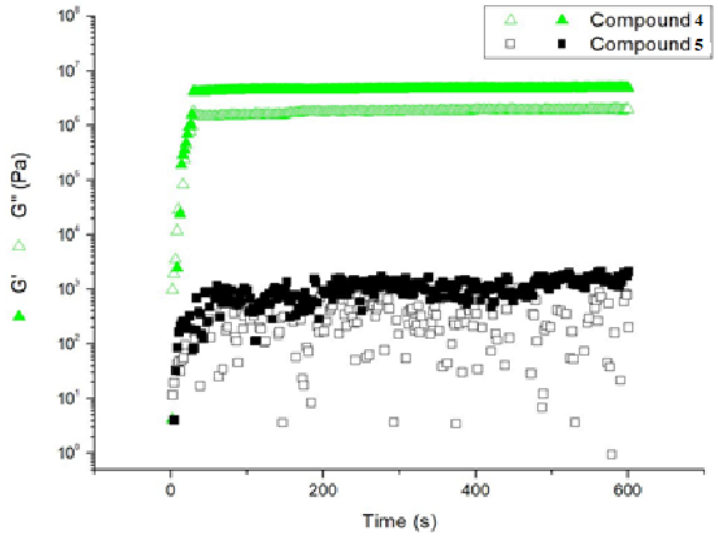

Figure 44: Elastic and viscous modulus during the second kinetic process of gelation for compounds **4** and **5** 0.2wt%.

From **Figure 44** it is possible to observe that the hydrogel obtained from dehydrotripeptide **5** reforms within one minute after the breakup, with a G` value of 1.38 x 10^3 Pa and a G`` value of 505 Pa. The lower G' values are expected following self-healing. The hydrogel from dehydrotripeptide **4** reformed under one minute and presented a G` value of 4.91 x $10^6$ Pa and a G`` value of 1.93 x 10^6 Pa. Interestingly, the G` value of the reformed hydrogel is higher than the initial G` value. This means that after the hydrogel is broken, it self-heals into a more elastic hydrogel, which to the best of our knowledge, has never been reported for supramolecular hydrogels. To explain this result, it was considered that dehydrotripeptide **4** could undergo a multistep self-assembly, where the formation of small aggregates competes with the formation of hydrogel fibers. This was already described for the hypergelator Fmoc-Lys(Fmoc)-Asp-OH which exhibited a morphological transformation from spheres to fibers over time, suggesting a molecular rearrangement of the gel structure (38). Moreover, the STEM images of the hydrogel of dehydrotripeptide **4** show a network of fibers together with spherical aggregates. A plausible rationale is that the initial hydrogel has both fibers and spherical aggregates and the aggregates are very slowly being converted into fibers, and by agitating and breaking the gel this process

is accelerated, by breaking both the fibers and the aggregates, which self-assemble a second time, this time as fibers only (**Figure 45**). This hypothesis would also explain why the hydrogel does not self-heal after breaking a second time. Additionally, if the assembly of compound **4** is a two-step process, it means that the first G` value observed in **Figure 41** would not be the final value, but instead the G` value of **Figure 44** would be the final one.

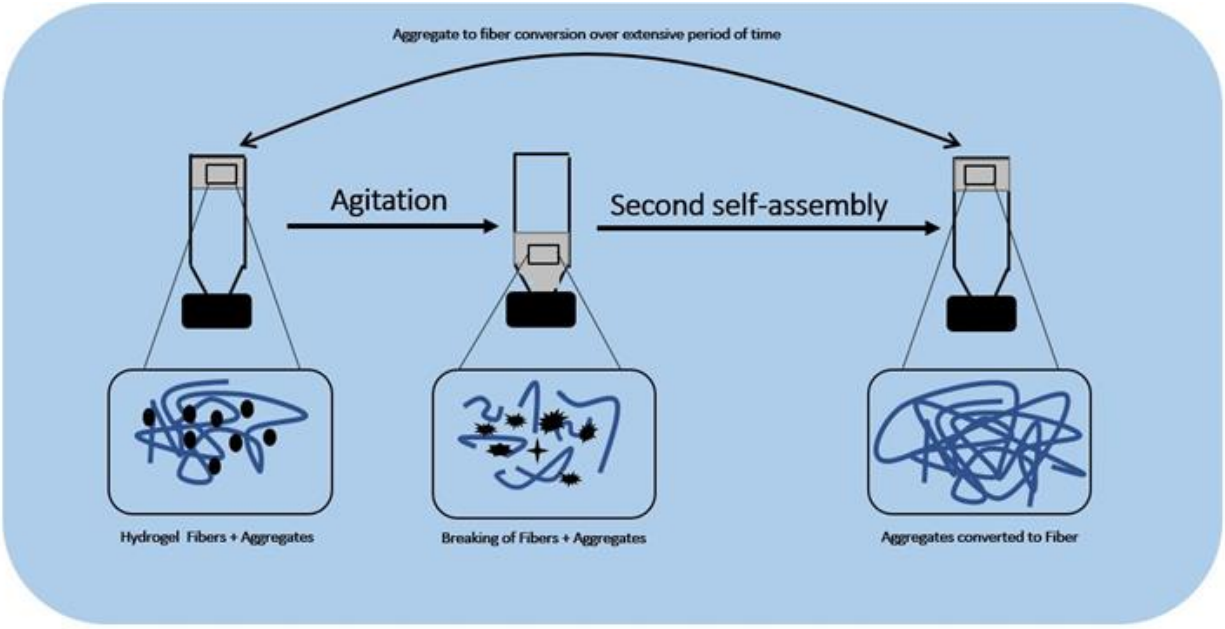

Figure 45: Illustrative scheme of the hypothesis for the second assembly of hydrogelator **4**.

Although this hypothesis explains the results obtained, it is important to bear in mind that both hydrogelators **4** and **5** are diastereomeric mixtures.

2.3 Hydrogelation properties of dipeptides targeted to the folate receptor

Two dipeptides studied were recently described by Huang *et al.* (92) and identified as ligands for the folate receptor (**Figure 46**). Since these compounds have a similar structure to the other small peptide hydrogelators we decided to study their ability to self-assemble. A folate receptor ligand as a hydrogelator is an interesting concept, as it potentially provides an opportunity to selectively target drug delivery to cancer cells, as these over-express folate receptors (92). These compounds contain D-4-benzylphenylalanine and D-homophenylalanine which are unusual amino acids - unnatural in both basic structure and enantiomeric configuration – and should provide enzymatic resistance. Their aromatic side-chains should make them ideal building blocks for self-assembly. Furthermore, the capping group of **6** is naproxen (**Figure 46**), a non-steroidal anti-inflammatory drug (NSAID). Naproxen has been successfully

incorporated into the structures of peptide hydrogelators previously, often resulting in retained or improved anti-inflammatory activity (26). The capping group of **7** is indole 3-propionic acid, which itself is an antibiotic.

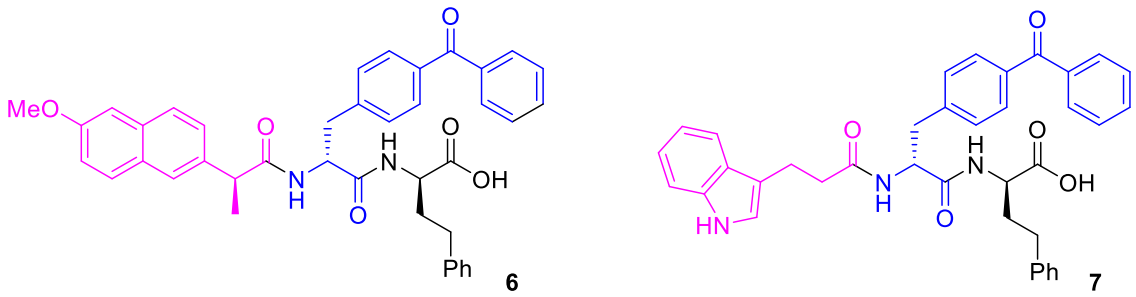

Figure 46: Structure of the dipeptides targeted to the folate receptor (92).

2.3.1 Synthesis of dipeptides 6 and 7

Dipeptides **6** and **7** were prepared according to a modified version of the procedure described by Huang *et al.* (92) (**Scheme 8**). Starting from D-homophenylalanine (H-D-HPhe-OH), an initial esterification using thionyl chloride in methanol afforded the corresponding methyl ester (H-D-HPhe-OMe). This reaction was followed by an amide coupling reaction with Boc-4-benzoyl-D-phenylalanine (Boc-D-BPhe-OH) in the presence of HBTU to afford Boc-D-BPhe-D-HPhe-OMe in 87% yield . The removal of the Boc group was achieved with trifluoroacetic acid. A second HBTU-mediated amide coupling with either (S)-naproxen (Npx) or 3-indolepropionic acid (Ind), afforded the *N*-capped dipeptides that after a basic hydrolysis gave the folate ligands **6** and **7**.

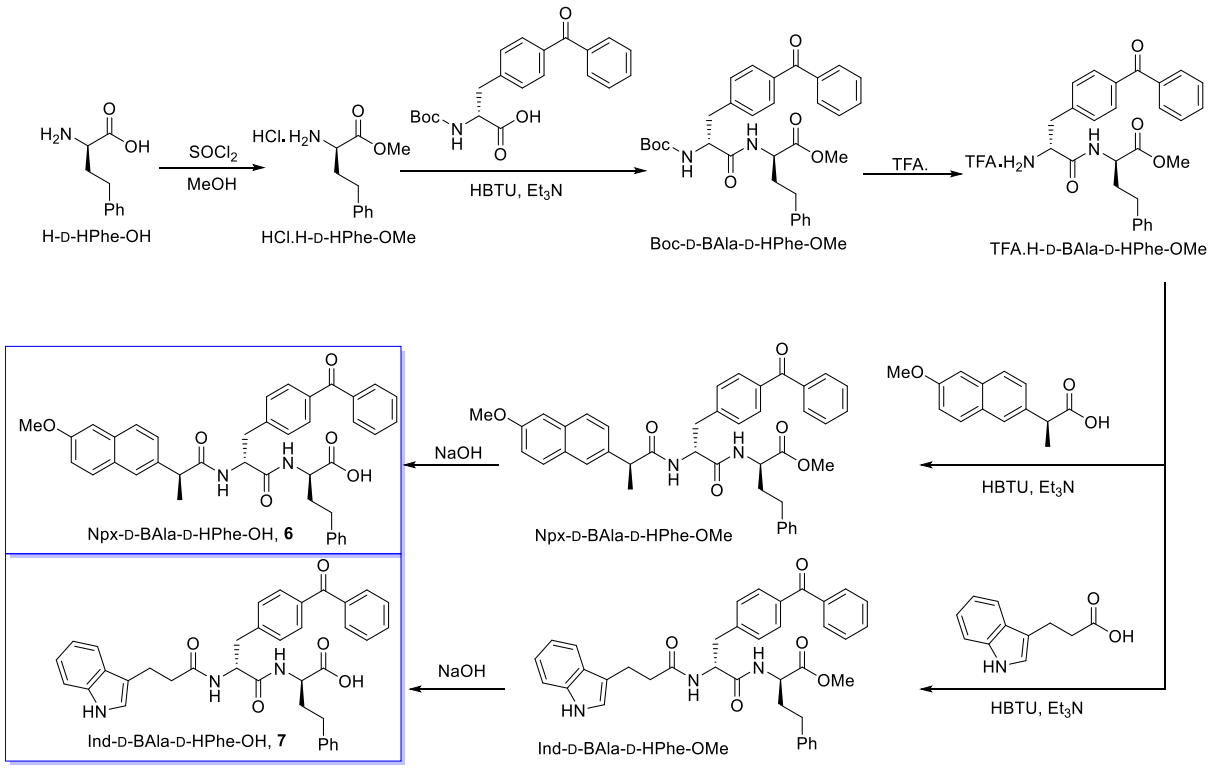

Scheme 8: Synthesis of the folate receptor ligands **6** and **7** (92).

The proton ^{1}H NMR spectrum of the dipeptide **6** in DMSO-d_6 (**Figure 47**) shows a three-proton doublet at 1.55 ppm that corresponds to the CH_3 of the naproxen, and also a three-proton singlet at 3.84 ppm, which is attributed to the OCH_3 of the naproxen.

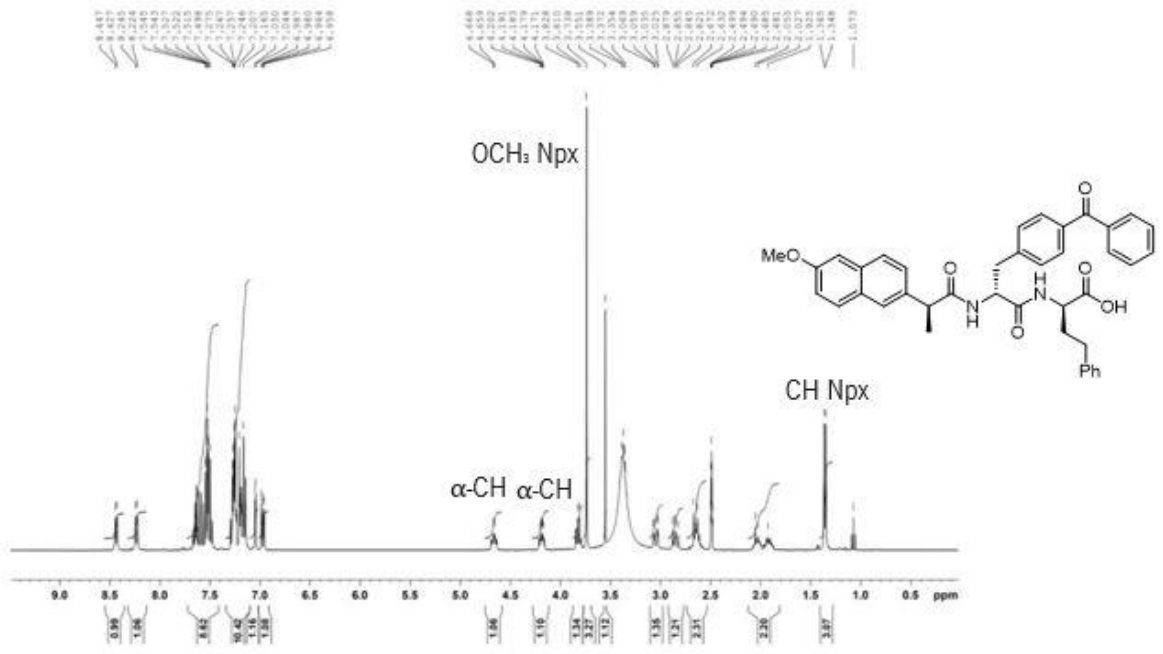

Figure 47: ^{1}H NMR spectrum of compound **6** in DMSO-d_6.

The proton ^{1}H NMR spectrum of the dipeptide **7** in DMSO-d_6 (**Figure 48**) displays a four-proton multiplet at 2.50-2.67 ppm, which corresponds to the CH_2 protons of the indole moiety and also to the γ-CH_2 of HPhe. In addition, it shows another four-proton multiplet, attributed to the other CH_2 protons of the indolyl group, and the β-CH_2 of BPhe.

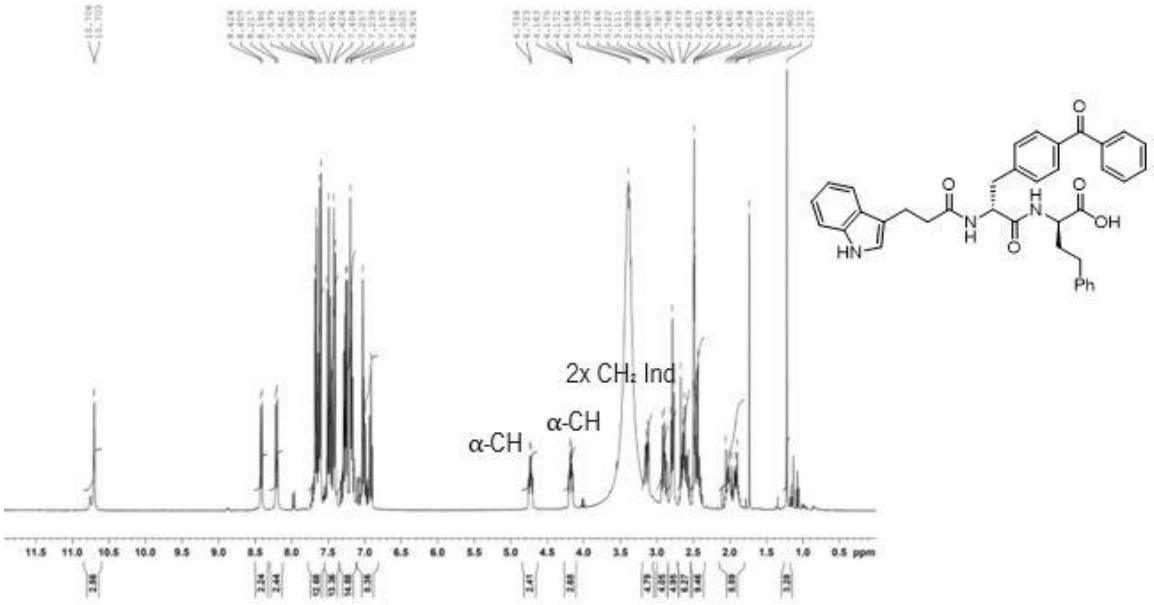

Figure 48: ^{1}H NMR spectrum of compound **7** in DMSO-d_6.

2.3.2 Preparation of hydrogels

The dipeptides **6** and **7** revealed limited solubility in buffer solutions in the physiological pH range (6.0-8.0). However, they were soluble in water upon pH adjustment to pH 10, by the addition of sodium hydroxide solution (1 M). Hydrogelation was attempted by the addition of D-glucono-δ-lactone (GdL). Compound **6** gave a self-standing hydrogel with a CGC of 0.03 wt% (0.5 mM; pH 5.5) (**Figure 49**). Although the calculated LogP of compound 5 is between 2.5 and 5.5 (4.34), this compound failed to give hydrogels using pH as trigger (**Table 8**). When compared with other dipeptides N-capped with naproxen, compound **6** show a considerably lower CGC (**Table 8**).

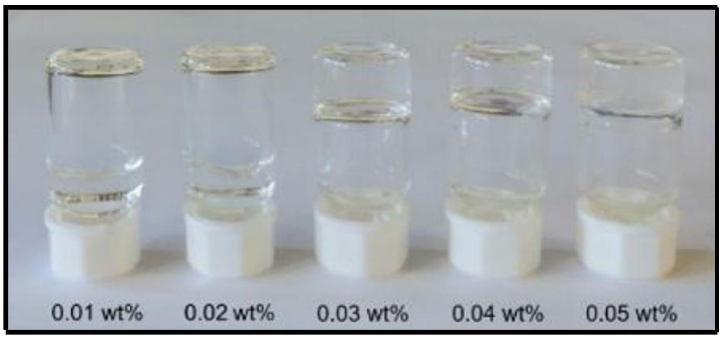

Figure 49: Optical images of hydrogelator **6** in concentrations ranging from 0.05wt% to 0.01wt%.

Table 8: CGC of compounds **6** and of several N-capped dipeptides reported in the literature.

Peptide	**Critical Gelation Concentration (CGC)**		**pH**	**cLogP***
	wt%	mM		
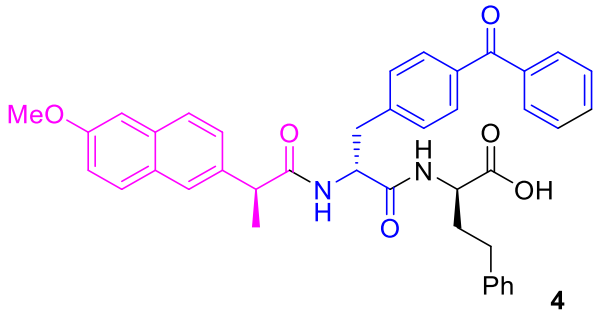 **4**	0.03	0.0005	5.5	5.69
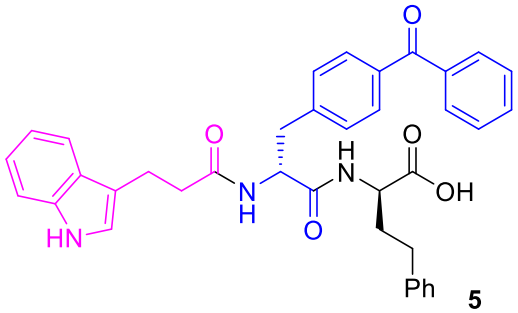 **5**	No hydrogel			4.34
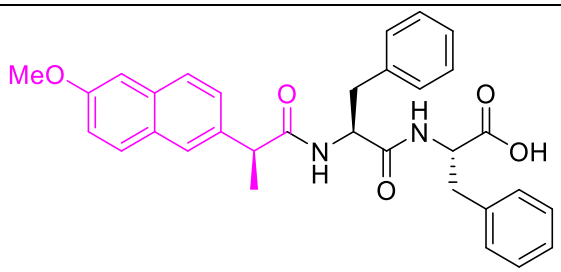	0.8	0.02	4.0	3.71

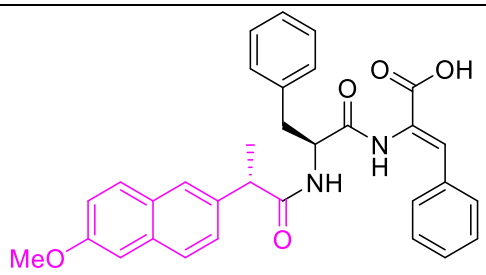	0.4	0.008	8.0	5.84
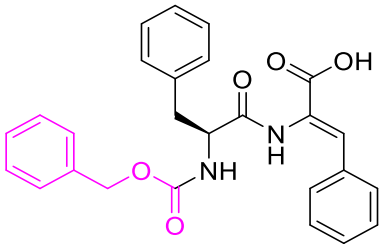	0.1	0.002	5.0	4.14

*cLogP value obtained from https//molinspiration.com

The CGC for compound **6** is lower when compared with the CGC of other *N*-capped dipeptides reported (**Table 8**) including dipeptide **1**. However, the value reported for the CGC of compound **6** is higher than the values reported for the hypergelator Fmoc-Lys(Fmoc)-Asp-OH (0.002 wt%, **Figure 21**) (38). As already mentioned, although the gelation conditions were not the same, the results point to the fact that the presence of two fluorenylmethoxycarbonyl groups in the structure of the dipeptide together with the two carboxylic acid moieties from Asp impart to this compound the ideal conditions to establish intermolecular bonds and to self-assemble at very low concentrations.

2.3.3 STEM

The STEM images of compounds **6** and **7** are shown in **Figure 50**.

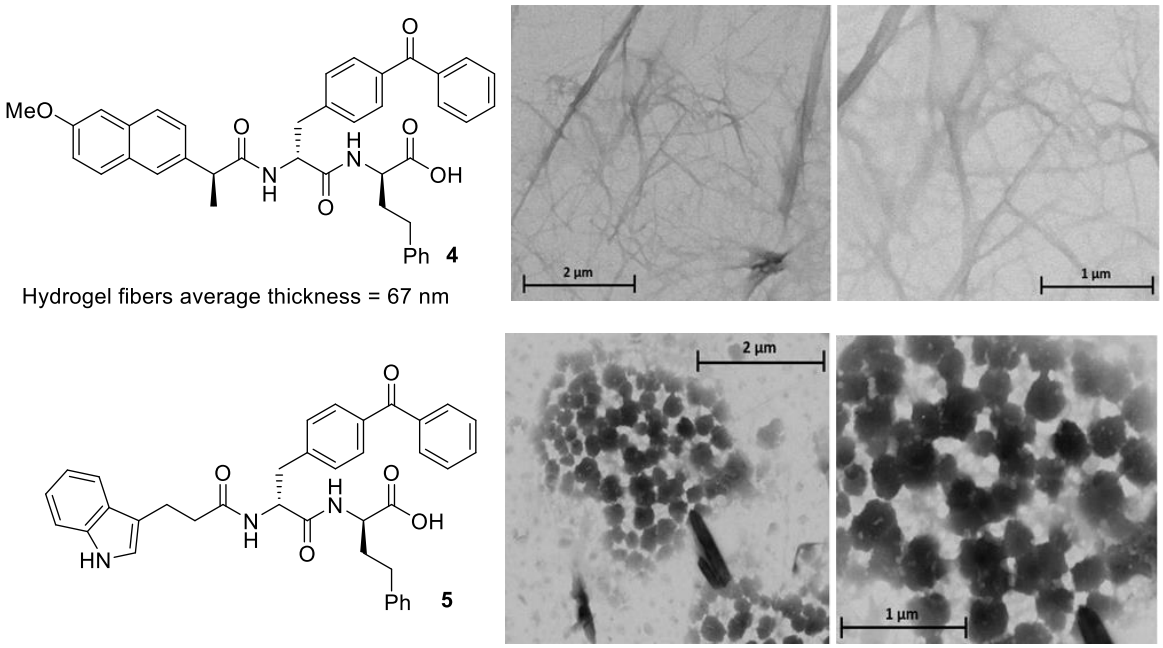

Figure 50: STEM images of compounds **6** and **7** at 0.2 wt%.

Compound **6** displays interlaced fibers that assemble into a 3D-network that can entrap water. The structure is similar to that observed for other hydrogels based on N-capped dipeptides. The STEM images of dipeptide **7** (**Figure 50**) revealed that this compound self-assembles into small spherical aggregates. This structure could be the reason for dipeptide **7** fail to give a self-standing hydrogel.

2.3.4 Circular Dichroism

The CD spectrum of dipeptides **6** and **7** displays a similar shape for both compounds, with negative bands at 213 nm and 220 nm, respectively (**Figure 51**). This data also points to a β-sheet aggregation pattern.

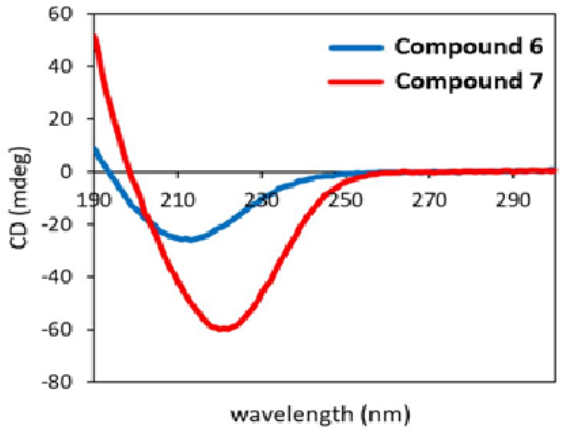

Figure 51: CD spectra of diluted aqueous solutions of compounds **6** and **7** (0.01 wt%).

2.3.5 Rheological studies

In **Figure 52** is represented the gelation kinetics of dipeptide **6.**

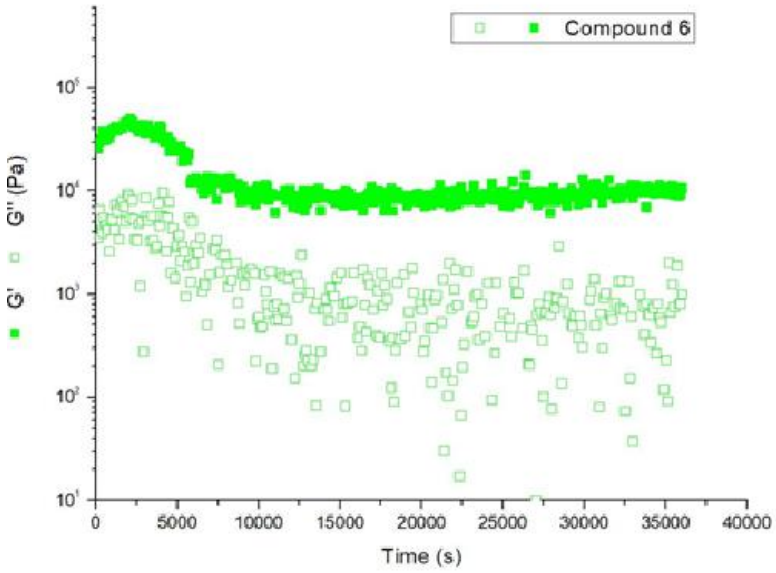

Figure 52: Elastic and viscous modulus during the kinetic process of gelation for compound **6** at 0.2wt%.

The data for dipeptide **6** displays an immediate increase in G` (storage or elastic modulus) relative to G` `(loss modulus or viscosity), which is unusual. Also, the general shape of the graph is unusual for a supramolecular hydrogel kinetics, and to the best of our knowledge, no spectral data similar to this has been reported for this type of hydrogels. This could be explained by the extremely fast gelation observed for dipeptide **6**. Therefore, it is likely that the hydrogel has already formed during the lag time required to the rheometer to begin taking the measurements making impossible to measure the kinetics.

After reaching the structural equilibrium established by the reading of G` and G`` with time, a frequency sweep from 100Hz down to 0.1 Hz was performed with a strain of 0.001% to give the mechanical spectra displayed in **Figure 53**.

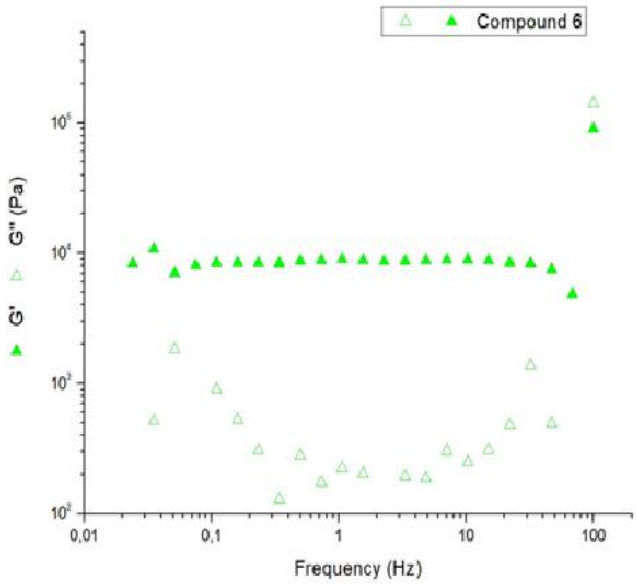

Figure 53: Frequency dependence of the shear elastic G' and G'' moduli for the compound **6** at 0.2wt%.

As seen with the previous dehydropeptide hydrogels, hydrogel **6** displays G` values which are constant over the frequency domain tested, whereas G`` values show a slight decrease. Hydrogel **6** has a G` value of 1 x $10^3$ Pa and a G`` value of 250 Pa. Comparing the G` of this hydrogel with the dehydropeptide hydrogels, it is possible to verify that this hydrogel has an elasticity higher the dehydrodipeptides **1-3**, but lower than both dehydrotripeptides **4** and **5**.

After the frequency sweep, the hydrogel of **6** was also submitted to a strain sweep, where the frequency was maintained at 1 Hz (**Figure 54**).

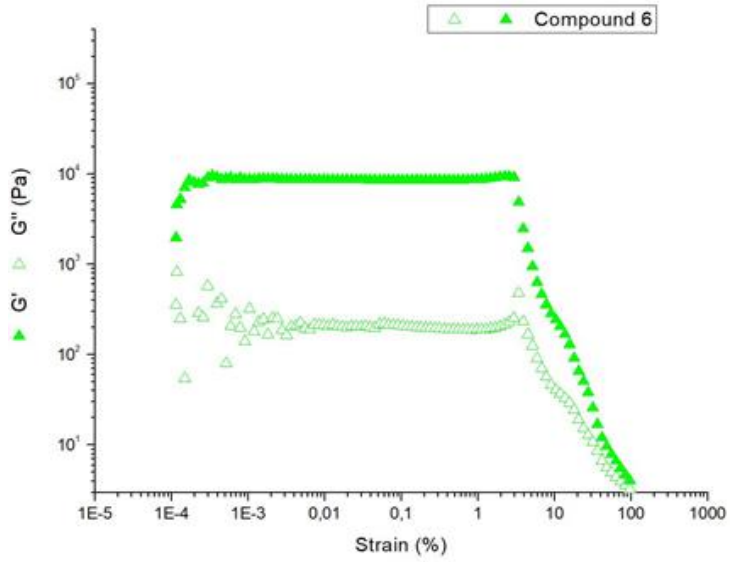

Figure 54: Strain dependence of the shear elastic G' and loss G'' moduli for compound **6** at 0.2 wt%.

The hydrogel of peptide **6** breaks up at 101% strain. Interestingly, this hydrogel is the one with the best elasticity/strength balance. The hydrogel from compound **1** has a comparable resistance to strain, but the hydrogel **6** has a significantly lower G` value, which makes it less elastic. The hydrogel from **4** has a higher G`but breaks up significantly easier.

Finally, a second kinetics was measured for ten minutes after the breakup (**Figure 55**). In this measurement, it is possible to see that in less than one minute the hydrogel self-heals with a lower value of G` (256 Pa). This highlights the hydrogel capacity to be injectable. Not only it can be injected in a liquid form and undergo a sol-gel transition inside the body, due to the fast kinetics, but also can be pre-gelled outside of the body and then injected by application of shear stress.

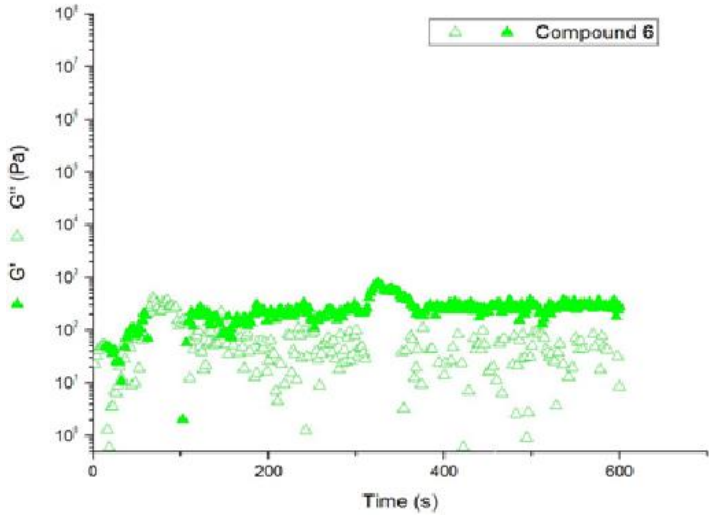

Figure 55: Elastic and viscous modulus during the second kinetic process of gelation for compound **6** at 0.2wt%.

2.3.6 Drug release assays

Hydrogels of peptide **6** were studied for their capability to release the model compounds: methylene blue (MB), methyl orange (MO) and ciprofloxacin (**Figure 56**) The release of each cargo molecule from the hydrogels was assessed using UV-Vis spectroscopy and HPLC (**Table 9, Figure 57**).

Figure 56: Representative images of hydrogels **6** layered with water after a saturating release study (7 days) loaded with MO (left), MB (centre) and ciprofloxacin (right).

Table 9: Percentage release of cargo from hydrogels **3** and **6** after 7 days.

Hydrogelator	MB released (%)	MO released (%)	Ciprofloxacin released (%)
6	0.8	40.3	18.1

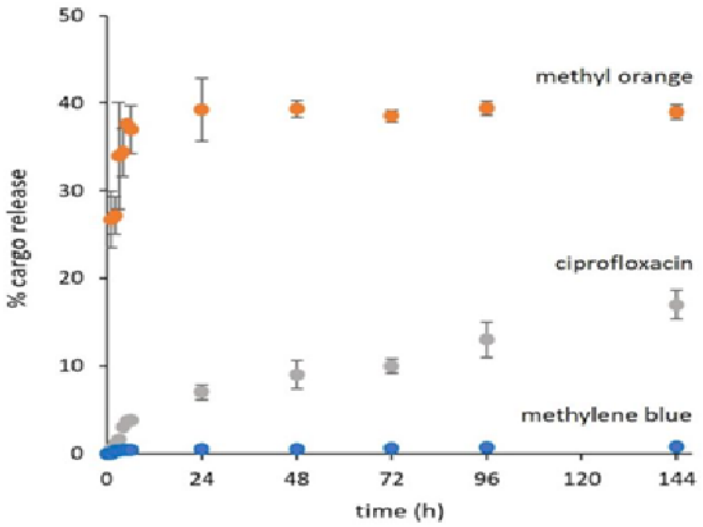

Figure 57: Percentage of cargo release vs time over 7 days. Release of methylene blue, methyl orange and ciprofloxacin from hydrogel **6**.

The values obtained for the release of the three model compounds are similar to those obtained

for the hydrogels of compound **1**. The application of the Korsmeyer-Peppa's model to the release of the cargo from the hydrogel **6** (**Figure 58, Table 10**) shows that release of ciprofloxacin is associated with a diffusion-controlled release mechanism and the release of methyl orange is more efficient for hydrogels from **6** than for hydrogels based on the dehydrodipeptide **1** (higher K and lower n).

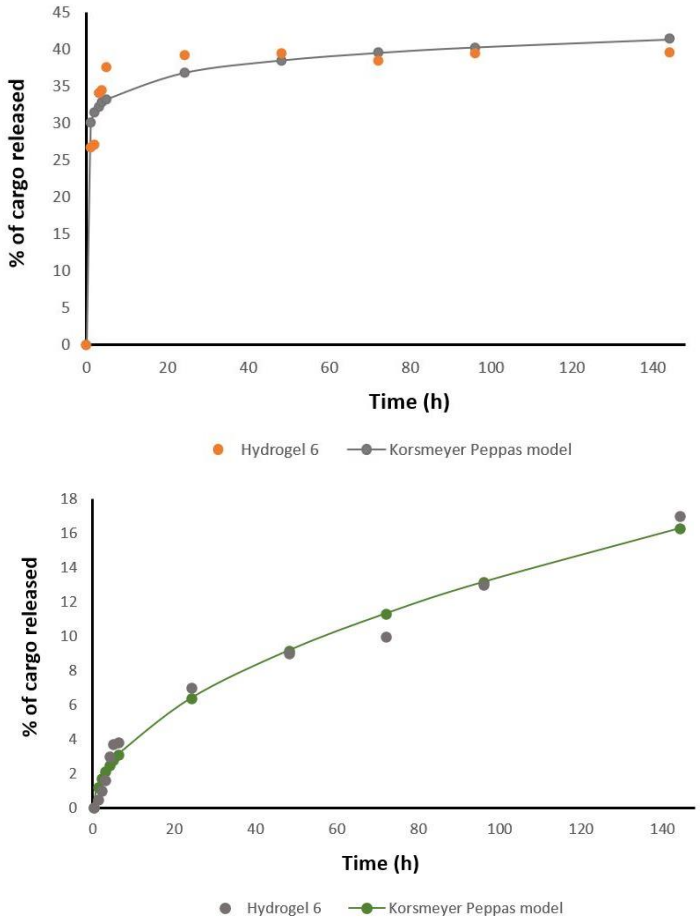

Figure 58: Data to Korsmeyer-Peppas Model to describe the release kinetics of (A) MO of hydrogel from **6**, (B) ciprofloxacin of hydrogel from **6**.

Table 10: Release coefficients of the Korsmeyer-Peppas model obtained for methyl orange and ciprofloxacin release profiles of hydrogels **6**.

Cargo	k	n	R^2
Methyl Orange	29.9747	0.0648	0.9763
Ciprofloxacin	1.2063	0.5236	0.9901

2.4 Biocompatibility and Cytotoxicity studies

All seven compounds prepared were evaluated for their potential impact on the viability of human keratinocytes, namely the HaCaT cell line. The results generally show that peptides **1** and **4-7**, show a significant impact in cell viability, while peptides **2** and **3** show almost no impact at all (**Figure 59**). Interestingly, peptides **5** and **6** exhibited a similar behaviour, with most concentrations tested eliciting a significant apparent loss of cell viability of around 40%, which was independent of concentration. In addition, peptides **5** and **7** also display a significantly loss of cell viability of 40%, but only at higher concentrations, being 50 μM and 25 μM, respectively. Also, dehydrodipeptide **1** reveals a clear higher impact on cell viability loss with the increase of peptide concentration, reaching a maximum of around 30% loss at 100 μM. Finally, peptides **2** and **3** were mostly devoid of any effect, with **3** showing a very small loss of cell viability of less than 10%.

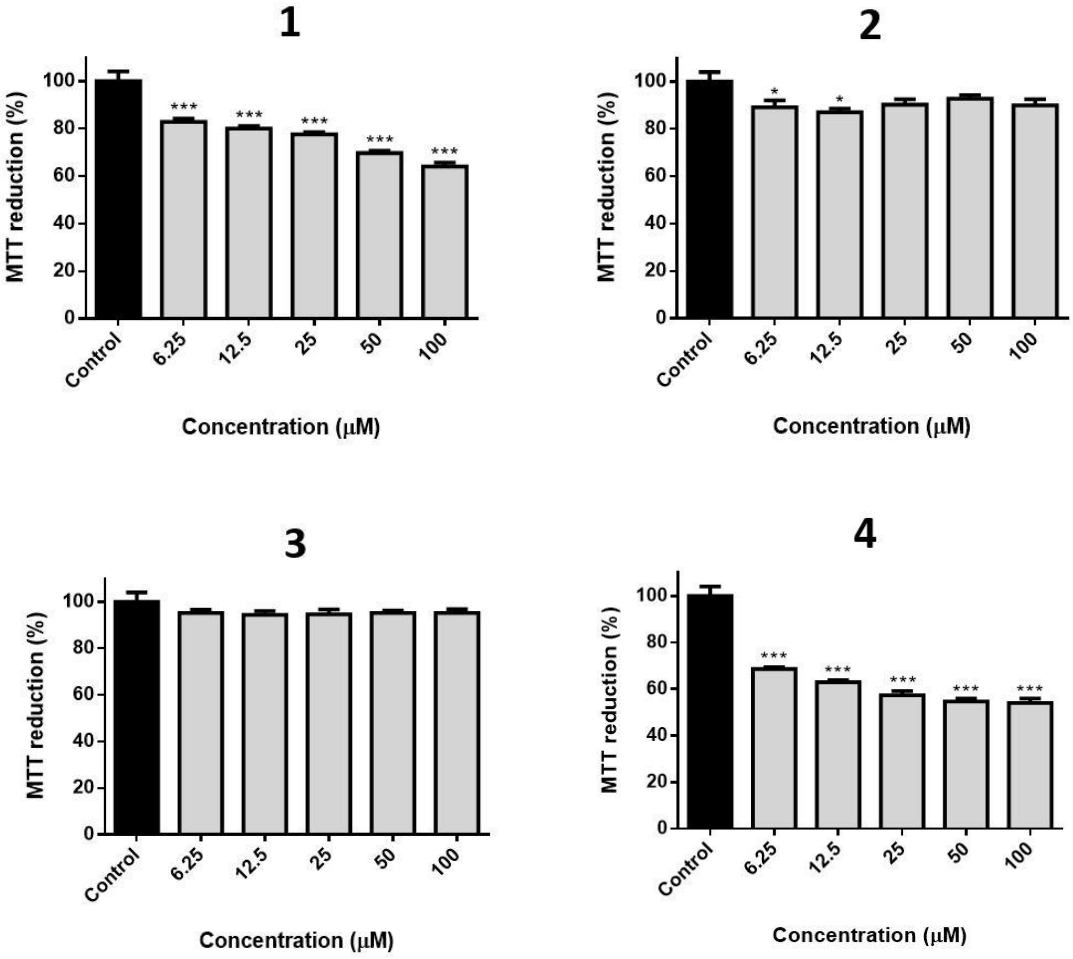

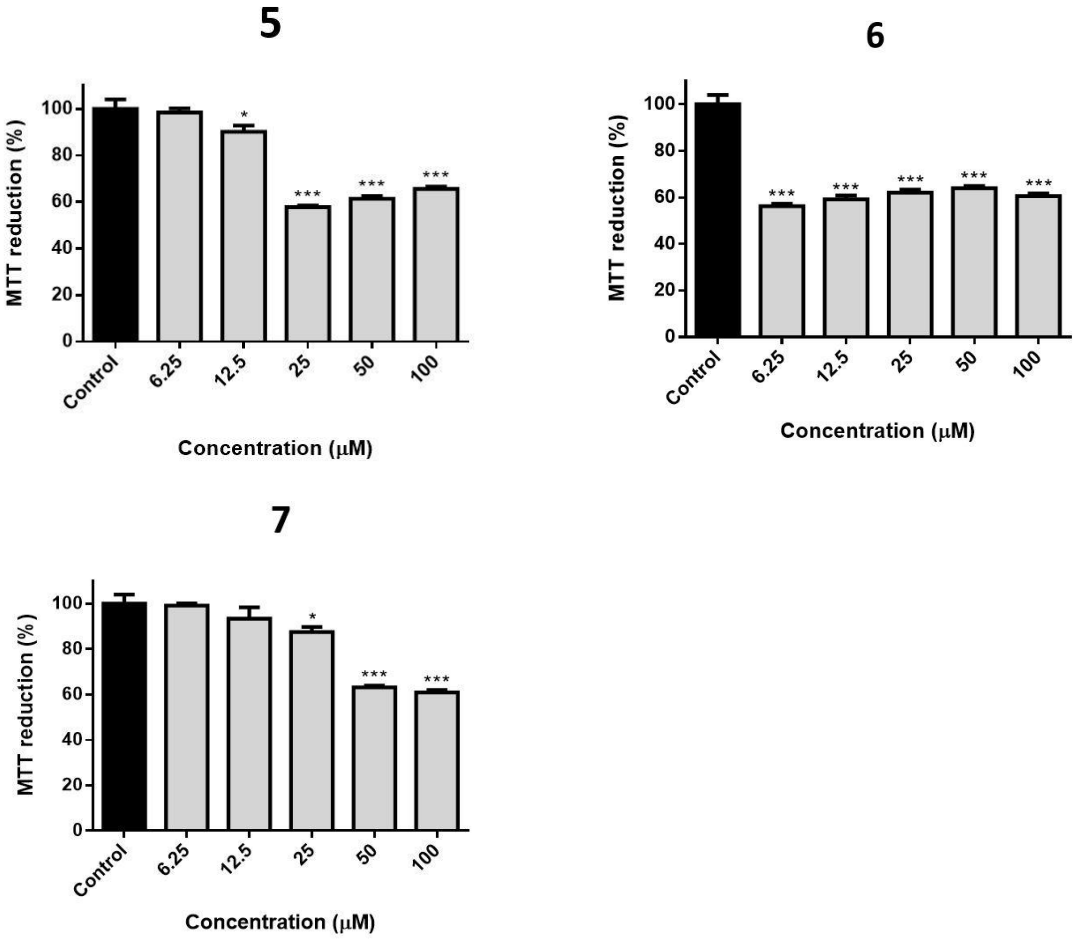

Figure 59: Viability of HaCaT cells treated with **1-7** for 24h, at the concentrations presented. *p<0.05, ***p<0.001.

Generally, all seven compounds did not show a critical cell viability loss, which suggests that all peptides are good for further studies for biological applications. Although a direct correlation between the structure of the peptides and the loss of cell viability cannot be established, it is safe to point out that from all compounds synthesized, the dehydrodipeptides **1-3** were the best ones, suggesting that the structure of these dipeptides is optimal regarding cell viability. Between the three dehydrodipeptides, it is possible to establish a direct relation between the aromatic capping groups and the loss of cell viability. The results suggest that the presence of Naph groups (**1**) in the Lys residue, decreases cell proliferation, while the presence of Cbz groups (**2**/**3**) has no/very small effect on cell proliferation. Further studies should be conducted to fully conclude if Cbz protecting groups are optimal for cell viability and the cause of the loss of cell viability when the Lys is protected with Naph groups.

Due to the small effect in cell viability, it was necessary to evaluate if the molecules could be eliciting necrosis in treated cells. To investigate this, the lactate dehydrogenase (LDH) release assay was conducted. Briefly, LDH is a cytosolic enzyme which presence in culture media is widely used as a suggestion that cells have lost membrane integrity, a hallmark of necrosis. As showcased in **Figure 60**, none of the peptides elicited loss of membrane integrity in the concentrations tested.

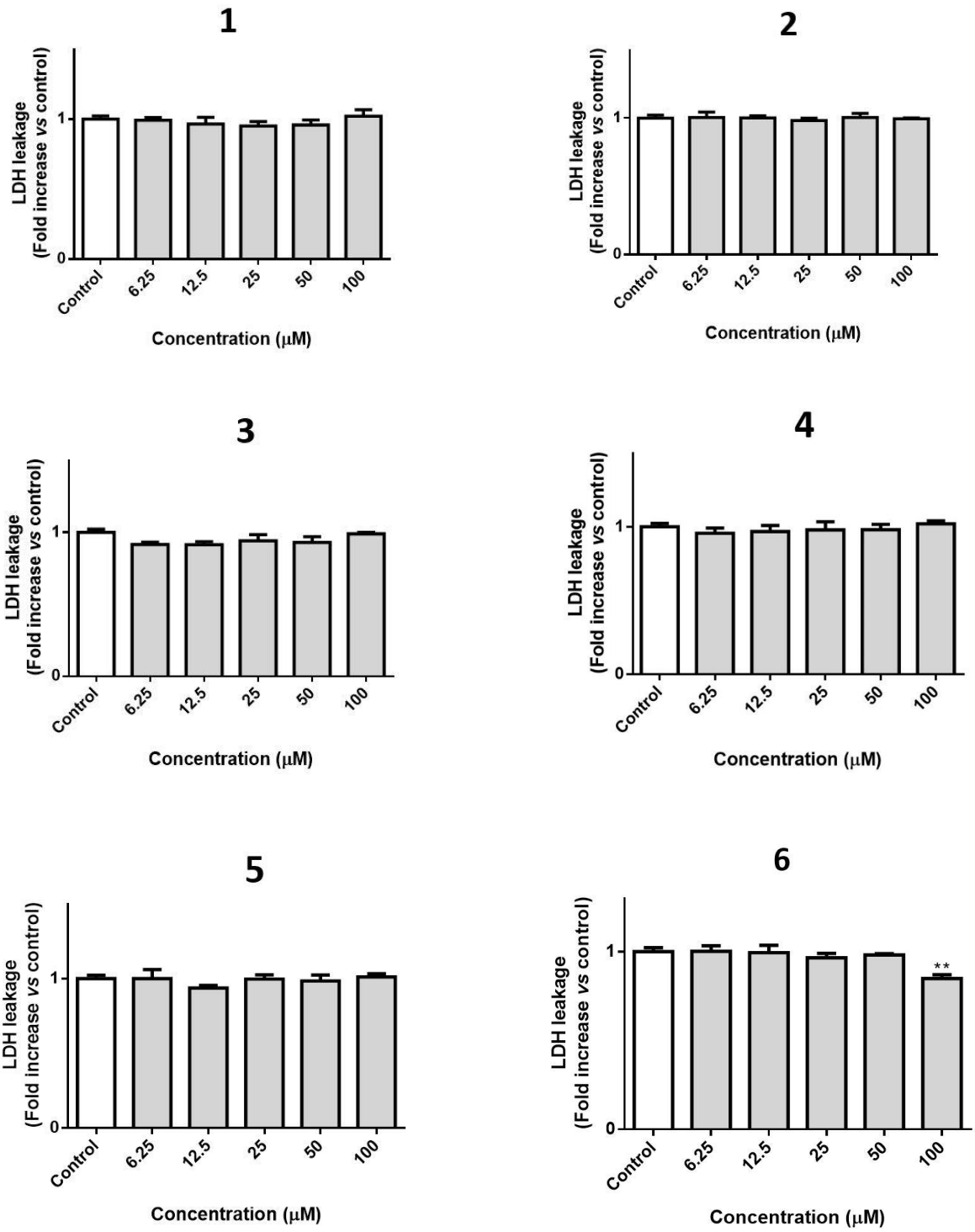

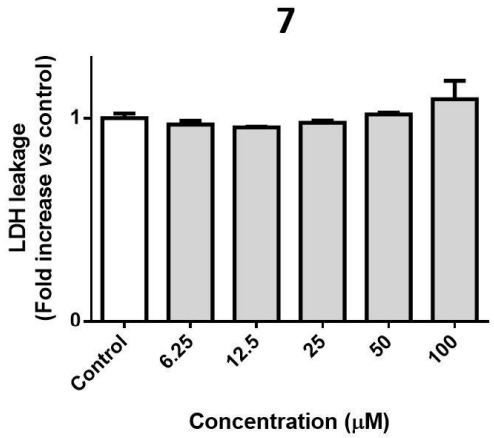

Figure 60: LDH activity found in the culture media of HaCaT cells treated with **1-7** for 24h, at the concentrations presented. Triton X-100 was used as positive control to lyse cells.

In general, the results suggest that all seven compounds are not cytotoxic, although some peptides have shown a small impact in cell viability. To fully conclude this, further characterization should be conducted as MTT viability assays have some drawbacks, one being that the absorbance values depend on the number of cells in each well. In order to clarify if the loss of viability identified could be related with fewer cells in hydrogelator-treated wells, the impact of the in-cell DNA and protein content should be evaluated in the future, as a strategy to identify potential changes in cell proliferation and thus total number of cells.

Chapter 3

Conclusions and Prospects

3 Conclusions and Prospects

In this work we describe the synthesis, characterisation, and gelation properties of seven new non-natural di- and tripeptides, which can be further divided into three sub-classes:

1) dehydro*di*peptides with a lysine residue *N*-capped with different aromatic moieties,
2) dehydro*tri*peptides also with a *N*-capped lysine residue and an aspartic acid residue with a free carboxylic acid, and
3) non-canonical D-dipeptides *N*-capped with two different aromatic groups.

For the first two groups, the unsaturated amino acid residue employed was dehydrophenylalanine, which had been previously studied by the research group. Six of the seven compounds synthesized are efficient hydrogelators, producing hydrogels with ultralow critical gelation concentration values between 0.2 - 0.03 wt%. The rheological properties of the new hydrogels displayed a storage modulus (G`) significantly higher than the loss modulus (G``), which confirmed a viscoelastic behaviour characteristic of supramolecular hydrogels. In addition, the rheological data showed that some of these hydrogels were self-healing. Scanning transmission electron microscopy revealed that all hydrogels display fibrillar structures. Also, in the particular case of the dehydrotripeptide Naph-Lys(Naph)-Asp-ΔPhe-OH, the images also showed small spheres/aggregates in between the fibers, which could be associated with a multi-step self-assembly in which the spheres slowly convert to fibers.

The two non-canonical D-configured dipeptides showed very different gelation properties, despite being very similar in structure. This result was corroborated by STEM microscopy, with the images of the successful gelator revealing fibres, whereas the dipeptide which failed to produce a hydrogel showed a self-assembly of the molecules into vesicle-like nanostructures.

The biocompatibility of these peptides was evaluated by cytotoxicity assays. The peptides were initially evaluated for their potential impact on the viability of human keratinocytes (HaCaT cell line). Generally, the results suggest that the peptides synthesized are not cytotoxic, despite having small impact in cell viability.

Lastly, in sustained release assays, the effects of the charge present on model drug compounds on the rate of cargo release from the hydrogel networks was studied using cationic (methylene blue), anionic (methyl orange) and neutral cargo (ciprofloxacin). Generally, the hydrogels retained methylene blue inside the hydrogel network, released 40% of methyl orange after 7 days, and 20% of ciprofloxacin after 7 days.

For the future, a lot of new perspectives and findings can be made by exploring these peptides. First, molecular dynamic simulations should be performed to better understand all the different self-

assembly patterns observed for the peptide hydrogelators described in this work. These simulations could also provide clues to explain why the dipeptide *N*-capped with the indol moiety was not able to provide a hydrogel. New rheological tests should be performed on all peptides synthesized, to assess if they are thermally reversible. In the particular case of dehydrotripeptides, new rheological test should be performed giving more time to measure the first kinetic, with the end goal of better understanding the self-assembly mechanism of these compounds. A new synthetic methodology to prepare the tripeptides should be carried out in order to obtain the pure diastereomer. Also, a new drug delivery tests should be performed, using a range of hydrogelator concentrations, to assess if there's an optimal concentration of gelator for sustained cargo release.

The main objective of these studies is to develop simple peptide molecules, which are efficient drug delivery systems and are free of any cytotoxicity, requiring low concentrations to produce hydrogels, and are easily injectable.

Chapter 4

Experimental procedures

4 Experimental procedures

4.1 Reagents and instrumentation

Analytical grade reagents were purchased from Sigma-Aldrich and Acros and used without further purification. Analytical grade solvents were used and dried by standard methods when required. Petroleum ether • refers to the fraction having a boiling point of 40-60 °C. Distilled water was used when aqueous medium was needed. The reactions were monitored by thin layer chromatography (TLC) on Merck-Kieselgel plates 60 F254 and detection was made by examination under UV light (240 nm) or by adsorption of iodine vapour. Organic phases were dried using anhydrous magnesium sulfate (Riedel). Chromatographic separations were performed on silica MN Kieselgel 60 M (230-400 mesh).

The ^{1}H and ^{13}C NMR spectra (assigned by DEPT, HSQC and HMBC techniques) were recorded on a Bruker Avance III 400 spectrometer, operating at 400.13 MHz and 100.62 MHz, for ^{1}H and ^{13}C NMR respectively. NMR spectra were recorded at 25 °C and in some cases at 80 °C, using the residual solvent signals as reference. Deuterated dimethyl sulfoxide (DMSO-d_6) and deuterated chloroform ($CDCl_3$) were used as solvents. Chemical shifts are given in parts per million (ppm) and the coupling constants in Hertz (Hz). HRMS data were recorded by the mass spectrometry service of the University of Vigo, Spain. MS was recorded by a Thermo Finnigan LxQ (Linear Ion Trap) Mass Detector with Electro Spray Ionization (ESI).

For the formation of the hydrogels, the compounds were weighed into a sample vial and water was added. While stirring, NaOH (1 M, 20 μL) was added, to provide a solution of pH 10. The mixture was sonicated and then GdL was added. The solutions were left standing overnight to form the hydrogel.

CD spectra were recorded under N_2 on a Jasco J815 CD spectrometer. The samples were prepared using a diluted version (final concentration: 0.1 mg/mL) of the procedure for hydrogel preparation.

The viscoelastic characterization of hydrogels was performed with a stress-controlled rotational rheometer Anton Paar MCR300 (Anton Paar GmbH, Graz, Austria). Gel forming solutions were loaded in the shearing geometry (a Couette cell with 1 mL volume and 0.5 mm gap) at 25 °C. The liquid sample was pre-sheared at a shear rate of 5 s^{-1} during one minute to homogenise the sample in the shearing geometry. Then, the gelation kinetics was monitored during 10 hours by applying a small amplitude (0.001 %) oscillatory shear at 1 Hz and recording both storage (G') and loss (G'') moduli at each second.

STEM images were recorded using a NanoSEM – FEI Nova 200 (FEI Technologies, Inc., Hillsboro, Oregon, USA), operating at 15 kV, coupled to an Electron Dispersive Spectroscopic analyzer (EDS) and

Electron Backscatter Diffraction EDAX – Pegasus X4M analyzer and detection system (EBSD) at SEMAT (Serviços de Caracterização de Materiais), Guimarães, Portugal.

The concentration of methylene blue or methyl orange released in the experiments of sustained release assays was determined by measuring the absorbance at λ_{max} of the dye (666 nm for methylene blue and 465 nm for methyl orange) using a microplate reader (VARIAN, 50 MPR Microplate Reader) and then converting the value to percentage release (using a standard calibration curve). The concentration of ciprofloxacin released was determined using analytical HPLC (Jasco, PU-980 Intelligent HPLC Pump; Jasco, UV-975, Intelligent UV/VIS Detector; Shimadzu, C-R6A, Chromatopac), where the integrated peak area was converted to a percentage release (using a standard calibration curve). The eluent used in the HPLC experiments was MeCN/water (50:50) containing small amount of TFA (1%), filtered and degassed, with a flow rate of 1 mL/min. Each experiment was performed in triplicate, and the mean percentage cargo release was plotted against time.

4.2 Synthesis

4.2.1 Synthesis of H-D,L-Phe(β-OH)-OMe.HCl:

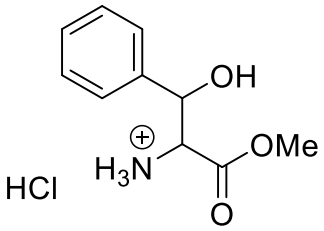

β-hydroxyphenylalanine monohydrate [H-D,L-Phe(β-OH)-OH.H_2O] (10 mmol, 1.80 g) was added to MeOH (40 mL) at 0 °C . With stirring, thionyl chloride 0.80 mL, 1.1 equiv) was added dropwise over 10 min and then the reaction mixture was allowed to warm to room temperature, before being heated at 40 °C for 4 h. The solvent was removed under reduced pressure and Et_2O was added and then removed under pressure. This process was repeated until a white solid of compound H-D,L-Phe(β-OH)-OMe.HCl was formed (85%, 2.02 g).

^{1}H NMR (400 MHz, DMSO-d_6) δ: 3.57 (3H, s, OCH_3); 4.11 (1H, br q, β-CH), 5.00 (1H, d, J 5.6 Hz, α-CH), 6.56 (1H, br s, OH), 7.31-7.38 (5H, m, ArH), 8.56 (3H, s, H_3N^+).

4.2.2 Synthesis of Boc-L-Lys(Boc)-OH:

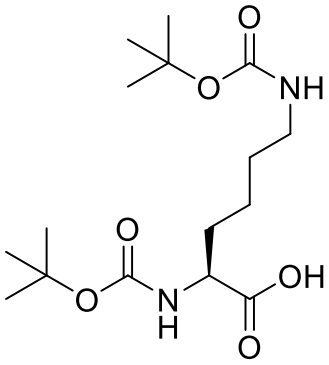

L-Lysine monohydrate (2.00g, 11.0 mmol) was dissolved in 1,4-dioxane (65 mL) and then a solution of NaOH 1.0 M (32.7 mL, 33.0 mmol) was added. The solution was left to stir for 10 minutes before Boc_2O (2.00 equiv, 4.5 g, 22.0 mmol) was added. The mixture was then stirred at rt overnight. The 1,4-dioxane solvent was removed under reduced pressure and the mixture was acidified with $KHSO_4$ (1.0 M) until pH 2-3. The aqueous phase was extracted with ethyl acetate (3 x 50 mL) and the organic phase dried with $MgSO_4$. Removal of the solvent under reduced pressure afforded Boc-L-Lys(Boc)-OH as a transparent oil (2.27 g, 60%).

^{1}H NMR (400 MHz, DMSO-d_6) δ: 1.19-1.40 (4H, m, γ-CH_2 and δ-CH_2), 1.42-1.69 (2H, m, β-CH_2),

2.81-2.90 (2H, m, ε-C*H*$_2$), 3.77-3.87 (1H, m, α-C*H*), 6.74 (1H, t, J = 18.0 Hz, δ-N*H*), 6.92 (1H, d, J 8.0 Hz, α-C*H*), 12.37 (1H, br s, CO_2*H* of Lys).

4.2.3 Synthesis of Boc-L-Lys(Boc)- D,L-Phe(β-OH)-OMe:

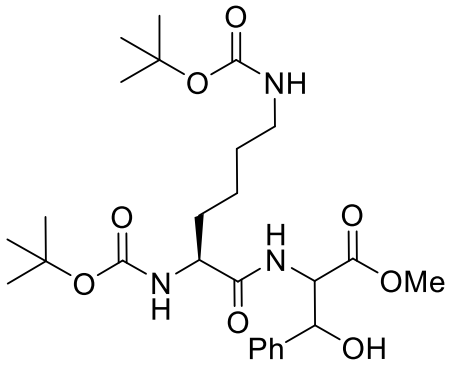

Boc-L-Lys(Boc)-OH (0.500 g, 1.50 mmol) was dissolved in MeCN (8 mL) and cooled to 0 °C. HBTU (1.1 equiv, 0.630 g, 1.65 mmol), H-D,L-Phe(β-OH)-OMe (1.00 equiv, 0.349 g, 1.50 mmol) and triethylamine (3 equiv, 0.7 mL, 4.50 mmol) were added sequentially, with 2 min between each addition. The mixture was stirred at rt overnight. The solvent was removed under reduced pressure to afford a residue that was partitioned between EtOAc (50 mL) and $KHSO_4$ (50 mL, 1 M). After separation of the phases, the organic layer was thoroughly washed with $KHSO_4$ (1 M, 2 x 50 mL), $NaHCO_3$ (1 M, 2 x 50 mL) and brine (2 x 50 mL) and then dried with $MgSO_4$. Filtration followed by removal of the solvent under reduced pressure afforded a diastereomeric mixture of Boc-L-Lys(Boc)- D,L-Phe(β-OH)-OMe as a white solid (0.557 g, 71%).

^{1}H NMR (400 MHz, DMSO) δ: 0.90-1.11 (4H, m, γ-C*H*$_2$ and δ-C*H*$_2$ of Lys), 1.16-1.29 (2H, m, β-C*H*$_2$ of Lys), 1.36 (9H, s, 1 x OC(C*H*$_3$)$_3$), 1.38 (9H, s, 1x OC(C*H*$_3$)$_3$)], 2.76-2.87 (2H, m, ε-C*H*$_2$ of Lys), 3.60 and 3.64 (3H, s, OC*H*$_3$), 3.76-3.85 and 3.88-3.94 (1H, m, α-C*H* of Phe), 4.53 (1H, dd, J=8.8 Hz, 2.8 Hz, α-C*H* of Lys), 5.09-5.15 (1H, m, β-C*H* of Phe), 5.89-5.97 (1H, m, 1x N*H*), 6.91 (1H, d, J=8.4 Hz, 1 x N*H*), 7.19-7.39 (5H, m, Ar*H*), 7.45 and 7.90 (1H, d, J = 8.8 Hz, 1x N*H*).

4.2.4 Synthesis of Boc-L-Lys(Boc)-*Z*-ΔPhe-OMe:

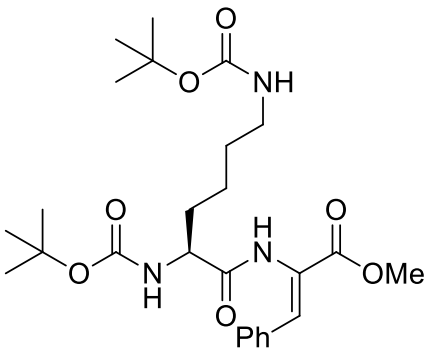

DMAP (0.11 equiv, 0.014 g, 0.12 mmol) and Boc_2O (1,1 equiv, 0.262 g, 1.20 mmol) were added to a solution of Boc-L-Lys(Boc)-D,L-Phe(β-OH)-OMe (0.5566 g, 1.09 mmol) in dry MeCN (8 mL, 1 M) under rapid stirring at rt. The mixture was monitored by ^{1}H NMR and stirred at rt until all the starting material was consumed (typically 5 h). *N,N,N',N'*-tetramethylguadinine (4 % in volume, 0.32 mL) was added. The mixture was stirred at rt and monitored by ^{1}H NMR until all the intermediate was consumed. Concentration under reduced pressure gave a residue that was partitioned between EtOAc (50 mL) and $KHSO_4$ (1 M, 30 mL). After separation of the phases, the organic phase was washed with $KHSO_4$ (1 M, 2 x 60 mL), $NaHCO_3$ (1 M, 2 x 60 mL) and brine (2 x 60 mL) and then dried with $MgSO_4$. Removal of the solvent afforded Boc-L-Lys(Boc)-*Z*-ΔPhe-OMe (0.363 g, 66%).

^{1}H NMR (400 MHz, DMSO-d_6) δ: 1.25-1.42 (4H, m, γ-C*H*$_2$ and δ-C*H*$_2$ of Lys), 1.36 (9H, s, OC(C*H*$_3$)$_3$), 1.40 (9H, s, OC(C*H*$_3$)$_3$), 1.49-1.71 (2H, m, β-C*H*$_2$ of Lys), 2.83-2.95 (2H, m, ε-C*H*$_2$ of Lys), 3.68 (3H, s, OC*H*$_3$), 4.00 (1H, dd, J = 14.4 Hz, 7.2 Hz, α-C*H* of Lys), 6.75 (1H, s, N*H*), 6.92 (1H, d, J 7.6 Hz, 1 x N*H*), 7.22 (1H, s, β-C*H* of ΔPhe); 7.33-7.41 (3H, m, Ar*H*); 7.65-7.74 (2H, m, Ar*H*), 9.59 (1H, s, N*H* of ΔPhe).

4.2.5 Synthesis of H-L-Lys-*Z*-ΔPhe-OMe.2TFA:

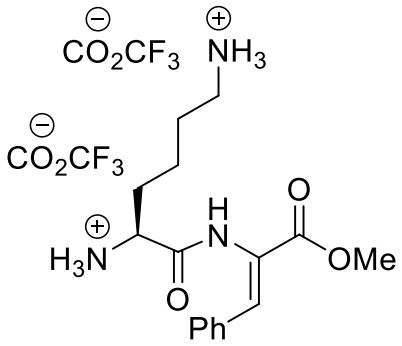

Boc-L-Lys(Boc)-*Z*-ΔPhe-OMe (0.363 g, 0.72 mmol) was dissolved in TFA (3.0 mL) and the reaction mixture was stirred at room temperature for 1 hour. The TFA was removed under reduced pressure. Traces of TFA were removed by the addition of CH_2Cl_2 (3 x 10 mL) followed by removal under reduced pressure, affording H-L-Lys-*Z*-ΔPhe-OMe.2TFA as a brown oil.

^{1}H NMR (400 MHz, DMSO-d_6) δ: 1.31-1.60 (4H, m, γ-C*H*$_2$ and δ-C*H*$_2$ of Lys), 1.73-1.88 (2H, m, β-C*H*$_2$ of Lys), 2.69-2.80 (2H, m, ε-C*H*$_2$ of Lys), 3.13 (3H, s, OC*H*$_3$), 3.95-4.06 (1H, m, α-C*H* of Lys), 7.36-7.47 (4H, m, Ar*H* and β-C*H* of ΔPhe), 7.63-7.69 (2H, m, Ar*H*), 7.74 (1H, br s, N*H*), 8.24 (3H, d, J = 3.6 Hz, *H*$_3$N$^+$ of Lys), 10.20 (1H, s, *H*$_3$N$^+$ of ΔPhe).

4.2.6 Synthesis of Naph-L-Lys(Naph)-*Z*-ΔPhe-OMe:

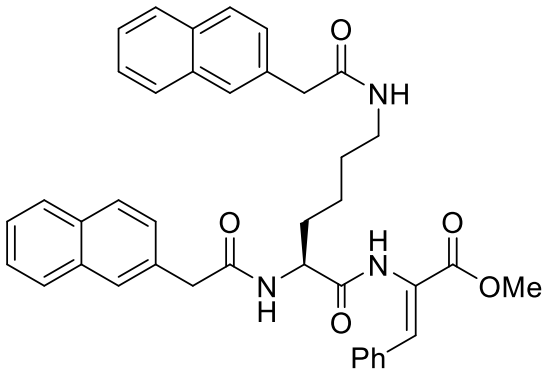

H-L-Lys-*Z*-ΔPhe-OMe.TFA (0.3826g, 0.72 mmol) was dissolved in MeCN (8 mL) and cooled to 0 °C. HBTU (1.1 equiv, 0.300 g, 0.79 mmol), 2-(Naphth-2-yl)-acetic acid (2.10 equiv, 0.281 g, 1.51 mmol) and triethylamine (3 equiv, 0.3 mL, 2.15 mmol) were added sequentially, with 2 min between each addition, and then the mixture was stirred at rt overnight. The solvent was removed under reduced pressure to afford a residue that was partitioned between EtOAc (50 mL) and $KHSO_4$ (50 mL, 1 M). After separation of the phases, the organic layer was thoroughly washed with $KHSO_4$ (1 M, 2 x 50 mL), $NaHCO_3$

(1 M, 2 x 50 mL) and brine (2 x 50 mL) and then dried with $MgSO_4$. Filtration followed by removal of the solvent under reduced pressure afforded Naph-L-Lys(Naph)-*Z*-ΔPhe-OMe as a white solid (0.400 g, 87%).

^{1}H NMR (400 MHz, DMSO) δ: 1.27-1.48 (4H, m, γ-C*H*$_2$ and δ-C*H*$_2$ of Lys), 1.57-1.81 (2H, m, β-C*H*$_2$ of Lys), 2.96-3.09 (2H, m, ε-C*H*$_2$ of Lys), 3.55 (3H, s, OC*H*$_3$ of ΔPhe), 3.66 (4H, s, 2x C*H*$_2$ of Naph), 4.33-4.45 (1H, m, α-C*H*$_2$ of Lys), 7.18-7.49 (10H, m, Ar*H* and β-C*H* of ΔPhe), 7.60-7.89 (10H, m, Ar*H* and N*H*), 8.06-8.13 (1H, m, Ar*H*), 8.40 (1H, d, J 8.4, 1x N*H*), 9.76 (1H, s, 1x N*H* of ΔPhe).

^{13}C NMR (100.6 MHz, DMSO-d_6, δ): 22.6 (CH_2, γ-*C*H$_2$ of Lys), 28.7 (CH_2, δ-*C*H$_2$ of Lys), 31.2 (CH_2, β-*C*H$_2$ of Lys), 38.5 (CH_2, ε-*C*H$_2$ of Lys), 42.0 (CH_2, 1 x *C*H$_2$ of Naph), 42.5 (CH_2, 1 x *C*H$_2$ of Naph), 52.1 (CH_3, O*C*H$_3$ of ΔPhe), 52.7 (CH, α-*C*H of Lys), 125.4 (CH, Ar), 126.0 (CH, Ar), 127.2 (CH, Ar), 127.30 (CH, Ar), 127.35 (CH, Ar), 127.4 (CH, Ar), 127.50 (CH, Ar), 127.55 (CH, Ar), 127.63 (CH, Ar), 127.67 (CH, Ar), 127.7 (CH, Ar), 127.8 (CH, Ar), 128.3 (CH, Ar), 128.4 (CH, Ar), 129.3 (CH, Ar), 129.9 (CH, Ar), 130.0 (CH, Ar), 131.7 (C, Ar), 131.9 (C, Ar), 132.0 (C, Ar), 132.1 (CH, β-CH of ΔPhe), 132.93 (C, Ar), 132.97 (C, Ar), 133.1 (C, α-C of ΔPhe), 134.1 (C, Ar), 134.2 (C, Ar), 165.3 (C, *C*=O), 169.9 (C, *C*=O of Naph), 170.2 (C, *C*=O of Naph), 171.9 (C, *C*=O).

4.2.7 Synthesis of Naph-L-Lys(Naph)-*Z*-ΔPhe-OH, 1:

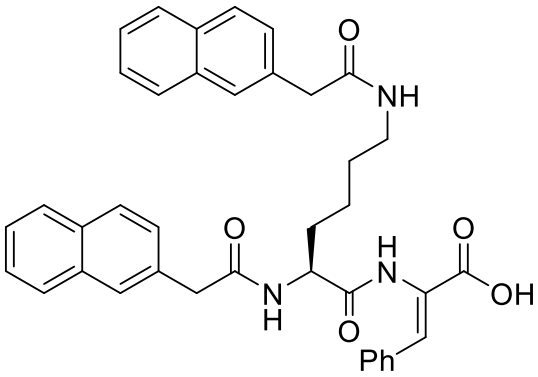

Naph-L-Lys(Naph)-*Z*-ΔPhe-OMe was dissolved in 1,4-dioxane (12.4 mL) and a solution of 1 M NaOH (1.6 equiv, 3.7 mL, 1.00 mmol) was added. The reaction was followed by TLC until no starting material was detected (typically about 4 hours). The organic solvent was removed under reduced pressure, and the reaction mixture was acidified to pH 2-3 with $KHSO_4$ (1M). The solid was collected by filtration and then washed with Et_2O. The solid was identified as Naph-L-Lys(Naph)-*Z*-ΔPhe-OH, **1** (0.247g, 66%).

^{1}H NMR (400 MHz, DMSO) δ: 1.29-1.49 (4H, m, γ-C*H*$_2$ and δ-C*H*$_2$ of Lys), 1.54-1.81 (2H, m, β-C*H*$_2$ of Lys), 2.91-3.12 (2H, m, ε-C*H*$_2$ of Lys), 3.55 (2H, s, 1 x C*H*$_2$ of Naph), 3.66 (2H, s, 1 x C*H*$_2$ of Naph), 4.39 (1H, m, α-C*H* of Lys), 7.23-7.30 (3H, m, Ar*H*), 7.39-7.51 (6H, m, Ar*H* and β-C*H* of ΔPhe), 7.57-7.64 (2H, m, Ar*H*), 7.70-7.89 (9H, m, Ar*H*), 8.07 (1H, t, J 4.8 Hz, 1 x N*H*), 8.35 (1H, d, J 8.0 Hz, 1 x N*H*), 9.56 (1H, s, N*H* of ΔPhe), 12.62 (1H, br s, CO$_2$*H* of ΔPhe).

^{13}C NMR (100.6 MHz, DMSO-*d*$_6$, δ): 22.7 (CH$_2$, γ-*C*H$_2$ of Lys), 28.8 (CH$_2$, δ-*C*H$_2$ of Lys); 31.3 (CH$_2$, β-*C*H$_2$ of Lys); 38.6 (CH$_2$, ε-*C*H$_2$ of Lys); 42.1 (CH$_2$, 1 x *C*H$_2$ of Naph), 42.6 (CH$_2$, 1 x *C*H$_2$ of Naph), 52.6 (CH, α-*C*H of Lys), 125.52 (CH, Ar), 125.53 (CH, Ar), 126.0 (CH, Ar), 126.1 (CH, Ar), 126.6 (CH, Ar), 127.2 (CH, Ar), 127.3 (CH, Ar), 127.40 (CH, Ar), 127.41 (CH, Ar), 127.50 (CH, Ar), 127.57 (CH, Ar), 127.6 (CH, Ar), 127.7 (CH, Ar), 128.4 (CH, Ar), 129.1 (CH, Ar), 130.0 (CH, Ar), 131.8 (C, Ar), 131.9 (CH, β-CH of ΔPhe), 133.0 (C, α-C of ΔPhe), 133.5 (C, Ar), 134.1 (C, Ar), 134.2 (C, Ar), 166.2 (C, *C*=O), 169.9 (C, *C*=O of Naph), 170.2 (C, *C*=O of Nah), 171.6 (C, *C*=O).

HRMS (ESI) *m/z*: [M + H]$^+$ calcd for $C_{39}H_{38}N_3O_5$ 628.28; found: 628.282.

4.2.8 Synthesis of Boc-L-Lys(Cbz)-D,L-Phe(β-OH)-OMe:

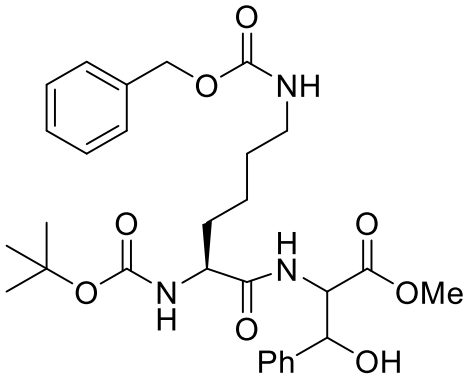

Boc-L-Lys(Cbz)-OH (0.800 g, 2.15 mmol) was dissolved in MeCN (5 mL) and cooled to 0 °C. HBTU (1.1 equiv, 0.900 g, 2.37 mmol), H-D,L-Phe(β-OH)-OMe 1.00 equiv, 0.500 g, 2.15 mmol) and triethylamine (3 equiv, 0.9 mL, 6.47 mmol) were added sequentially, with 2 min between each addition, and then the mixture was stirred at rt overnight. The solvent was removed under reduced pressure to afford a residue that was partitioned between EtOAc (50 mL) and $KHSO_4$ (50 mL, 1 M). After separation of the phases, the organic layer was thoroughly washed with $KHSO_4$ (1 M, 2 x 50 mL), $NaHCO_3$ (1 M, 2 x 50 mL) and brine (2 x 50 mL) and then dried with $MgSO_4$. Filtration followed by removal of the solvent under reduced pressure afforded a diastereomeric mixture of Boc-L-Lys(Cbz)-D,L-Phe(β-OH)-OMe as a

white solid (1.146 g, 96%).

^{1}H NMR (400 MHz, DMSO-*d*$_6$) δ: 0.91-1.04 (4H, m, γ-C*H*$_2$ and δ-C*H*$_2$ of Lys), 1.29-1.43 (2H, m, β-C*H*$_2$ of Lys), 1.36 and 1.37 (9H, 2 s, OC(C*H*$_3$)$_3$), 2.81-2.95 (2H, m, ε-C*H*$_2$ of Lys), 3.60 and 3.64 (3H, 2 s, OC*H*$_3$), 3.77-3.89 and 3.88-3.97 [1H, m, α-C*H* of Phe(β-OH)], 4.54 (1H, dd, J 9.2 Hz, and 2.8 Hz, α-C*H* of Lys), 4.99 (2H, s, C*H*$_2$ of Cbz), 5.09-5.18 (1H, m, β-C*H* of Phe(β-OH)), 5.88-5.95 (1H, m, 1 x N*H*), [6.72 and 6.96 (1H, d, J=8.4 Hz, 1 x N*H*)], 7.10-7.39 (10H, m, Ar*H*), 7.74 and 7.91 (1H, 2 d, J 8.8 Hz, 1 x N*H*).

4.2.9 Synthesis of Boc-L-Lys(Cbz)-*Z*-ΔPhe-OMe:

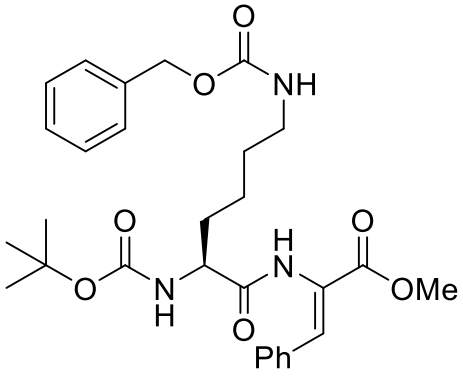

DMAP (0.11 equiv, 0.026 g, 0.23 mmol) and Boc$_2$O (1,1 equiv, 0.493 g, 2.26 mmol) were added to a solution of Boc-L-Lys(Cbz)-D,L-Phe(β-OH)-OMe (1.1459 g, 2.05 mmol) in MeCN (10 mL, 1 M) under rapid stirring at rt. The mixture was monitored by ^{1}H NMR and stirred at rt until all the starting material was consumed (typically 5 h). *N*,*N*,*N*',*N*'-tetramethylguadinine (4 % in volume, 0.4 mL) was added. The mixture was stirred at rt and monitored by ^{1}H NMR until all the intermediate was consumed. Concentration under reduced pressure gave a residue that was partitioned between EtOAc (50 mL) and KHSO$_4$ (1 M, 30 mL). After separation of the phases, the organic phase was washed with KHSO$_4$ (1 M, 2 x 60 mL), NaHCO$_3$ (1 M, 2 x 60 mL) and brine (2 x 60 mL) and then dried with MgSO$_4$. Removal of the solvent afforded Boc-L-Lys(Cbz)-*Z*-ΔPhe-OMe (0.8604g, 78%).

^{1}H NMR (400 MHz, DMSO-*d*$_6$) δ: 1.25-1.43 (4H, m, γ-C*H*$_2$ and δ-C*H*$_2$ of Lys), 1.40 (9H, s, OC(C*H*$_3$)$_3$), 1.49-1.71 (2H, m, β-C*H*$_2$ of Lys), 2.91-3.02 (2H, m, ε-C*H*$_2$ of Lys), 3.67 (3H, s, OC*H*$_3$ of ΔPhe), 3.96-4.09 (1H, m, α-C*H* of Lys), 4.99 (2H, s, C*H*$_2$ of Cbz), 6.90-6.98 (1H, d, J 7.6 Hz, N*H*), 7.19-7.39 (10H, m, Ar*H* and β-C*H* of ΔPhe and 1 N*H*), 7.67-7.75 (2H, m, Ar*H*), 9.59 (1H, s, N*H* of ΔPhe).

4.2.10 Synthesis of H-L-Lys(Cbz)-*Z*ΔPhe-OMe.TFA:

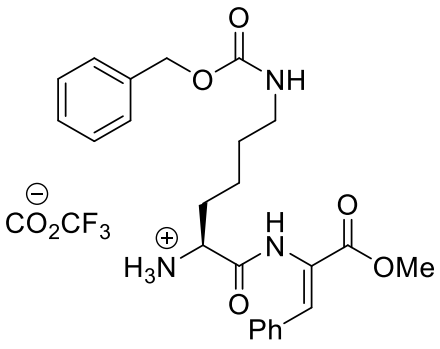

Boc-L-Lys(Cbz)-*Z*-ΔPhe-OMe (0.358 g, 0.88 mmol) was dissolved in TFA (3.0 mL) and the reaction mixture was stirred at room temperature for 1 hour. The TFA was then removed under reduced pressure. Traces of residue TFA were removed by the addition of CH_2Cl_2 (3 x 10 mL) followed by removal under reduced pressure, affording H-L-Lys(Cbz)-*Z*-ΔPhe-OMe.TFA as a brown oil.

^{1}H NMR (400 MHz, DMSO-d_6) δ: 1.28-1.49 (4H, m, γ-CH_2 and δ-CH_2 of Lys), 1.71-1.89 (2H, m, β-CH_2 of Lys), 2.91-3.04 (2H, m, ε-CH_2 of Lys), 3.73 (3H, s, OCH_3 of ΔPhe), 3.90-4.08 (1H, m, α-C*H* of Lys), 4.99 (2H, s, CH_2 of Cbz), 7.28 (1H, t, J 5.6 Hz, 1 x N*H*), 7.10-7.46 (9H, m, Ar*H*), 7.62-7.68 (2H, m, Ar*H*), 8.21 (3H, d, J 3.6 Hz, H_3N^+); 10.19 (1H, s, N*H* of ΔPhe).

4.2.11 Synthesis of Naph-L-Lys(Cbz)-*Z*-ΔPhe-OMe:

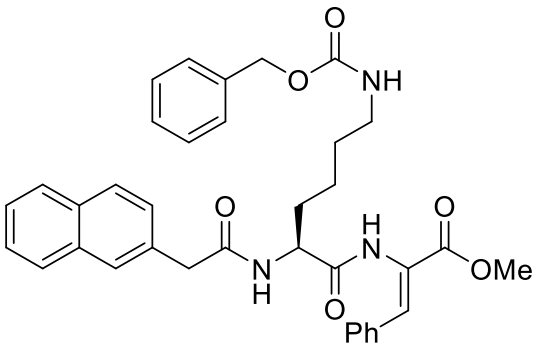

H-L-Lys(Cbz)-Z-ΔPhe-OMe.TFA (0.5374g, 0.98 mmol) was dissolved in MeCN (8 mL) and cooled to 0 °C. 2-(Naphth-2-yl)-acetic acid (1.00 equiv, 0.182 g, 0.98 mmol), triethylamine (3 equiv, 0.4 mL, 2.94 mmol) and HBTU (1.1 equiv, 0.409 g, 1.08 mmol) were added sequentially, with 2 min between each addition, and then the mixture was stirred at rt overnight. The solvent was removed under reduced pressure to afford a residue that was partitioned between EtOAc (50 mL) and $KHSO_4$ (50 mL, 1 M). After separation of the phases, the organic layer was thoroughly washed with $KHSO_4$ (1 M, 2 x 50 mL), $NaHCO_3$ (1 M, 2 x 50 mL) and brine (2 x 50 mL) and then dried with $MgSO_4$. Filtration followed by removal of the solvent under reduced pressure afforded Naph-L-Lys(Cbz)-*Z*-ΔPhe-OMe as a white solid (0.572 g, 98%).

^{1}H NMR (400 MHz, DMSO-d_6) δ: 1.22-1.48 (4H, m, γ-CH_2 and δ-CH_2 of Lys), 1.54-1.79 (2H, m, β-CH_2 of Lys), 2.91-3.01 (2H, m, ε-CH_2 of Lys), 3.67 (3H, s, OCH_3 of ΔPhe), 3.68 (2H, s, CH_2 of Naph), 4.37-4.43 (1H, m, α-CH of Lys), 4.99 (2H, s, CH_2 of Cbz), 7.19-7.88 (19H, m, ArH and β-CH of ΔPhe and 1x NH), 8.39 (1H, d, J 7.6 Hz, NH), 9.74 (1H, s, NH of ΔPhe).

^{13}C NMR (100.6 MHz, DMSO-d_6, δ): 22.6 (CH_2, γ-CH$_2$ of Lys), 29.1 (CH_2, δ-CH$_2$ of Lys), 31.3 (CH_2, β-CH$_2$ of Lys), 40.2 (CH_2, ε-CH$_2$ of Lys), 42.1 (CH_2, CH$_2$ of Naph), 48.6 (CH_3, OCH$_3$ of ΔPhe), 52.7 (CH, α-CH of Lys), 65.1 (CH_2, CH$_2$ of Cbz), 125.5 (CH, Ar), 126.0 (CH, Ar), 127.33 (CH, Ar), 127.39 (CH, Ar), 127.50 (CH, Ar), 127.56 (CH, Ar), 127.7 (CH, Ar), 128.4 (CH, Ar), 128.5 (CH, Ar), 129.1 (CH, Ar), 129.4 (CH, Ar), 130.0 (CH, Ar), 130.1 (CH, Ar), 131.9 (CH, β-CH of ΔPhe), 139.1 (C, Ar), 132.9 (C, α-C of ΔPhe), 133.1 (CH, Ar), 133.4 (C, Ar), 134.1 (C, Ar), 137.2 (C, Ar), 156.0 (C, C=O), 166.1 (C, C=O), 170.2 (C, C=O), 171.5 (C, C=O).

4.2.12 Synthesis of Naph-L-Lys(Cbz)-*Z*-ΔPhe-OH, 2:

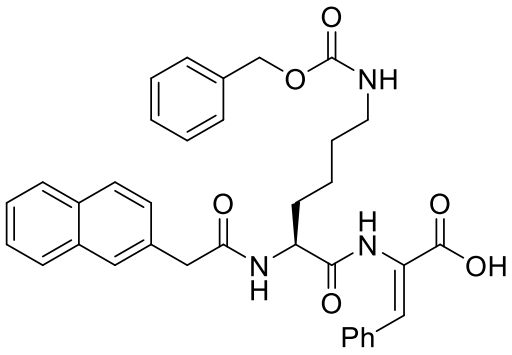

Naph-L-Lys(Cbz)-*Z*-ΔPhe-OMe was dissolved in 1,4-dioxane (11 mL) and a solution of 1 M NaOH (1.6 equiv, 3.2 mL, 1.50 mmol) was added. The reaction was followed by TLC until no starting material was detected (typically about 4 hours). The organic solvent was removed under reduced pressure, and the reaction mixture was acidified to pH 2-3 with $KHSO_4$ (1M). The solid was collected by filtration and then washed with Et_2O. The solid was identified as Naph-L-Lys(Cbz)-*Z*-ΔPhe-OH, **2** (0.474g, 85%).

^{1}H NMR (400 MHz, DMSO-d_6)δ: 1.21-1.42 (4H, m, γ-CH_2 and δ-CH_2 of Lys), 1.55-1.80 (2H, m, β-CH_2 of Lys), 2.79-2.96 (2H, m, ε-CH_2 of Lys), 3.64 (1H, d, J 14.0 Hz, CH_AH$_B$ of Naph), 3.69 (1H, d, J 14.0 Hz, CH$_A$CH_B of Naph), 4.40 (1H, dd, J 13.2 Hz, 8.4 Hz, α-CH_2 of Lys), 4.99 (2H, s, CH_2 of Cbz), 7.18-7.50 (10H, m, ArH and β-CH of ΔPhe and 1 x NH), 7.56-7.67 (3H, m, ArH), 7.61-7.89 (6H, m, ArH), 8.34 (1H, d, J 8.0 Hz, NH), 9.54 (1H, s, NH of ΔPhe).

^{13}C NMR (100.6 MHz, DMSO-d_6, δ): 22.6 (CH_2, γ-CH_2 of Lys), 29.2 (CH_2, δ-CH_2 of Lys), 31.4 (CH_2, β-CH_2 of Lys), 40.2 (CH_2, ε-CH_2 of Lys), 42.1 (CH_2, CH_2 of Naph), 52.7 (CH, α-CH of Lys), 65.1 (CH_2, CH_2 of Cbz), 125.5 (CH, Ar), 126.01 (CH, Ar), 126.04 (C, Ar), 126.6 (CH, Ar), 127.3 (CH, Ar), 127.40 (CH, Ar), 127.46 (CH, Ar), 127.5 (CH, Ar), 127.6 (CH, Ar), 127.7 (CH, Ar), 128.35 (CH, Ar), 128.39 (CH, Ar), 129.1 (CH, Ar), 129.9 (CH, Ar), 131.7 (C, Ar), 131.8 (CH, β-CH of ΔPhe), 132.9 (C, α-C of ΔPhe), 133.6 (C, Ar), 134.2 (C, Ar), 137.2 (C, Ar), 156.1 (C, *C*=O), 166.2 (C, *C*=O), 170.1 (C, *C*=O), 171.6 (C, *C*=O).

HRMS (ESI) *m/z*: $[M + H]^+$ calcd for $C_{35}H_{36}N_3O_6$ 594.26; found: 594.258.

4.2.13 Synthesis of Cbz-L-Lys(Cbz)-Phe(β-OH)-OMe:

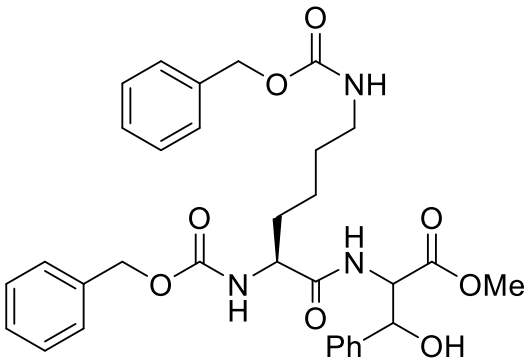

Cbz-L-Lys(Cbz)-OH (1.78 g, 4.30 mmol) was dissolved in MeCN (10 mL) and cooled to 0 °C. HBTU (1.1 equiv, 1.79 g, 4.73 mmol), HCl.H-Phe-β-OH)-OMe (1.00 equiv, 1.00 g, 4.30 mmol) and triethylamine (3 equiv, 1.8 mL, 12.90 mmol) were added sequentially, with 2 min between each addition, and then the mixture was stirred at rt overnight. The solvent was removed under reduced pressure to afford a residue that was partitioned between EtOAc (50 mL) and $KHSO_4$ (50 mL, 1 M). After separation of the phases, the organic layer was thoroughly washed with $KHSO_4$ (1 M, 2 x 50 mL), $NaHCO_3$ (1 M, 2 x 50 mL) and brine (2 x 50 mL) and then dried with $MgSO_4$. Filtration followed by removal of the solvent under reduced pressure afforded a diastereomeric mixture of Cbz-L-Lys(Cbz)-Phe(β-OH)-OMe as a white solid (1.82 g, 71%).

^{1}H NMR (400 MHz, DMSO-d_6) δ: 0.98-1.17 (4H, m, γ-CH_2 and δ-CH_2 of Lys), 1.30-1.42 (2H, m, β-CH_2 of Lys), 2.81-2.96 (2H, m, ε-CH_2 of Lys), 3.59 and 3.64 (3H, s, OCH_3), 3.91-4.08 (1H, m, α-C*H* of Phe), 4.49-4.60 (1H, m, α-C*H* of Lys), 5.09 and 5.15 (4H, s, 2x CH_2 of Cbz), 5.07-5.19 (1H, m, β-C*H* of Phe), 5.89-5.97 (1H, m, N*H*), 7.14-7.39 (16H, m, Ar*H* and N*H*), 7.89 and 8.02 (1H, 2 d, J 9.2 Hz, N*H*)].

4.2.14 Synthesis of Cbz-L-Lys(Cbz)-*Z*-ΔPhe-OMe:

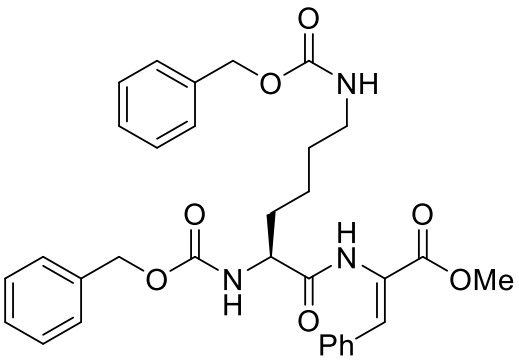

DMAP (0.11 equiv, 0.025 g, 0.21 mmol) and Boc_2O (1,1 equiv, 0.451 g, 2.07 mmol) were added to a solution of Cbz-L-Lys(Cbz)-Phe(β-OH)-OMe (1.114 g, 1.88 mmol) in dry MeCN (8 mL, 1 M) under rapid stirring at rt. The mixture was monitored by ^{1}H NMR and stirred at rt until all the starting material was consumed (typically 5 h). *N,N,N',N'*-tetramethylguadinine (4 % in volume, 0.32 mL) was added. The mixture was stirred at rt and monitored by ^{1}H NMR until all the intermediate was consumed. Concentration under reduced pressure gave a residue that was partitioned between EtOAc (50 mL) and $KHSO_4$ (1 M, 30 mL). After separation of the phases, the organic phase was washed with $KHSO_4$ (1 M, 2 x 60 mL), $NaHCO_3$ (1 M, 2 x 60 mL) and brine (2 x 60 mL) and then dried with $MgSO_4$. Filtration followed by removal of the solvent afforded Cbz-L-Lys(Cbz)-*Z*-ΔPhe-OMe (0.785 g, 73%).

^{1}H NMR (400 MHz, DMSO-d_6) δ: 1.28-1.47 (4H, m, γ-CH_2 and δ-CH_2 of Lys), 1.52-1.77 (2H, m, β-CH_2 of Lys), 2.90-3.00 (2H, m, ε-CH_2 of Lys), 3.67 (3H, s, OCH_3), 4.01 (1H, dd, J 37.6 Hz, 6.0 Hz, α-C*H* of Lys), 4.99 (2H, s, 1 x CH_2 of Cbz), 5.05 (2H, s, 1x CH_2 of Cbz), 7.17-7.40 (15H, m, Ar*H* and β-C*H* of ΔPhe and 1 x N*H*), 7.46 (1H, d, J 7.6 Hz, 1 x N*H*), 7.64-7.71 (2H, m, Ar*H*), 9.67 (1H, s, N*H* of ΔPhe).

^{13}C NMR (100.6 MHz, DMSO-d_6, δ): 22.6 (CH_2, γ-CH_2 of Lys), 29.0 (CH_2, δ-CH_2 of Lys), 30.9 (CH_2, β-CH_2 of Lys), 40.1 (CH_2, ε-CH_2 of Lys), 52.8 (CH_3, OCH_3 of ΔPhe), 54.7 (CH, α-C*H* of Lys), 65.2 (CH_2, 1 x CH_2 of Cbz), 65.4 (CH_2, 1 x CH_2 of Cbz), 126.0 (C, Ar), 127.72 (CH, Ar), 127.75 (CH, Ar), 127.8 (CH, Ar), 128.3 (CH, Ar), 128.5 (CH, Ar), 129.4 (CH, Ar), 129.5 (CH, Ar), 130.0 (CH, Ar), 130.1 (CH, Ar), 132.0 (CH, β-CH of ΔPhe), 133.2 (C, α-C of ΔPhe), 137.0 (C, Ar), 137.2 (C, Ar), 156.1 (C, 2 x *C*=O of Cbz), 165.3 (C, *C*=O), 172.3 (C, *C*=O).

4.2.15 Synthesis of Cbz-L-Lys(Cbz)-*Z*-ΔPhe-OH, 3:

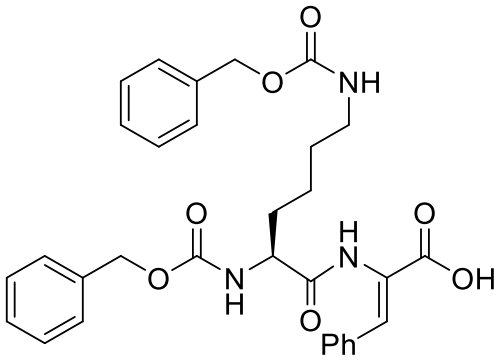

Cbz-L-Lys(Cbz)-*Z*-ΔPhe-OMe was dissolved in 1,4-dioxane (13.5 mL) and a solution of 1 M NaOH (1.5 equiv, 2.02 mL, 2.02 mmol) was added. The reaction was followed by TLC until no starting material was detected (typically about 4 hours). The organic solvent was removed under reduced pressure, and the reaction mixture was acidified to pH 2-3 with $KHSO_4$ (1M). The solid was collected by filtration and then washed with Et_2O. The solid was identified as Cbz-L-Lys(Cbz)-*Z*-ΔPhe-OH, **3** (0.749 g, 99%).

^{1}H NMR (400 MHz, DMSO-d_6) δ: 1.24-1.47 (4H, m, γ-CH_2 and δ-CH_2 of Lys), 1.51-1.78 (2H, m, β-CH_2 of Lys), 2.91-3.03 (2H, m, ε-CH_2 of Lys), 4.05-4.14 (1H, m, α-CH of Lys), 4.99 (2H, s, 1 x CH_2 of Cbz), 5.05 (2H, s, 1 x CH_2 of Cbz), 7.17-7.39 (15H, m, ArH and β-CH of ΔPhe and NH), 7.43-7.61 (3H, m, ArH and NH), 9.43 (1H, s, NH of ΔPhe).

^{13}C NMR (100.6 MHz, DMSO-d_6, δ): 22.7 (CH_2, γ-CH$_2$ of Lys), 29.0 (CH_2, δ-CH$_2$ of Lys), 31.2 (CH_2, β-CH$_2$ of Lys), 40.1 (CH_2, ε-CH$_2$ of Lys), 54.9 (CH, α-CH of Lys), 65.1 (CH_2, 1 x CH$_2$ of Cbz), 65.4 (CH_2, 1 x CH$_2$ of Cbz), 126.3 (CH, Ar), 126.5 (CH, Ar), 127.4 (C, Ar), 127.7 (CH, Ar), 127.8 (CH, Ar), 128.0 (CH, Ar), 128.2 (CH, Ar), 128.3 (CH, Ar), 128.7 (CH, Ar), 129.1 (CH, Ar), 129.8 (CH, β-CH of ΔPhe), 134.1 (C, α-C of ΔPhe), 137.0 (C, 2 x *C* of Cbz), 156.0 (C, 2x *C*=O of Cbz), 166.3 (C, *C*=O), 171.3 (C, *C*=O).

HRMS (ESI) *m/z*: $[M + H]^+$ calcd for $C_{31}H_{34}N_3O_7$ 560.24; found: 560.2397.

4.2.16 Synthesis of Boc-L-Asp(OMe)-D,L-Phe(β-OH)-OMe:

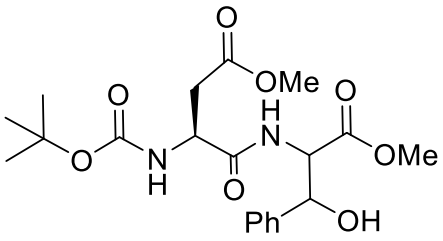

Boc-L-Asp(OMe)-OH (0.532 g, 2.15 mmol) was dissolved MeCN (5 mL) and cooled to 0 °C. HBTU (1.1 equiv, 0.900 g, 2.37 mmol), (H-Phe-D,L-β-OH)-OMe 1.00 equiv, 0.500 g, 2.15 mmol) and triethylamine (3 equiv, 0.9 mL, 6.47 mmol) were added sequentially, with 2 min between each addition, and then the mixture was stirred at rt overnight. The solvent was removed under reduced pressure to afford a residue that was partitioned between EtOAc (50 mL) and $KHSO_4$ (50 mL, 1 M). After separation of the phases, the organic layer was thoroughly washed with $KHSO_4$ (1 M, 2 x 50 mL), $NaHCO_3$ (1 M, 2 x 50 mL) and brine (2 x 50 mL) and then dried with $MgSO_4$. Filtration followed by removal of the solvent under reduced pressure afforded a diastereomeric mixture of Boc-L-Asp(Me)-D,L-Phe(β-OH)-OMe as a white solid (0.425 g, 47%).

^{1}H NMR (400 MHz, DMSO-*d*$_6$) δ: 1.46 and 1.47 (9H, 2 s, OC(C*H*$_3$)$_3$, 2.48-2.49 and 2.51-2.57 (2H, d, J 6.0 Hz, β-C*H*$_2$ of Asp), 2.69-2.73 and 2.76-2.81 (1H, m, α-C*H* of Phe), 3.69 and 3.71 (3H, s, 1 x OC*H*$_3$), 3.76 and 3.77 (3H, s, 1 x OC*H*$_3$), 4.41-4.48 and 4.49-4.57 (1H, m, β-C*H* of Phe), 4.79-4.87 (1H, m, α-C*H* of Asp), [5.29 and 5.33 (1H, d, J 4.0 Hz, N*H*)], 7.27-7.40 (6H, Ar*H* and N*H*).

4.2.17 Synthesis of Boc-L-Asp(OH)-*z*-ΔPhe-OMe:

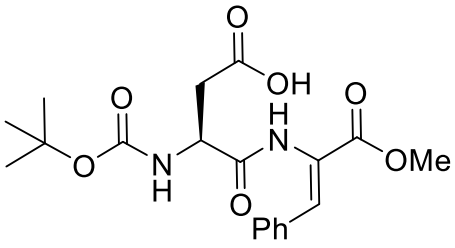

DMAP (0.11 equiv, 0.022 g, 0.18 mmol) and Boc_2O (1,1 equiv, 0.376 g, 1.72 mmol) were added to a solution of Boc-L-Asp(Me)-D,L-Phe(β-OH)-OMe (0.6712 g, 1.58 mmol) in dry MeCN (10 mL, 1 M) under rapid stirring at rt. The mixture was monitored by ^{1}H NMR and stirred at rt until all the starting material was consumed (typically 5 h). *N*,*N*,*N*',*N*'-tetramethylguadinine (4 % in volume, 0.40 mL) was added. The mixture was stirred at rt and monitored by ^{1}H NMR until all the intermediate was consumed. Concentration under reduced pressure gave a residue that was partitioned between EtOAc (50 mL) and

$KHSO_4$ (1 M, 30 mL). After separation of the phases, the organic phase was washed with $KHSO_4$ (1 M, 2 x 60 mL), $NaHCO_3$ (1 M, 2 x 60 mL) and brine (2 x 60 mL) and then dried with $MgSO_4$. Filtration followed by removal of the solvent afforded Boc-L-Asp(OH)-*Z*-ΔPhe-OMe (0.358 g, 57%).

^{1}H NMR (400 MHz, DMSO-d_6) δ: 1.42 (9H, s, OC(C*H*$_3$)$_3$, 2.84 (1H, dd, J 18.0 Hz, 6.4 Hz, β-C*H*$_A$H$_B$ of Asp), 3.16 (1H, dd, J 18.0 Hz, 9.2 Hz, β-CH$_A$C*H*$_B$ of Asp), 3.75 (3H, s, CO_2CH_3), 4.47 (1H, dd, J 16.4 Hz, 7.2 Hz, α-C*H* of Asp), 7.32-7.52 (5H, Ar*H* and β-C*H* of ΔPhe), 7.71-7.80 (2H, m, Ar*H* and N*H*), 7.96 (1H, s, N*H* of ΔPhe).

4.2.18 Synthesis of H-L-Asp(OMe)-*Z*-ΔPhe-OMe.HCl:

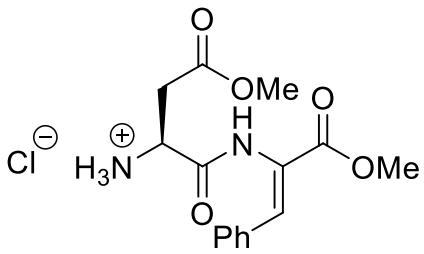

Boc-L-Asp(OH)-*Z*-ΔPhe-OMe (0.358 g, 0.88 mmol) was dissolved in TFA (3.0 mL) and the reaction mixture was stirred at room temperature for 1 hour. The TFA was then removed under reduced pressure. Traces of residual TFA were removed by the addition of $CHCl_3$ (3 x 10 mL) followed by removal under reduced pressure, affording H-L-Asp(OMe)-*Z*-ΔPhe-OMe • HCl as a brown oil.

^{1}H NMR (400 MHz, DMSO-d_6) δ: 2.95 (1H, dd, J 15.3 Hz, 5.8 Hz, β-C*H*$_A$CH$_B$ of Asp), 3.04 (1H, dd, J 17.2 Hz, 4.0 Hz, β-CH$_A$C*H*$_B$ of Asp), 3.68 (3H, s, OC*H*$_3$), 3.70 (3H, s, OC*H*$_3$), 4.33 (1H, dd, J 7.6 Hz, 4.4 Hz α-C*H* of Asp), 7.29-7.47 (5H, m, Ar*H* and β-*H* of ΔPhe and N*H*), 7.61-7.72 (2H, m, Ar*H*), 8.40 (3H, br s, *H*$_3$N$^+$).

4.2.19 Synthesis of Cbz-L-Lys(Cbz)-L-Asp(OMe)-*Z*-ΔPhe-OMe:

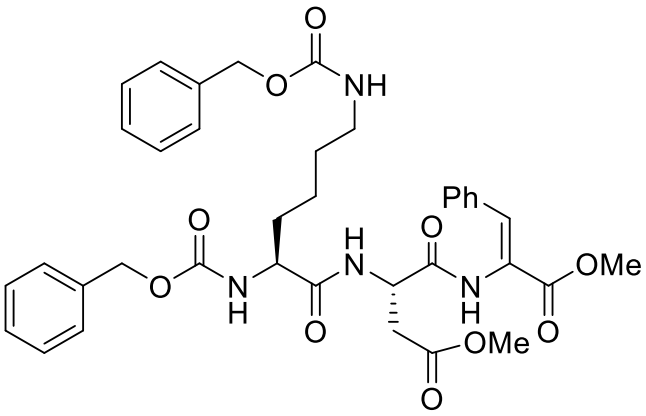

H-L-Asp(OMe)-*Z*-ΔPhe-OMe.HCl (0.358 g, 0.85 mmol) was dissolved in MeCN (8 mL) and cooled to 0 °C. Cbz-L-Lys(Cbz)-OH (1.00 equiv, 0.351 g, 0.85 mmol), triethylamine (3 equiv, 0.40 mL, 2.55 mmol) and HBTU (1.1 equiv, 0.353 g, 0.93 mmol) were added sequentially, with 2 min between each addition, and then the mixture was stirred at rt overnight. The solvent was removed under reduced pressure to afford a residue that was partitioned between EtOAc (50 mL) and $KHSO_4$ (50 mL, 1 M). After separation of the phases, the organic layer was thoroughly washed with $KHSO_4$ (1 M, 2 x 50 mL), $NaHCO_3$ (1 M, 2 x 50 mL) and brine (2 x 50 mL) and then dried with $MgSO_4$. Filtration followed by removal of the solvent under reduced pressure afforded Cbz-L-Lys(Cbz)-L-Asp(OMe)-*Z*-ΔPhe-OMe as a white solid (0.446 g, 75%).

^{1}H NMR (400 MHz, DMSO-d_6) δ: 1.13-1.40 (4H, m, γ-C*H*$_2$ and δ-C*H*$_2$ of Lys), 1.45-1.69 (2H, m,β-C*H*$_2$ of Lys), 2.62-2.73 (1H, m, β-C*H*$_A$H$_B$ of Asp), 2.81 (1H, dd, J 36.0 Hz, 6.0 Hz, β-CH$_A$C*H*$_B$ of Asp), 2.90-3.02 (2H, m, ε-C*H*$_2$ of Lys), 3.60 (3H, s, OC*H*$_3$), 3.68 (3H, s, OC*H*$_3$), 3.91-4.02 (1H, m, α-C*H* of Lys), 4.59-4.71 (1H, m, α-C*H* of Asp), 4.98 (2H, s, 1 x C*H*$_2$ of Cbz), 4.99 (4H, s, 1 x C*H*$_2$ of Cbz), 7.15-7.49 (16H, Ar*H* and β-*H* of ΔPhe and 2 x N*H*), 7.60-7.69 (2H, m, Ar*H*), 8.34 (1H, d, J 8.0 Hz, 1 x N*H*), 9.80 (1H, s, N*H* of ΔPhe).

^{13}C NMR (100.6 MHz, DMSO-d_6, δ): 22.6 (CH$_2$, γ-*C*H$_2$ of Lys), 29.0 (CH$_2$, δ-*C*H$_2$ of Lys), 31.5 (CH$_2$, β-*C*H$_2$ of Lys), 36.7 (CH$_2$, β-*C*H$_2$ of Asp), 40.18 (CH$_2$, ε-*C*H$_2$ of Lys), 48.59 (CH, α-*C*H of Asp), 52.1 (CH$_3$, 1 x O*C*H$_3$); 52.8 (CH$_3$, 1 x O*C*H$_3$), 54.4 (CH, α-*C*H of Lys), 65.0 (CH$_2$, 1 x *C*H$_2$ of Cbz), 65.3 (CH$_2$, 1 x *C*H$_2$ of Cbz), 126.0 (CH, Ar), 127.71 (CH, Ar), 128.3 (CH, Ar), 128.5 (CH, Ar), 128.6 (CH, Ar), 129.4 (CH, Ar), 129.9 (CH, Ar), 131.3 (CH, β-CH of ΔPhe), 133.22 (C, α-C of ΔPhe), 133.24 (C, Ar), 137.0 (C, Ar), 137.2 (C, Ar), 156.06 (C, 2 x *C*=O), 165.3 (C, *C*=O); 169.1 (C, *C*=O); 171.3.3 (C, *C*=O), 171.9 (*C*, C=O).

4.2.20 Synthesis of Cbz-L-Lys(Cbz)-L-Asp(OH)-*Z*-ΔPhe-OH, 5:

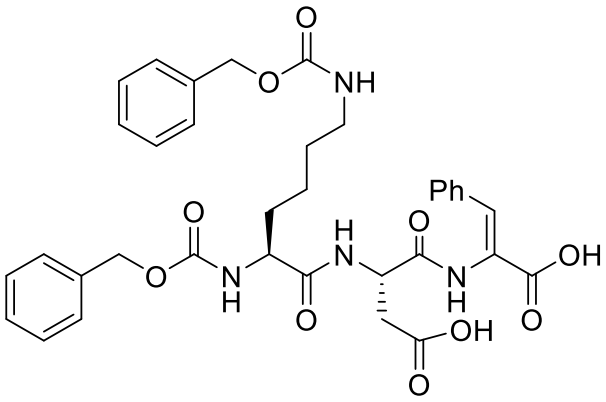

Cbz-L-Lys(Cbz)-L-Asp(OMe)-*Z*-ΔPhe-OMe was dissolved in 1,4-dioxane (27.5 mL) and a solution of 1.0 M NaOH (3.0 equiv, 16 mL, 0.824 mmol) was added. The reaction was followed by TLC until no starting material was detected (typically about 4 hours). The organic solvent was removed under reduced pressure, and the reaction mixture was acidified to pH 2-3 with $KHSO_4$ (1 M). The solid was collected by filtration and then washed with Et_2O. The solid was identified as Cbz-L-Lys(Cbz)-L-Asp(OH)-*Z*-ΔPhe-OH, **5** (0.196 g, 50%).

^{1}H NMR (400 MHz, DMSO-D6) δ: 1.13-1.41 (4H, m, γ-C*H*$_2$ and δ-C*H*$_2$ of Lys), 1.48-1.69 (2H, m,β-C*H*$_2$ of Lys), 2.59-2.71 (1H, m, β-C*H*$_A$H$_B$ of Asp), 2.78-2.87 (1H, m, β-CH$_A$C*H*$_B$ of Asp), 2.88-2.97 (2H, m, ε-C*H*$_2$ of Lys), 3.90-4.02 (1H, m, α-C*H* of Lys), 4.51-4.65 (1H, m, α-C*H* of Asp), 4.99 (2H, s, 1 x C*H*$_2$ of Cbz), 5.03 (2H, s, 1 x C*H*$_2$ of Cbz), 7.10-7.42 (16H, Ar*H* and β-*H* of ΔPhe and 2 x N*H*), 7.59-7.71 (2H, m, Ar*H*), 8.20 (1H, d, J 8.0 Hz, N*H* of Asp), 9.57 (1H, s, N*H* of ΔPhe), 12.45 (2H, s, CO_2*H* of Asp and CO_2*H* of ΔPhe).

^{13}C NMR (100.6 MHz, DMSO-d_6, δ): 22.7 (CH_2, γ-*C*H$_2$ of Lys), 29.1 (CH_2, δ-*C*H$_2$ of Lys), 31.6 (CH_2, β-*C*H$_2$ of Lys), 36.9 (CH_2, β-*C*H$_2$ of Asp), 40.1 (CH_2, ε-*C*H$_2$ of Lys), 48.5 (CH, α-*C*H of Asp), 54.5 (CH, α-*C*H of Lys), 65.1 (CH_2, 1 x *C*H$_2$ of Cbz), 65.4 (CH_2, 1 x *C*H$_2$ of Cbz), 127.70 (CH, Ar), 127.76 (CH, Ar), 128.3 (CH, Ar), 128.5 (CH, Ar), 128.6 (CH, Ar), 129.1 (CH, Ar), 129.4 (CH, Ar), 130.01 (CH, Ar), 130.08 (CH, Ar), 131.2 (CH, β-CH of ΔPhe), 133.6 (C, α-C of ΔPhe), 137.0 (C, Ar), 137.3 (C, Ar), 165.4 (C, *C*=O), 166.3 (C, *C*=O), 169.2 (C, *C*=O), 169.5 (C, *C*=O), 171.8 (C, *C*=O); 172.5 (C, *C*=O).

4.2.21 Synthesis of Boc-L-Lys(Boc)-L-Asp(OMe)-*Z*-ΔPhe-OMe:

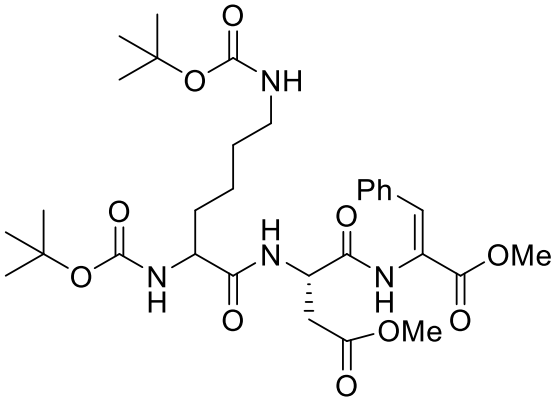

H-L-Asp(OMe)-*Z*-ΔPhe-OMe • HCl (0.346g, 0.82 mmol) was dissolved in MeCN (8 mL) and cooled to 0 °C. Boc-L-Lys(Boc)-OH (1.00 equiv, 0.274 g, 0.82 mmol), triethylamine (3 equiv, 0.4 mL, 2.46 mmol) and HBTU (1.1 equiv, 0.342 g, 0.90 mmol) were added sequentially, with 2 min between each addition, and then the mixture was stirred at rt overnight. The solvent was removed under reduced pressure to afford a residue that was partitioned between EtOAc (50 mL) and $KHSO_4$ (50 mL, 1 M). After separation of the phases, the organic layer was thoroughly washed with $KHSO_4$ (1 M, 2 x 50 mL), $NaHCO_3$ (1 M, 2 x 50 mL) and brine (2 x 50 mL) and then dried with $MgSO_4$. Filtration followed by removal of the solvent under reduced pressure afforded Boc-L-Lys(Boc)-L-Asp(OMe)-*Z*-ΔPhe-OMe as a white solid (0.450 g, 87%).

^{1}H NMR (400 MHz, DMSO-d_6) δ:[1.35 and 1.36 (18H, s, OC(C*H*$_3$)], 1.15-1.40 (4H, m, γ-C*H*$_2$ and δ-C*H*$_2$ of Lys), 1.35 (9H, s, 1 x OC(C*H*$_3$)$_3$), 1.36 (9H, s, 1 x OC(C*H*$_3$)$_3$), 1.43-1.64 (2H, m, β-C*H*$_2$ of Lys), 2.61-2.90 (2H, m, β-C*H*$_2$ of Asp), 2.72-2.91 (2H, m, ε-C*H*$_2$ of Lys), 3.60 (3H, s, 1 x OC*H*$_3$), 3.69 (3H, s, 1 x OC*H*$_3$), 3.81-3.95 (1H, m, α-C*H* of Lys); 4.68-4.81 (1H, m, α-C*H* Asp); 6.72 (1H, s, 1 x N*H*); 7.21-7.42 (5H, m, Ar*H* and β-C*H* of ΔPhe and 1x N*H*); 7.60-7.69 (2H, m, Ar*H*), 8.20 (1H, d, J 7.6 Hz, N*H*), 9.48 (1H, s, N*H* of ΔPhe).

4.2.22 Synthesis of H-L-Lys-L-Asp(OMe)-*Z*-ΔPhe-OMe.2TFA:

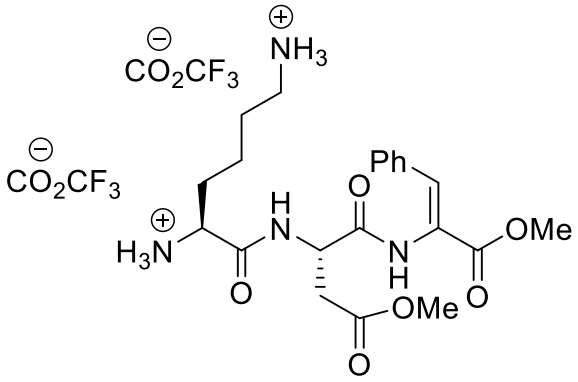

Boc-L-Lys(Boc)-L-Asp(OMe)-*Z*-ΔPhe-OMe (0.4501 g, 0.72 mmol) was dissolved in TFA (2.0 mL) and the reaction mixture was stirred at room temperature for 1 hour. The TFA was then removed under reduced pressure. Traces of residue TFA were removed by the addition of $CHCl_3$ (3 x 10 mL) followed by removal under reduced pressure, affording H-L-Lys-L-Asp(OMe)-*Z*-ΔPhe-OMe.2TFA as a brown oil.

^{1}H NMR (400 MHz, DMSO-d_6) δ: 1.22-1.58 (4H, m, γ-C*H*$_2$ and δ-C*H*$_2$ of Lys), 1.62-1.79 (2H, m, β-C*H*$_2$ of Lys), 2.61-2.72 (2H, m, ε-C*H*$_2$ of Lys), 2.80-2.91 (2H, m, β-C*H*$_2$ of Asp), 3.61 and 3.64 (3H, s, OC*H*$_3$)], 3.81-3.95 (1H, m, α-C*H* of Lys), 4.79-4.90 (1H, m, α-C*H* Asp), 7.15-7.46 (5H, m, Ar*H* and 1x *H*$_3$N$^+$), 7.61-7.86 (2H, m, Ar*H* and β-C*H* of ΔPhe), 8.11-8.29 (2H, m, Ar*H*), 8.86 and 8.94 (3H, d, J=7.2 Hz, 1 x *H*$_3$N$^+$); [9.84 and 9.94 (1H, s, N*H* of ΔPhe).

4.2.23 Synthesis of Naph-L-Lys(Naph)-L-Asp(OMe)-*Z*-ΔPhe-OMe:

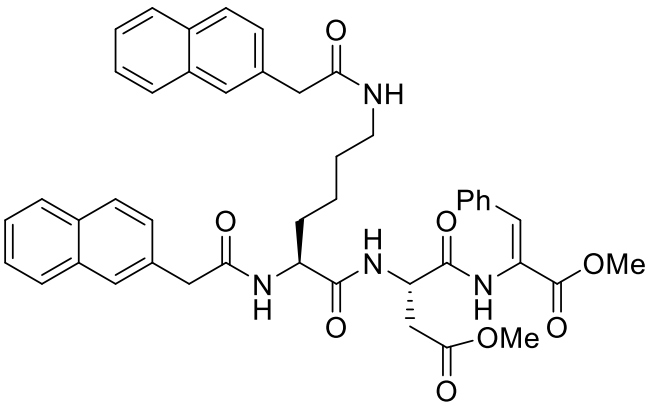

H-L-Lys-L-Asp(OMe)-*Z*-ΔPhe-OMe.TFA (0.4567g, 0.86 mmol) was dissolved in MeCN (8 mL) and cooled to 0 °C. 2-(Naphth-2-yl)-acetic acid (2.00 equiv, 0.320 g, 1.72 mmol), triethylamine (3 equiv, 0.4 mL, 2.58 mmol) and HBTU (1.1 equiv, 0.357 g, 0.94 mmol) were added sequentially, with 2 min between each addition, and then the mixture was stirred at rt overnight. The solvent was removed under reduced

pressure to afford a residue that was partitioned between EtOAc (50 mL) and $KHSO_4$ (50 mL, 1 M). After separation of the phases, the organic layer was thoroughly washed with $KHSO_4$ (1 M, 2 x 50 mL), $NaHCO_3$ (1 M, 2 x 50 mL) and brine (2 x 50 mL) and then dried with $MgSO_4$. Filtration followed by removal of the solvent under reduced pressure afforded Naph-L-Lys(Naph)-L-Asp(OMe)-*Z*-ΔPhe-OMe as a white solid (0.210 g, 33%).

^{1}H NMR (400 MHz DMSO-d_6) δ: 1.16-1.43 (4H, m, γ-CH_2 and δ-CH_2 of Lys), 1.43-1.72 (2H, m, β-CH_2 of Lys), 2.63 (1H, m, β-CH_AH$_B$ of Asp), 2.81 (1H, m, β-CH$_A$CH_B of Asp), 2.90-3.03 (2H, m, ε-CH_2 of Lys), 3.51-3.62 (4H, m, 2 x CH_2 of Naph), 3.57 (3H, s, 1 x OCH_3), 3.65 (3H, s, 1 x OCH_3), 4.20-4.31 (1H, m, α-CH of Lys), 4.68-4.82 (1H, m, α-CH of Asp), 7.22-7.50 (10H, m, ArH and β-CH of ΔPhe), 7.56-7.7.87 (11H, m, ArH and 2 x NH), 7.99-8.07 (1H, m, ArH), 8.38 (1H, d, J = 8.0 Hz, NH), 8.59 (1H, d, J = 8.0 Hz, NH), 9.61 (1H, s, NH of ΔPhe).

^{13}C NMR (100.6 MHz, DMSO-d_6, δ): 22.6 (CH_2, γ-CH$_2$ of Lys), 28.7 (CH_2, δ-CH$_2$ of Lys), 31.9 (CH_2, β-CH$_2$ of Lys), 38.2 (CH_2, β-CH$_2$ of Asp), 38.6 (CH_2, ε-CH$_2$ of Lys), 42.1 (CH_2, 1 x CH$_2$ of Naph), 42.5 (CH_2, 1 x CH$_2$ of Naph), 48.5 (CH, α-CH of Asp), 52.0 (CH_3, 1 x OCH$_3$), 52.2 (CH, α-CH of Lys), 52.8 (CH_3, 1 x OCH$_3$), 125.4 (CH, Ar), 126.01 (CH, Ar), 126.04 (CH, Ar), 127.2 (CH, Ar), 127.30 (CH, Ar), 127.36 (CH, Ar), 127.4 (CH, Ar), 127.51 (CH, Ar), 127.56 (CH, Ar), 127.60 (CH, Ar), 127.65 (CH, Ar), 128.4 (CH, Ar), 128.5 (CH, Ar), 128.6 (CH, Ar), 129.1 (C, Ar), 129.8 (CH, Ar), 129.9 (CH, Ar), 130.1 (CH, Ar), 131.3 (CH, β-CH of ΔPhe), 131.7 (C, Ar), 132.9 (C, Ar), 134.1 (C, Ar), 134.2 (C, Ar), 169.8 (C, C=O), 170.0 (C, C=O), 171.41 (C, C=O), 171.45 (C, C=O).

4.2.24 Synthesis of Naph-L-Lys(Naph)-L-Asp(OH)-*Z*-ΔPhe-OH, 4:

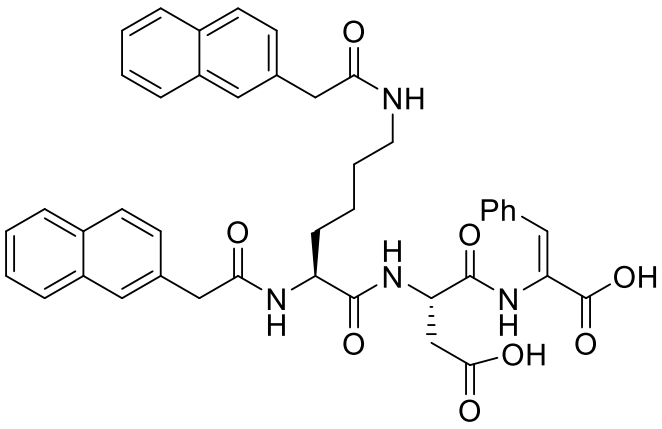

Naph-L-Lys(Naph)-L-Asp(OMe)-*Z*-ΔPhe-OMe was dissolved in 1,4-dioxane (27.5 mL) and a solution of 1 M NaOH (3.0 equiv, 16 mL, 0.824 mmol) was added. The reaction was followed by TLC until no

starting material was detected (typically about 4 hours). The organic solvent was removed under reduced pressure, and the reaction mixture was acidified to pH 2-3 with $KHSO_4$ (1 M). The solid was collected by filtration and then washed with Et_2O. The solid was identified as Naph-L-Lys(Naph)-L-Asp(OH)-*Z*-ΔPhe-OH, **4** (0.200g, 98%).

^{1}H NMR (400 MHz, DMSO-d_6) δ: 1.16-1.41 (4H, m, γ-CH_2 and δ-CH_2 of Lys), 1.43-1.71 (2H, m, β-CH_2 of Lys), 2.53-2.62 (1H, m, β-CH_AH$_B$ of Asp), 2.66-2.75 (1H, m, β-CH$_A$CH_B of Asp), 2.86-3.07 (2H, m, ε-CH_2 of Lys), 3.53-3.68 (4H, m, 2 x Naph CH_2), 4.22-4.32 (1H, m, α-CH of Lys), 4.53-4.62 (1H, m, α-CH of Asp), 7.15-7.50 (10H, m, ArH and β-CH of ΔPhe), 7.53-7.90 (10H, m, ArH and 2 x NH), 7.99-8.10 (1H, m, ArH), 8.22-8.37 (2H, m, 2 x NH), 9.62 (1H, br s, 1 x NH of ΔPhe).

^{13}C NMR (100.6 MHz, DMSO-d_6, δ): 22.7 (CH_2, γ-CH$_2$ of Lys), 28.8 (CH_2, δ-CH$_2$ of Lys), 32.0 (CH_2, β-CH$_2$ of Lys), 36.9 (CH_2, β-CH$_2$ of Asp), 38.6 (CH_2, ε-CH$_2$ of Lys), 42.2 (CH_2, 1 x CH$_2$ of Naph), 42.5 (CH_2, 1 x CH$_2$ of Naph), 48.5 (CH, α-CH of Asp), 52.3 (CH, α-CH of Lys), 125.5 (CH, Ar), 126.10 (CH, Ar), 126.14 (CH, Ar), 127.2 (CH, Ar), 127.4 (CH, Ar), 127.5 (CH, Ar); 127.62 (CH, Ar), 127.67 (CH, Ar), 127.7 (CH, Ar), 128.5 (CH, Ar), 128.62 (CH, Ar), 128.63 (CH, Ar), 129.2 (CH, Ar), 130.01 (CH, Ar), 130.06 (CH, Ar), 130.1 (CH, Ar), 130.2 (CH, Ar), 131.3 (CH, β-CH of ΔPhe), 131.8 (C, Ar), 133.04 (C, Ar), 133.05 (C, Ar), 133.5 (C, α-C of ΔPhe), 133.6 (C, Ar), 134.15 (C, Ar), 134.16 (C, Ar), 134.2 (C, Ar), [166.3 and 166.4 (C, C=O)], [169.2 and 169.3 (C, C=O)], [170.01 and 170.03 (C, C=O)], [170.11 and 170.13 (C, C=O)], [171.64 and 171.67 (C, C=O)], 172.5 (C, C=O).

4.2.25 Synthesis of H-D-HPhe-OMe.HCl:

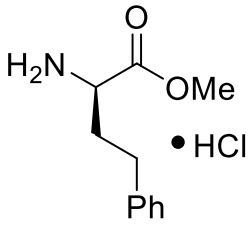

Thionyl chloride (1.21 mL, 16.7 mmol) was slowly added to cooled (0 °C) MeOH (12 mL) over 5 min. D-Homophenylalanine (1.00 g, 5.58 mmol) was then added slowly, and the temperature of the mixture was raised to 40 °C and left for 4 h. The solvent was removed under reduced pressure to afford a white solid, which was washed with Et_2O (12 mL). Removal of residual Et_2O under reduced pressure afforded H-D-HPhe-OMe.HCl as a white solid (1.20 g, 94%).

^{1}H NMR (300 MHz DMSO-d_6, δ): 2.04-2.13 (1H, m, γ-CH_2Ph), 2.56-2.68 (1H, m, β-CH_AH$_B$), 2.70-

2.80 (1H, m, β-CH_AH_B), 3.73 (3H, s, CO_2CH_3), 4.00 (1H, m, α-C*H*), 7.17-7.23 (3H, m, Ph*H*), 7.27-7.33 (2H, m, Ph*H*), 8.65 (br s, NH_3+).

^{13}C NMR (100.6 MHz, DMSO-d_6: δ): 30.2 (CH_2, γ-*C*H_2 of HPhe), 31.1 (CH_2, γ-*C*H_2 of HPhe), 51.5 (CH, α-C*H* of HPhe), 52.7 (CH_3, CO_2*C*H_3), 126.2 (CH, Ar), 128.3 (CH, Ar), 128.4 (CH, Ar), 140.2 (C, Ar), 169.7 (C, *C*=O). The data were consistent with those reported previously in the literature (92).

4.2.26 Synthesis of Boc-D-BPhe-D-HPhe-OMe:

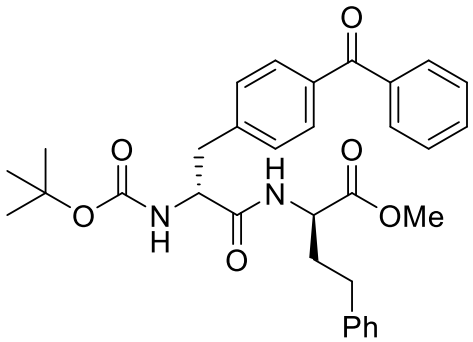

Boc-D-BPhe-OH (200 mg, 0.54 mmol) was dissolved in MeCN (5 mL) and cooled to 0 °C. H-D-HPhe-OMe.HCl (124 mg, 0.54 mmol), Et_3N (225 uL, 1.62 mmol) and HBTU (225 mg, 0.59 mmol) were added sequentially, with 2 min between each addition, and the mixture was stirred at rt overnight. The solvent was removed under reduced pressure to afford a residue that was partitioned between EtOAc (50 mL) and $KHSO_4$ (50 mL, 1 M). After separation of the phases, the organic phase was thoroughly washed with $KHSO_4$ (1 M, 2 × 50 mL), $NaHCO_3$ (1 M, 3 × 50 mL), and brine (3 × 50 mL) and then dried with $MgSO_4$. Filtration followed by removal of the solvent under reduced pressure afforded Boc-D-BPhe-D-HPhe-OMe (248 mg, 87%).

^{1}H-NMR (400 MHz, $CDCl_3$, δ): 1.42 (9H, s, O(CH_3)$_3$), 1.96-2.05 (1H, m, β-CH_AH_B of HPhe), 2.14-2.23 (1H, m, β-CH_AH_B), 2.61 (2H, app. t, J = 8.0, γ-CH_2 of HPhe), 3.08 (1H, dd, J = 13.4 6.8, β-CH_AH_B of BPhe), 3.20 (1H, dd, J = 13.4, 6.4, β-CH_AH_B of BPhe), 3.69 (3H, s, CO_2CH_3), 4.40-4.42 (1H, m, α-C*H* of HPhe), 4.60 (app. q, J = 6.6, α-C*H* of BPhe), 5.00 (1H, d, J = 6.6, N*H*), 6.53 (1H, d, J = 7.6, N*H*), 7.14 (2H, d, J = 6.8, Ar*H*), 7.20 (1H, d, J = 7.2, Ar*H*), 7.23-7.29 (2H, m, Ar*H*), 7.33 (2H, d, J = 8.0, Ar*H*), 7.47 (2H, t, J = 6.4, Ar*H*), 7.57-7.62 (1H, m, Ar*H*), 7.72-7.81 (4H, m, Ar*H*).

^{13}C NMR (100.6 MHz, $CDCl_3$, δ): 28.2 (CH_3, OC(*C*H_3)$_3$), 31.4 (CH_2, γ-*C*H_2 of HPhe), 33.6 (CH_2, β-*C*H_2 of HPhe), 38.0 (CH_2, β-*C*H_2 of BPhe), 52.1 (CH, α-*C*H of BPhe), 52.4 (CH_3, CO_2*C*H_3), 55.5 (CH, α-*C*H of HPhe), 80.4 (C, O*C*(CH_3)$_3$) 126.2 (CH, Ar), 128.2 (CH, Ar), 128.3 (CH, Ar), 128.5 (CH, Ar), 129.3 (CH, Ar), 129.9 (CH, Ar), 130.4 (CH, Ar), 132.4 (CH, Ar), 136.2 (C, Ar), 137.6 (C, Ar), 140.5 (C, Ar),

141.6 (C, Ar), 155.3 (C, *C*=O), 170.6 (C, *C*=O), 172.0 (C, *C*=O), 196.3 (C, *C*=O).

4.2.27 Synthesis of Npx-D-BPhe-D-HPhe-OMe:

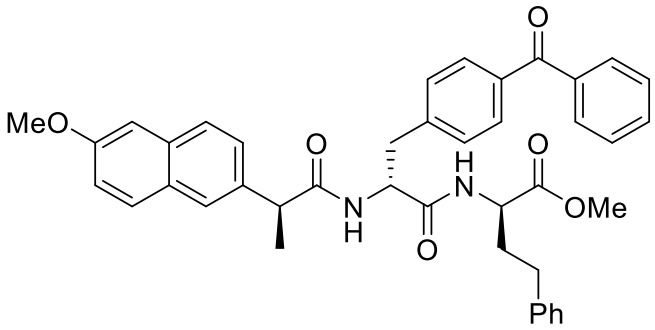

Boc-D-BPhe-D-HPhe-OMe (229 mg, 0.42 mmol) was dissolved in TFA (2.0 mL) and the reaction mixture was stirred at rt for 30 minutes. The mixture was diluted with $CHCl_3$ (10 mL) and concentrated under reduced pressure. Additional $CHCl_3$ (2 × 10 mL) was added and then removed under reduced pressure (to completely remove the residual TFA), to afford H-D-BPhe-D-HPhe-OMe.TFA as a white solid, which was dissolved in MeCN (6 mL) and cooled to 0 °C. Naproxen (106 mg, 0.46 mmol), Et_3N (175 uL, 1.26 mmol), and HBTU (175 mg, 0.46 mmol) were added sequentially, with 2 min between each addition, and the mixture was stirred at rt overnight. The solvent was removed under reduced pressure to afford a residue that was partitioned between EtOAc (50 mL) and $KHSO_4$ (1M, 50 mL). After separation of the phases, the organic phase was thoroughly washed with $KHSO_4$ (1 M, 3 × 50 mL), NaHCO3 (1 M, 3 × 50 mL), and brine (3 × 50 mL) and then dried with $MgSO_4$. Filtration followed by removal of the solvent under reduced pressure afforded Npx-D-BPhe-D-HPhe-OMe as a white solid (234 mg, 85%).

^{1}H NMR (400 MHz, $CDCl_3$, δ): 1.55 (3H, d, J = 7.2, C*H*$_3$ of Npx), 1.94-2.01 (1H, m, β-C*H*$_A$H$_B$ of HPhe), 2.12-2.22 (1H, m, β-CH$_A$*H*$_B$ of HPhe), 2.56 (2H, app. t, J = 8.0, γ-C*H*$_2$ of HPhe), 2.99 (2H, m, β--C*H*$_2$ of BPhe), 3.70 (3H, s, CO$_2$C*H*3), 3.84 (3H, s, OC*H*$_3$ of Npx), 4.55 (1H, app. dt, J = 7.6, 5.2, α-C*H* of HPhe), 4.77 (1H, app. dt, J = 14.0, 7.2, α-C*H* of BPhe), 6.02 (1H, br d, J = 8.0, N*H*), 6.75 (1H, br d, J = 8.0, N*H*), 6.94 (2H, d, J = 8.0, Ar*H*), 7.01-7.13 (4H, m, Ar*H*), 7.13-7.29 (4H, m, Ar*H*), 7.40-7.48 (4H, m, Ar*H*), 7.56-7.65 (4H, m, Ar*H*), 7.68-7.72 (2H, m, Ar*H*).

^{13}C NMR (100.6 MHz, $CDCl_3$, δ): 17.9 (CH_3, CH*C*H$_3$ of Npx), 31.4 (CH_2, γ-CH_2 of HPhe), 33.6 (CH_2, β-*C*H$_2$ of HPhe), 37.4 (CH_2, β-*C*H$_2$ of BPhe), 46.8 (CH, *C*HCH$_3$ of Npx), 52.1 (CH, α-*C*H of HPhe), 52.4 (CH_3, CO$_2$*C*H$_3$), 53.6 (CH, α-*C*H of BPhe), 55.2 (CH_3, O*C*H$_3$ of Npx), 105.6 (CH, Ar), 119.3 (CH, Ar), 125.7 (CH, Ar), 126.1 (CH, Ar), 126.2 (CH, Ar), 127.7 (CH, Ar), 128.2 (CH, Ar), 128.3 (CH, Ar), 128.5

(CH, Ar), 128.8 (C, Ar), 129.1 (CH, Ar), 129.9 (CH, Ar), 130.2 (CH, Ar), 132.3 (CH, Ar), 133.7 (C, Ar), 135.7 (C, Ar), 135.9 (C, Ar), 137.5 (C, Ar), 140.4 (C, Ar), 140.9 (C, Ar), 157.7 (C, Ar), 170.3 (C, *C*=O), 172.1 (C, *C*=O), 174.4 (C, *C*=O), 196.1 (C, *C*=O). 1 x (CH, Ar) is not observed due to resonance overlap.

4.2.28 Synthesis of Npx-D-BPhe-D-HPhe-OH, 6:

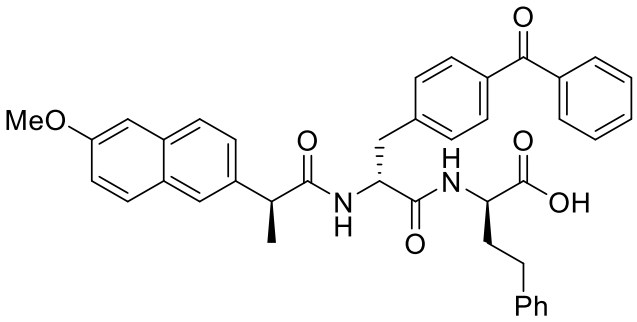

Npx-D-BPh-D-HPhe-OMe (210 mg, 0.32 mmol) was dissolved in 1,4-dioxane (3.2 mL) and NaOH (1.0 M, 0.96 mL, 0.96 mmol). The reaction was monitored by TLC. When all the starting material was consumed (typically 4 h), the organic solvent was removed under reduced pressure and the reaction mixture was acidified to pH 3 with $KHSO_4$ (1.0 M). The solid precipitate was filtered to afford Npx-D-BPh-D-HPhe-OH **6,** as a white solid (146 mg, 71%).

^{1}H NMR (400 MHz, DMSO-d_6, δ): 1.36 (3H, d, J = 6.8, CH_3 of Npx), 1.86-2.09 (1H, m, β-CH_AH$_B$ of HPhe), 1.98-2.09 (1H, m, β-CH$_A$$H_B$ of HPhe), 2.57-2.70 (2H, m, γ-CH_2 of HPhe), 2.85 (1H, dd, J = 13.6, 9.4, β-CH_AH$_B$ of BPhe), 3.05 (1H, dd, J = 13.6, 3.8, β-CH$_A$$H_B$ of BPhe), 3.74 (3H, s, OCH_3 of Npx), 4.18 (1H, m, α-CH of HPhe), 4.66 (1H, app. td, J = 9.4 and 3.8, α-CH of BPhe), 6.97 (1H, dd, J = 9.2, 2.8, ArH), 7.05 (1H, d, J = 2.4, ArH), 7.12-7.21 (5H, m, ArH), 7.21-7.30 (5H, m, ArH), 7.48-7.56 (5H, m, ArH).

^{13}C NMR (100.6 MHz, DMSO-d_6: δ): 17.8 (CH$_3$, CHCH$_3$ of Npx), 31.3 (CH$_2$, γ-CH$_2$ of HPhe), 32.8 (CH$_2$, β-CH$_2$ of HPhe), 37.4 (CH$_2$, β-CH$_2$ of BPhe), 44.5 (CH, CHCH$_3$ of Npx), 51.4 (CH, α-CH of HPhe), 52.3 (CH$_3$, CO$_2$$CH_3$), 53.2 (CH, α-$C$H of BPhe), 105.5 (CH, Ar), 118.4 (CH, Ar), 125.3 (CH, Ar), 126.0 (CH, Ar), 126.3 (CH, Ar), 128.2 (C, Ar), 128.37 (CH, Ar), 128.41 (CH, Ar), 128.44 (CH, Ar), 128.9 (CH, Ar), 129.2 (CH, Ar), 129.3 (CH, Ar), 129.4 (CH, Ar), 132.4 (CH, Ar), 133.0 (C, Ar), 134.7 (C, Ar), 137.0 (C, Ar), 137.1 (C, Ar), 141.0 (C, Ar), 142.8 (C, Ar), 156.8 (C, Ar), 171.2 (C, *C*=O), 173.3 (C, *C*=O), 173.4 (C, *C*=O), 195.3 (C, *C*=O).

4.2.29 Synthesis of Ind-D-BPhe-D-HPhe-OMe:

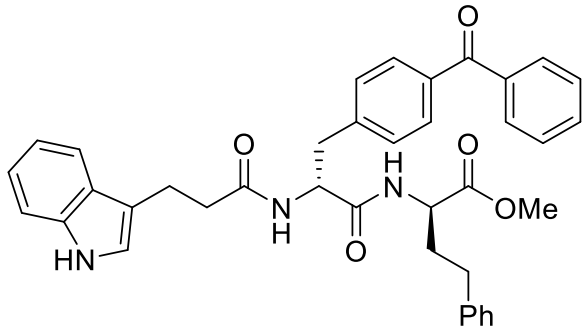

Boc-D-BPhe-D-HPhe-OMe (218 mg, 0.40 mmol) was dissolved in TFA (2 mL) and the reaction mixture was stirred at rt for 30 minutes. The mixture was diluted with $CHCl_3$ (10 mL) and concentrated under reduced pressure. Additional $CHCl_3$ (2 × 10 mL) was added and then removed under reduced pressure (to completely remove the residual TFA), to afford H-D-BPhe-D-HPhe-OMe • TFA as a white solid, which was dissolved in MeCN (6 mL) and cooled to 0 °C. 3-Indolepropionic acid (83 mg, 0.44 mmol), Et_3N (167 uL, 1.20 mmol), and HBTU (167 mg, 0.44 mmol) were added sequentially, with 2 min between each addition, and the mixture was stirred at rt overnight. The solvent was removed under reduced pressure to afford a residue that was partitioned between EtOAc (50 mL) and $KHSO_4$ (1M, 50 mL). After separation of the phases, the organic phase was thoroughly washed with $KHSO_4$ (1 M, 3 × 50 mL), $NaHCO_3$ (1 M, 3 × 50 mL), and brine (3 × 50 mL) and then dried with $MgSO_4$. Filtration followed by removal of the solvent under reduced pressure afforded Ind-D-BPhe-D-HPhe-OMe as a white solid (202 mg, 82%).

^{1}H NMR (400 MHz, $CDCl_3$, δ): 1.94-2.01 (1H, m, β-C*H*$_A$H$_B$ of HPhe), 2.10-2.21 (1H, m, β-CH$_A$*H*$_B$ of HPhe), 2.50-2.67 (4H, m, γ-C*H*$_2$ of HPhe and C*H*$_2$ of Ind), 2.90-3.13 (4H, m, β-C*H*$_2$ of BPhe and C*H*$_2$ of Ind), 3.70 (3H, s, CO_2CH_3), 4.54 (1H, app. dt, J = 7.6, 5.2, α-C*H* of HPhe), 4.76 (1H, app. q, J = 7.2 α-C*H* of BPhe), 5.99 (1H, br d, J = 8.4, N*H*), 6.57 (1H, br d, J = 8.0, N*H*), 7.07-7.26 (10H, m, Ar*H*), 7.33 (1H, d, J = 8.0, Ar*H*), 7.48 (2H, t, J = 8.0, Ar*H*), 7.54-7.65 (4H, m, Ar*H*), 7.68-7.72 (2H, m, Ar*H*), 8.22 (1H, br s, N*H*).

^{13}C NMR (100.6 MHz, $CDCl_3$, δ): 21.1 (CH_2, 1 x CH_2 of Ind), 31.2 (CH_2, γ-CH_2 of HPhe), 32.6 (CH_2, β-CH_2 of HPhe), 36.1 (CH_2, 1 x CH_2 of Ind), 37.6 (CH_2, , β-CH_2 of BPhe), 51.4 (CH, α-CH of HPhe), 51.9 (CH_3, CO_2CH_3), 53.2 (CH_2, α-CH of BPhe), 111.3 (CH, Ar), 113.7 (C, Ar), 118.1 (CH, Ar), 118.2 (CH, Ar), 120.8 (CH, Ar), 122.1 (CH, Ar), 126.0 (CH, Ar), 127.0 (C, Ar), 128.3 (CH, Ar), 128.4 (CH, Ar), 128.5 (CH, Ar), 129.46 (CH, Ar), 129.5 (CH, Ar), 132.5 (CH, Ar), 135.1 (C, Ar), 136.2 (C, Ar), 137.2 (C, Ar), 140.8 (C, Ar), 143.2 (C, Ar), 171.4 (C, C=O), 172.0 (C, C=O), 172.3 (C, C=O), 195.5 (C, C=O).

4.2.30 Synthesis of Ind-D-BPhe-D-HPhe-OH, 7:

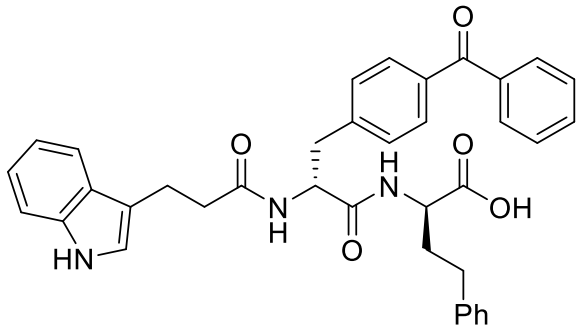

Ind-D-BPhe-D-HPhe-OMe (180 mg, 0.29 mmo) was dissolved in 1,4-dioxane (2.9 mL) and NaOH (1.0 M, 0.87 mL, 0.87mmol). The reaction was monitored by TLC. When all the starting material was consumed (typically 4 h), the organic solvent was removed under reduced pressure and the reaction mixture was acidified to pH 3 with KHSO4 (1.0 M). The solid precipitate was filtered to afford Ind-D-BPhe-D-HPhe-OH **7**, as a white solid (127 mg, 73%).

^{1}H NMR (400 MHz, DMSO-d_6, δ): 1.88-2.09 (1H, m, β-CH_AH$_B$ of HPhe), 2.10-2.21 (1H, m, β-CH$_A$$H_B$ of HPhe), 2.39-2.51 (2H, m, γ-CH_2 of HPhe), 2.53-2.70 (2H, m, CH_2 of Ind), 2.79 (2H, t, J = 8.0, CH_2 of Ind), 2.89 (1H, dd, J = 13.6, 9.0, β-CH_ACH$_B$ of BPhe), 3.13 (1H, dd, J = 13.6, 4.4, β-CH$_A$CH_B of BPhe), 4.17 (1H, app. td, J = 9.2, 4.8, α-CH of HPhe), 4.73 (1H, app. td, J = 9.0, 4.4, α-CH BPhe), 6.92 (1H, td, J = 7.2, 0.8, ArH), 6.98-7.05 (2H, m, ArH), 7.15-7.20 (3H, m, ArH), 7.23-7.30 (3H, m, ArH), 7.41 (2H, d, J = 8.0, ArH), 7.46 (1H, d, J = 8.8, ArH), 7.50 (2H, d, J = 8.0, ArH), 7.59-7.70 (5H, m, ArH), 8.21 (1H, d, J = 8.4, NH), 8.41 (1H, d, J = 7.6, NH), 10.70 (1H, s, NH).

^{13}C NMR (100.6 MHz, DMSO-d_6, δ): 21.1 (CH$_2$, 1 x CH$_2$ of Ind), 31.4 (CH$_2$, γ-CH$_2$ of HPhe), 32.8 (CH$_2$, β-CH$_2$ of HPhe), 36.2 (CH$_2$, 1 x CH$_2$ of Ind), 37.6 (CH$_2$, β-CH$_2$ of BPhe), 51.4 (CH, α-CH of HPhe), 53.3 (CH, α-CH of BPhe), 111.3 (CH, Ar), 113.8 (C, Ar), 118.1 (CH, Ar), 118.3 (CH, Ar), 120.9 (CH, Ar), 122.1 (CH, Ar), 126.0 (CH, Ar), 127.0 (C, Ar), 128.37 (CH, Ar), 128.43 (CH, Ar), 128.5 (CH, Ar), 129.5 (CH, Ar), 129.6 (CH, Ar), 132.5 (CH, Ar), 135.1 (C, Ar), 136.3 (C, Ar), 137.3 (C, Ar), 141.0 (C, Ar), 143.3 (C, Ar), 171.3 (C, C=O), 172.1 (C, C=O), 173.4 (C, C=O), 195.6 (C, C=O).

4.3 Sustained release assays

Hydrogels of **1** and **6**, were prepared as described before to form 1 mL hydrogels containing the same concentration of the hydrogelators described above and the appropriate cargo – methylene blue (0.1 nM), methyl orange (0.2 nM) or ciprofloxacin (0.2 nM), in a slightly modified version of the procedure described by Abraham *et al.* (97). After allowing to stand overnight, 1 mL of water was carefully added to the surface of the hydrogels. Aliquots of the layered solution (100 μL) were removed at 1h, 2h, 3h, 4h, 6h, 24h, 72h and 6 days from the time the water was initially layered on top of the hydrogel. After removing each aliquot, the volume water was immediately replaced by and equal volume of water. The concentration of methylene blue or methyl orange in each aliquot was determined by measuring the absorbance at λ_{max} of the dye (666 nm for methylene blue and 465 nm for methyl orange) using a microplate reader and then converting the value to percentage release (using a standard calibration curve). The concentration of ciprofloxacin in each aliquot was determined using analytical HPLC, where the integrated peak area was converted to a percentage release (using a standard calibration curve). Each experiment was performed in triplicate, and the mean percentage cargo release was plotted against time.

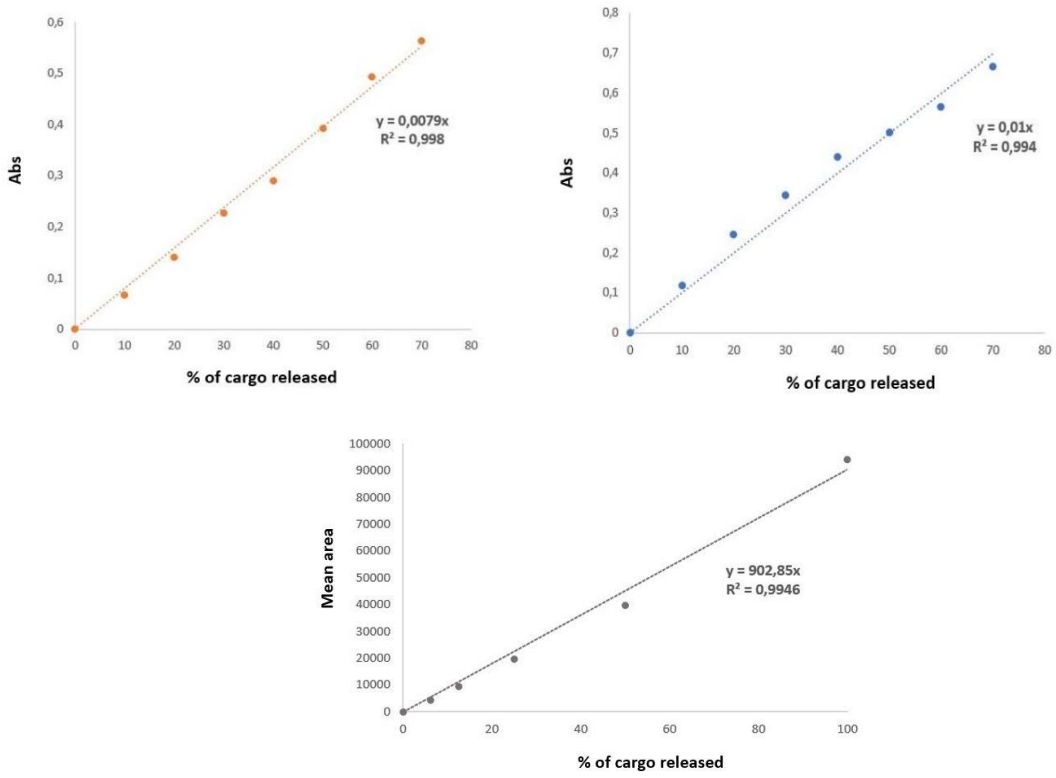

Figure 61: Calibration curve to determine the amount of cargo present in the layered solution above the hydrogel. (A) Methylene orange was measured by UV-Vis spectroscopy by absorbance at 666 nm. Equation of linear correlation: y=0.0079x. (B) Methyl blue was measured by UV-Vis spectroscopy by absorbance at 465 nm. Equation of linear correlation: y=0.01x. (C) Ciprofloxacin was measured by HPLC by area under the curve of the ciprofloxacin peak. Equation of linear correlation: y=902.85x.

4.4 Cell Culture

Human keratinocytes cell line HaCaT was from ATCC. Cells were cultured in DMEM supplemented with 10% FBS and 1% penicillin/streptomycin and were incubated in an incubator at 37°C, in a humidified atmosphere of 5% CO_2.

4.5 MTT assay

Cells were seeded in 96-well plates (1.5×10^4 cells/well) and left to attach for 24h. After this period, cells were incubated with different concentrations of the molecules under study for another 24h. After this period, cell viability was evaluated based on the ability of metabolically active cells to convert MTT to formazan over the course of 2 hours. Absorbances were measured at 570 nm in a Multiskan GO plate reader (Thermo Fisher Scientific; Waltham, MA, USA) and results were expressed as percentage of the respective control and correspond to the mean ± standard error of the mean (SEM) of at least three independent experiments performed in triplicate.

Chapter 5

References

5 References

1. Thakur S, Thakur VK, Arotiba OA. History, Classification, Properties and Application of Hydrogels: An Overview. *Springer Singapore*; **2018**. 29–50 p. Available from: http://dx.doi.org/10.1007/978-981-10-6077-9_2
2. Wichterle O, Lim D. Hydrophilic Gels for Biological Use. *Nature Publishing Group*. **1960**.
3. Buwalda SJ, Boere KWM, Dijkstra PJ, Feijen J, Vermonden T, Hennink WE. Hydrogels in a historical perspective: From simple networks to smart materials. *J Control Release*. **2014**;190:254–73. Available from: http://dx.doi.org/10.1016/j.jconrel.2014.03.052
4. Yahia Lh. History and Applications of Hydrogels. *J Biomed Sci*. **2015**;04(02):1–23.
5. Yadav N, Chauhan MK, Chauhan VS. Short to ultrashort peptide-based hydrogels as a platform for biomedical applications. *Biomater Sci.* **2020**;8(1):84–100.
6. Ferreira NN, Ferreira LMB, Cardoso VMO, Boni FI, Souza ALR, Gremião MPD. Recent advances in smart hydrogels for biomedical applications: From self-assembly to functional approaches. *Eur Polym J*. **2018**;117–33. Available from: https://doi.org/10.1016/j.eurpolymj.2017.12.004
7. Fichman G, Gazit E. Self-assembly of short peptides to form hydrogels: Design of building blocks, physical properties and technological applications. *Acta Biomater*. **2014**;10(4):1671–82. Available from: http://dx.doi.org/10.1016/j.actbio.2013.08.013
8. Hoare TR, Kohane DS. Hydrogels in drug delivery: Progress and challenges. *Polymer (Guildf)*. **2008**;49(8):1993–2007. Available from: http://dx.doi.org/10.1016/j.polymer.2008.01.027
9. Hamidi M, Azadi A, Rafiei P. Hydrogel nanoparticles in drug delivery. *Adv Drug Deliv Rev*. **2008**;60(15):1638–49.
10. Martens PJ, Bryant SJ, Anseth KS. Tailoring the degradation of hydrogels formed from multivinyl poly(ethlene glycol) and poly(vinyl alcohol) macromers for cartilage tissue engineering. *Biomacromolecules*. **2003**;4(2):283–92.
11. Drozdov AD, deClaville Christiansen J. Mechanical response and equilibrium swelling of thermoresponsive copolymer hydrogels. *Polym Int*. **2020**;69(10):974–84.
12. Overstreet DJ, McLemore RY, Doan BD, Farag A, Vernon BL. Temperature-responsive graft copolymer hydrogels for controlled swelling and drug delivery. *Soft Mater*. **2013**;11(3):294–304.
13. Reinicke S, Schmelz J, Lapp A, Karg M, Hellweg T, Schmalz H. Smart hydrogels based on double responsive triblock terpolymers. *Soft Matter*. **2009**;5(13):2648–57.
14. He C, Kim SW, Lee DS. In situ gelling stimuli-sensitive block copolymer hydrogels for drug delivery. *J Control Release*. **2008**;127(3):189–207.

15. Jonker AM, Lo DWPM, Hest JCM Van. Peptide- and Protein-Based Hydrogels. *Chem. Mater.* **2012**; 24, 5, 754-773.
16. Mantha S, Pillai S, Khayambashi P, Upadhyay A, Zhang Y. Smart Hydrogels in Tissue Engineering and. *Materials (Basel)*. **2019**;12(3323):33. Available from: https://www.ncbi.nlm.nih.gov/pmc/articles/PMC68/
17. Sikdar P, Uddin MM, Dip TM, Islam S, Hoque MS, Dhar AK, et al. Recent advances in the synthesis of smart hydrogels. *Mater Adv*. **2021**;2(14):4532–73.
18. McCloskey AP, Gilmore BF, Laverty G. Evolution of antimicrobial peptides to self-assembled peptides for biomaterial applications. *Pathogens*. **2014**;3(4):792–821.
19. Shibata Y, Kurokawa T, Aizawa T, Gong JP. Bactericidal effect of cationic hydrogels prepared from hydrophilic polymers. *J Appl Polym Sci*. **2020**;137(48):1–10.
20. He Q, Kusumi R, Kimura S, Kim UJ, Wada M. Cationic hydrogels prepared from regioselectively azidated (1→3)-α-D-glucan via crosslinking and amination: Physical and adsorption properties. *Carbohydr Polym*. **2020**;245(June):116543. Available from: https://doi.org/10.1016/j.carbpol.2020.116543
21. Kim B, La Flamme K, Peppas NA. Dynamic swelling behavior of pH-sensitive anionic hydrogels used for protein delivery. *J Appl Polym Sci*. **2003**;89(6):1606–13.
22. Brzonova I, Kozliak EI, Andrianova AA, LaVallie A, Kubátová A, Ji Y. Production of lignin based insoluble polymers (anionic hydrogels) by C. versicolor. *Sci Rep*. **2017**;7(1):1–13.
23. Draper ER, Adams DJ. Low-Molecular-Weight Gels: The State of the Art. *Chem*. **2017**;3(3):390–410. Available from: https://doi.org/10.1016/j.chempr.2017.07.012
24. Dong R, Pang Y, Su Y, Zhu X. Supramolecular hydrogels: synthesis, properties and their biomedical applications. *Biomater Sci*. **2015**;3(7):937–54.
25. Raeburn J, Cardoso AZ, Adams DJ. The importance of the self-assembly process to control mechanical properties of low molecular weight hydrogels. *Chem Soc Rev*. **2013**;42(12):5143–56.
26. Vilaça H, Hortelão ACL, Castanheira EMS, Queiroz MJRP, Hilliou L, Hamley IW, et al. Dehydrodipeptide Hydrogelators Containing Naproxen N-Capped Tryptophan: Self-Assembly, Hydrogel Characterization, and Evaluation as Potential Drug Nanocarriers. *Biomacromolecules*. **2015**;16(11):3562–73.
27. Yan X, Zhu P, Li J. Self-assembly and application of diphenylalanine-based nanostructures. *Chem Soc Rev.* **2010**;39(6):1877–90.

28. Li J, Xing R, Bai S, Yan X. Recent advances of self-assembling peptide-based hydrogels for biomedical applications. *Soft Matter*. **2019**;15(8):1704–15.

29. Colherinhas G, Fileti E. Molecular dynamics study of surfactant-like peptide based nanostructures. *J Phys Chem B*. **2014**;118(42):12215–22.

30. Smadbeck J, Chan KH, Khoury GA, Xue B, Robinson RC, Hauser CAE, et al. De Novo Design and Experimental Characterization of Ultrashort Self-Associating Peptides. *PLoS Comput Biol*. **2014**;10(7).

31. Ruan L, Luo H, Zhang H, Xing Z. Effect of sonication on a novel designed peptide. *J Wuhan Univ Technol Mater Sci Ed.* **2013**;28(3):622–6.

32. Jervis PJ, Amorim C, Pereira T, Martins JA, Ferreira PMT. Dehydropeptide supramolecular hydrogels and nanostructures as potential peptidomimetic biomedical materials. *Int J Mol Sci*. **2021**;22(5):1–19.

33. Veloso SRS, Magalhães CAB, Rodrigues ARO, Vilaça H, Queiroz MJRP, Martins JA, et al. Novel dehydropeptide-based magnetogels containing manganese ferrite nanoparticles as antitumor drug nanocarriers. *Phys Chem Chem Phys*. **2019**;21(20):10377–90.

34. Johnson EK, Adams DJ, Cameron PJ. Peptide based low molecular weight gelators. *J Mater Chem*. **2011**;21(7):2024–7.

35. Adams DJ. Dipeptide and Tripeptide Conjugates as Low-Molecular-Weight Hydrogelators. *Macromol Biosci*. **2011**;11(2):160–73.

36. Wang K, Keasling JD, Muller SJ. Effects of the sequence and size of non-polar residues on self-assembly of amphiphilic peptides. *Int J Biol Macromol*. **2005;**36(4):232–40.

37. Tian Y, Wang H, Liu Y, Mao L, Chen W, Zhu Z, et al. A peptide-based nanofibrous hydrogel as a promising DNA nanovector for optimizing the efficacy of HIV vaccine. *Nano Lett*. **2014**;14(3):1439–45.

38. Chakraborty P, Tang Y, Yamamoto T, Yao Y, Guterman T, Zilberzwige-Tal S, et al. Unusual Two-Step Assembly of a Minimalistic Dipeptide-Based Functional Hypergelator. *Adv Mater*. **2020**;32(9):1–11.

39. Tao K, Levin A, Adler-Abramovich L, Gazit E. Fmoc-modified amino acids and short peptides: Simple bio-inspired building blocks for the fabrication of functional materials. *Chem Soc Rev.* **2016**;45(14):3935–53. Available from: http://dx.doi.org/10.1039/C5CS00889A

40. Vegners R, Shestakova I, Kalvinsh I, Ezzell RM, Janmey PA. Use of a gel-forming dipeptide derivative as a carrier for antigen presentation. *J Pept Sci*. **1995**;1(6):371–8.

41. Truong WT, Su Y, Gloria D, Braet F, Thordarson P. Dissolution and degradation of Fmoc-diphenylalanine self-assembled gels results in necrosis at high concentrations in vitro. *Biomater Sci*. **2015**;3(2):298–307.

42. Martin AD, Thordarson P. Beyond Fmoc: A review of aromatic peptide capping groups. *J Mater Chem B*. **2020**;8(5):863–77.

43. d`Orlyê F, Alfonso LT, Lescot C, Pinvidic M, Doan BT, Verenne A. Synthesis, characterization and evaluation of peptide nanostructures for biomedical applications. *Molecules*. **2021**; 26, 4587.

44. Vilaça H, Castro T, Costa FMG, Melle-Franco M, Hilliou L, Hamley IW, et al. Self-assembled RGD dehydropeptide hydrogels for drug delivery applications. *J Mater Chem B*. **2017**;5(43):8607–17.

45. Carvalho A, Gallo J, Pereira DM, Valentão P, Andrade PB, Hilliou L, et al. Magnetic dehydrodipeptide-based self-assembled Hydrogels for Theragnostic applications. *Nanomaterials*. **2019**;9(4).

46. Jervis PJ, Amorim C, Pereira T, Martins JA, Ferreira PMT. Exploring the properties and potential biomedical applications of NSAID-capped peptide hydrogels. *Soft Matter*. **2020**;16(44):10001–12.

47. Jervis PJ, Hilliou L, Pereira RB, Pereira DM, Martins JA, Ferreira PMT. Evaluation of a model photo-caged dehydropeptide as a stimuli-responsive supermolecular hydrogel. *Nanomaterials*. **2021**;11(3):1–21.

48. Veloso SRS, Jervis PJ, Silva JFG, Hilliou L, Moura C, Pereira DM, et al. Supramolecular ultra-short carboxybenzyl-protected dehydropeptide-based hydrogels for drug delivery. *Mater Sci Eng C*. **2021**;122.

49. Du X, Zhou J, Shi J, Xu B. Supramolecular Hydrogelators and Hydrogels: From Soft Matter to Molecular Biomaterials. *Chem Rev*. **2015**;115(24):13165–307.

50. Adams DJ, Butler MF, Frith WJ, Kirkland M, Mullen L, Sanderson P. A new method for maintaining homogeneity during liquid-hydrogel transitions using low molecular weight hydrogelators. *Soft Matter*. **2009**;5(9):1856–62.

51. Wang H, Yang Z, Adams DJ. Controlling peptide-based hydrogelation. *Mater Today*. **2012**;15(11):500–7.

52. Yang Z, Liang G, Ma M, Gao Y, Xu B. In vitro and in vivo enzymatic formation of supramolecular hydrogels based on self-assembled nanofibers of a β-amino acid derivative. *Small*. **2007**;3(4):558–62.

53. Toledano S, Williams RJ, Jayawarna V, Ulijn R V. Enzyme-triggered self-assembly of peptide

hydrogels via reversed hydrolysis. *J Am Chem Soc*. **2006**;128(4):1070–1.

54. Yang Z, Liang G, Xu B. Enzymatic hydrogelation of small molecules. *Acc Chem Res*. **2008**;41(2):315–26.
55. Mcewen H, Du EY, Mata JP, Thordarson P, Martin AD. Tuning hydrogels through metal-based gelation triggers. *J Mater Chem B*. **2017**;5(47):9412–7.
56. Knerr PJ, Branco MC, Nagarkar R, Pochan DJ, Schneider JP. Heavy metal ion hydrogelation of a self-assembling peptide via cysteinyl chelation. *J Mater Chem*. **2012**;22(4):1352–7.
57. Chen L, Pont G, Morris K, Lotze G, Squires A, Serpell LC, et al. Salt-induced hydrogelation of functionalised-dipeptides at high pH. *Chem Commun*. **2011**;47(44):12071–3.
58. Yu G, Yan X, Han C, Huang F. Characterization of supramolecular gels. *Chem Soc Rev*. **2013**;42(16):6697–722.
59. Bakshi K, Liyanage MR, Volkin DB, Middaugh CR. Circular dichroism of peptides. *Methods Mol Biol*. **2014**;1088:247–53.
60. Greenfield NJ. Using circular dichroism spectra to estimate protein secondary structure. *Nat Protoc*. **2007**;1(6):2876–90.
61. Jayawarna V, Ali M, Jowitt TA, Miller AF, Saiani A, Gough JE, et al. Nanostructured hydrogels for three-dimensional cell culture through self-assembly of fluorenylmethoxycarbonyl-dipeptides. *Adv Mater.* **2006**;18(5):611–4.
62. Langer R. Drug delivery and targeting. Vol. 392, *Nature*. **1998.** p. 5–10.
63. Liechty WB, Kryscio DR, Slaughter B V., Peppas NA. Polymers for drug delivery systems. *Annu Rev Chem Biomol Eng*. **2010**;1:149–73.
64. Florence AT, Jani PU. Novel Oral Drug Formulations. *Drug Saf*. **1994**;10(3):233–66.
65. Manuscript A, Adhesives M. Mussel-Inspired Adhesives and Coatings, *Annu Rev Mater Res 41* **2011**;99–132.
66. Lee BP, Messsersmith PB, Isrealachvili JN, Waite JH. Mussel-inspired adhesives and coatings. *Annu Rev Mater Res*. **2011**; 41:99-132.
67. Brubaker CE, Kissler H, Wang LJ, Kaufman DB, Messersmith PB. Biological performance of mussel-inspired adhesive in extrahepatic islet transplantation. *Biomaterials.* **2010**;31(3):420–7. Available from: http://dx.doi.org/10.1016/j.biomaterials.2009.09.062
68. Li J, Kuang Y, Shi J, Gao Y, Zhou J, Xu B. The conjugation of nonsteroidal anti-inflammatory drugs (NSAID) to small peptides for generating multifunctional supramolecular nanofibers/hydrogels. *Beilstein J Org Chem.* **2013**;9:908–17.

69. Moreira R, Jervis PJ, Carvalho A, Ferreira PMT, Martins JA, Valentão P, et al. Biological evaluation of naproxen–dehydrodipeptide conjugates with self-hydrogelation capacity as dual LOX/COX inhibitors. *Pharmaceutics.* **2020**;12(2).

70. Tiwari G, Tiwari R, Bannerjee S, Bhati L, Pandey S, Pandey P, et al. Drug delivery systems: An updated review. *Int J Pharm Investig*. **2012**;2(1):2.

71. Silva EA, Mooney DJ. Spatiotemporal control of vascular endothelial growth factor delivery from injectable hydrogels enhances angiogenesis. *J Thromb Haemost.* **2007**;5(3):590–8.

72. Hiemstra C, Zhong Z, Van Tomme SR, van Steenbergen MJ, Jacobs JJL, Otter W Den, et al. In vitro and in vivo protein delivery from in situ forming poly(ethylene glycol)-poly(lactide) hydrogels. *J Control Release.* **2007**;119(3):320–7.

73. Jin R, Teixeira LSM, Krouwels A, Dijkstra PJ, Van Blitterswijk CA, Karperien M, et al. Synthesis and characterization of hyaluronic acid-poly(ethylene glycol) hydrogels via Michael addition: An injectable biomaterial for cartilage repair. *Acta Biomater*. **2010**;6(6):1968–77. Available from: http://dx.doi.org/10.1016/j.actbio.2009.12.024

74. Xiao Y, Gu Y, Qin L, Chen L, Chen X, Cui W, et al. Injectable thermosensitive hydrogel-based drug delivery system for local cancer therapy. *Colloids Surfaces B Biointerfaces*. **2021**;200. Available from: https://doi.org/10.1016/j.colsurfb.2021.111581

75. Wei W, Tang J, Li H, Huang Y, Yin C, Li D, et al. Antitumor effects of self-assembling peptide-emodin in situ hydrogels in vitro and in vivo. *Int J Nanomedicine*. **2021**;16:47–60.

76. Guvendiren M, Lu HD, Burdick JA. Shear-thinning hydrogels for biomedical applications. *Soft Matter.* **2012**;8(2):260–72.

77. Simonovsky E, Miller Y. Controlling the properties and self-assembly of helical nanofibrils by engineering zinc-binding β-hairpin peptides. *J Mater Chem B*. **2020**;8(33):7352–5.

78. Ren P, Li J, Zhao L, Wang A, Wang M, Li J, et al. Dipeptide Self-assembled Hydrogels with Shear-Thinning and Instantaneous Self-healing Properties Determined by Peptide Sequences. *ACS Appl Mater Interfaces.* **2020**;12(19):21433–40.

79. Bencherif SA, Sands RW, Bhatta D, Arany P, Verbeke CS, Edwards DA, et al. Injectable preformed scaffolds with shape-memory properties. *Proc Natl Acad Sci U S A*. **2012;**109(48):19590–5.

80. Sheridan MH, Shea LD, Peters MC, Mooney DJ. Bioabsorbable polymer scaffolds for tissue engineering capable of sustained growth factor delivery. *J Control Release*. **2000;**64(1–3):91–102.

81. Zhou S, Bismarck A, Steinke J. Ion-responsive alginate based macroporous injectable hydrogel

scaffolds prepared by emulsion templating. *J Mater Chem B*. **2013**;1(37), 4736.

82. Hassan CM, Peppas NA. Structure and morphology of freeze/thawed PVA hydrogels. *Macromolecules*. **2000**;33(7):2472–9.

83. Berillo D, Mattiasson B, Galaev IY, Kirsebom H. Formation of macroporous self-assembled hydrogels through cryogelation of Fmoc-Phe-Phe. *J Colloid Interface Sci*. **2012**;368(1):226–30.

84. Lyu L, Liu F, Wang X, Hu M, Mu J, Cheong H, et al. Stimulus-Responsive Short Peptide Nanogels for Controlled Intracellular Drug Release and for Overcoming Tumor Resistance. *Chem - An Asian J.* **2017;**12(7):744–52.

85. Lu J, Wang X. Biomimetic Self-Assembling Peptide Hydrogels for Tissue Engineering Applications. *Biomimetic Medical Materials, Advances in Experimental Medicine and Biology.* 18.1. **2018**;297–312.

86. Liyanage W, Vats K, Rajbhandary A, Benoit DSW, Nilsson BL. Multicomponent dipeptide hydrogels as extracellular matrix-mimetic scaffolds for cell culture applications. *Chem Commun*. **2015**;51(56):11260–3. Available from: http://dx.doi.org/10.1039/C5CC03162A

87. Panda JJ, Dua R, Mishra A, Mittra B, Chauhan VS. 3D cell growth and proliferation on a RGD functionalized nanofibrillar hydrogel based on a conformationally restricted residue containing dipeptide. *ACS Appl Mater Interfaces.* **2010**;2(10):2839–48.

88. Liu X, Sun X, Liang G. Peptide-based supramolecular hydrogels for bioimaging applications. *Biomater Sci.* **2021**;9(2):315–27.

89. Lian M, Chen X, Lu Y, Yang W. Self-Assembled Peptide Hydrogel as a Smart Biointerface for Enzyme-Based Electrochemical Biosensing and Cell Monitoring. *ACS Appl Mater Interfaces*. **2016**;8(38):25036–42.

90. Kim JH, Lim SY, Nam DH, Ryu J, Ku SH, Park CB. Self-assembled, photoluminescent peptide hydrogel as a versatile platform for enzyme-based optical biosensors. *Biosens Bioelectron*. **2011**;26(5):1860–5. Available from: http://dx.doi.org/10.1016/j.bios.2010.01.026

91. Souza SF, Kogikoski S, Silva ER, Alves WA. Nanostructured antigen-responsive hydrogels based on peptides for leishmaniasis detection. *J Braz Chem Soc.* **2017**;28(9):1619–29.

92. Huang Y, Meng L, Nie Q, Zhou Y, Chen L, Yang S, et al. Selection of DNA-encoded chemical libraries against endogenous membrane proteins on live cells. *Nat Chem*. **2021**;13(1):77–88. Available from: http://dx.doi.org/10.1038/s41557-020-00605-x

93. Ferreira PMT, Monteiro LS, Pereira G, Ribeiro L, Sacramento J, Silva L. Reactivity of dehydroamino acids and dehydrodipeptides towards N- bromosuccinimide: Synthesis of β-bromo- and β,β-

dibromodehydroamino acid derivatives and of substituted 4-imidazolidinones. *European J Org Chem*. **2007**;(35):5934–49.

94. Valeur E, Bradley M. Amide bond formation: Beyond the myth of coupling reagents. *Chem Soc Rev*. **2009**;38(2):606–31.
95. Jervis PJ, Martins JA, Ferreira PM. Unpublished results.
96. Wei Y, Thyparambil AA, Latour RA. Protein helical structure determination using CD spectroscopy for solutions with strong background absorbance from 190 to 230 nm. *Biochim Biophys Acta - Proteins Proteomics*. **2014**;1844(12):2331–7.
97. Abraham BL, Toriki ES, Tucker NJ, Nilsson BL. Electrostatic interactions regulate the release of small molecules from supramolecular hydrogels. *J Mater Chem B*. **2020**;8(30):6366–77.
98. Nurhan AD. Dash, Murthy. Kinetic Modeling On Drug Release From Controlled Drug Delivery Systems. *Polish Pharm Soc*. **2010**;67(3):217–23.
99. Kini S, Bahadur D, Panda D. Mechanism of anti-cancer activity of benomyl loaded nanoparticles in multidrug resistant cancer cells. *J Biomed Nanotechnol*. **2015**;11(5):877–89.
100. Fichman G, Guterman T, Damron J, Adler-Abramovich L, Schmidt J, Kesselman E, et al. Supramolecular Chemistry: Spontaneous structural transition and crystal formation in minimal supramolecular polymer model. *Sci Adv*. **2016**;2(2):1–11.
101. Martin AD, Robinson AB, Mason AF, Wojciechowski JP, Thordarson P. Exceptionally strong hydrogels through self-assembly of an indole-capped dipeptide. *Chem Commun*. **2014**;50(98):15541–4. Available from: http://dx.doi.org/10.1039/C4CC07941H